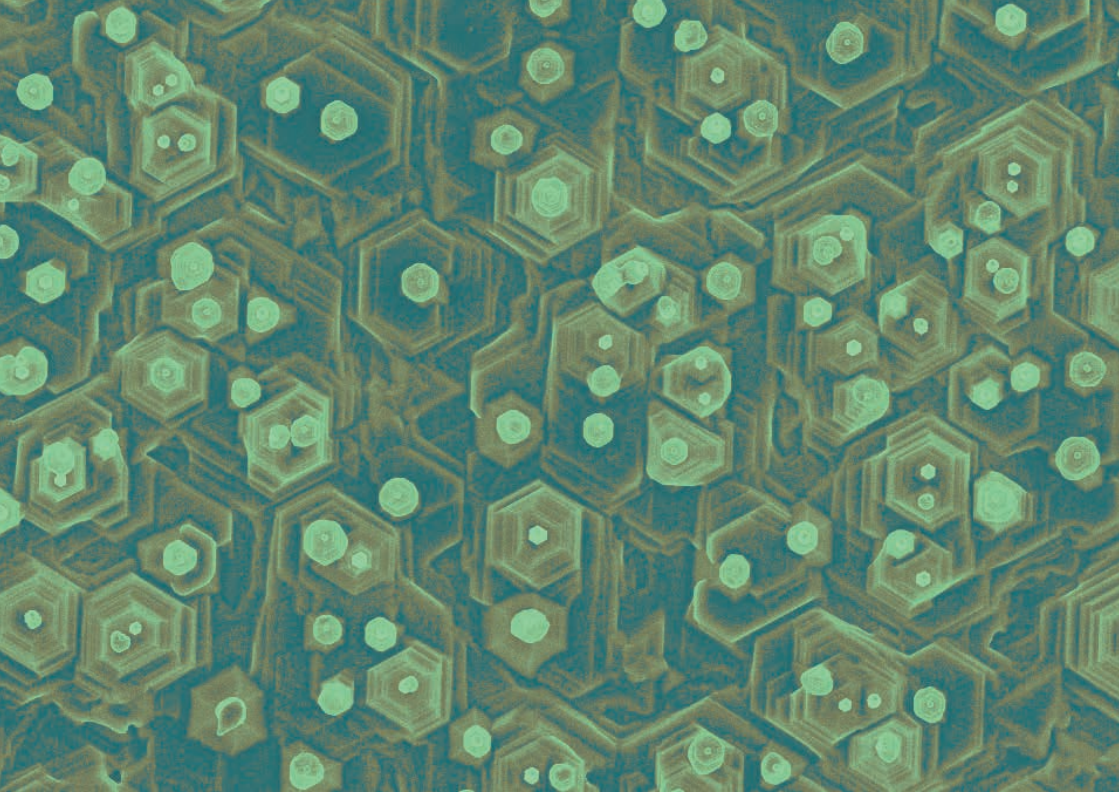

ACTIVITY REPORT 2024

CNR NANO

ISTITUTO NANOSCIENZE CONSIGLIO NAZIONALE DELLE RICERCHE

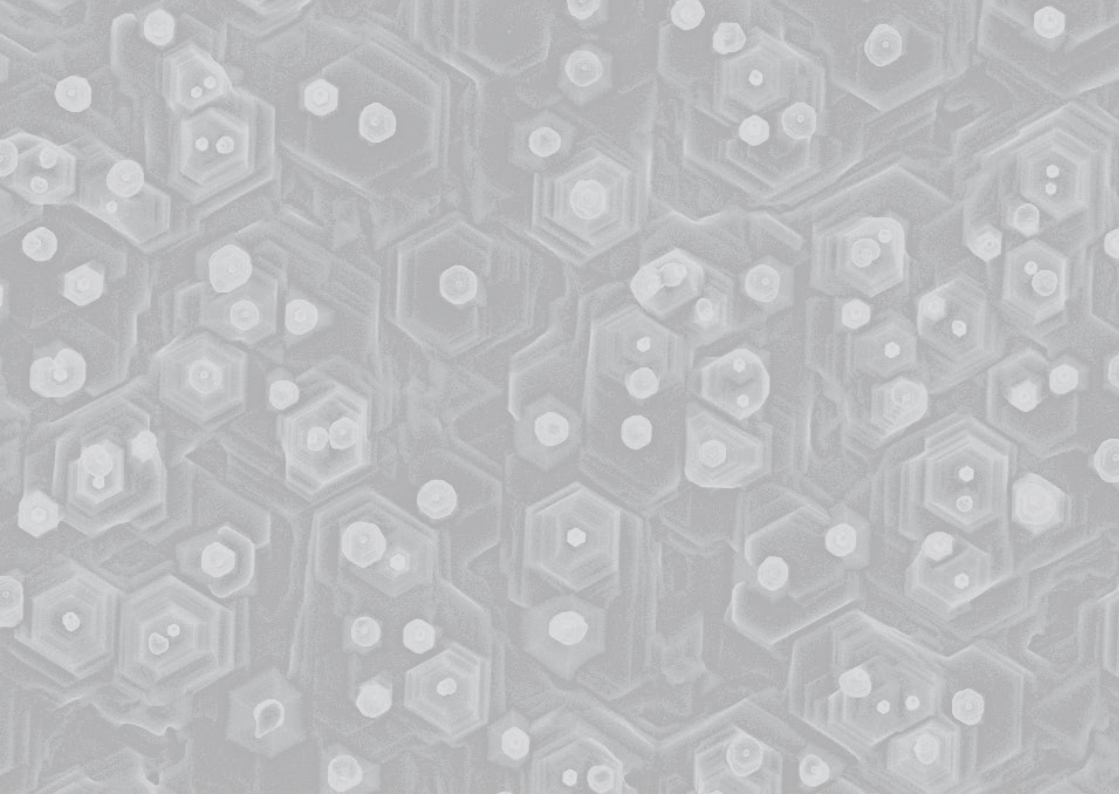

ACTIVITY REPORT 2024

CNRNANO

ISTITUTO NANOSCIENZE CONSIGLIO NAZIONALE DELLE RICERCHE

Cover image
Scanning electron microscope top view image of InSb nanowires.

Table of contents

Institute director
Lucia Sorba

Coordinators of units
Modena: Massimo Rontani
Pisa: Lucia Sorba

Administrative director
Giovanna Diprima

Executive board
Cnr researchers
Stefania Benedetti, Giorgia Brancolini, Marco Cecchini, Stefan Heun, Valentina Tozzini, Filippo Troiani

Cnr technical/administrative staff
Maria Grazia Angelini

Affiliated researchers
Elisa Molinari, Alessandro Tredicucci

Contacts
Piazza San Silvestro, 12
I-56127 Pisa, Italy
ph. +39 050 509418
website: www.nano.cnr.it
e-mail: segreteria.nest@nano.cnr.it

Modena unit
via Campi, 213A
I-41125 Modena, Italy
ph. +39 059 2055629
website: www.nano.cnr.it
e-mail: segreteria.s3@nano.cnr.it

Foreword

This is the seventh biennial report of the Nanoscience Institute of the National Research Council (Cnr Nano).

Following the scheme of the previous editions, we have collected the scientific highlights of the activities carried out during the years 2022-2023 within the research areas of the Institute, such as solid-state quantum technology, fundamental and translational nanobiophysics, nanoscale theory, modelling and computation, physics and technology of light at the nanoscale, and surface and interfaces: nanofabrication, imaging, and spectroscopy. To give a more complete overview of the Cnr Nano outcomes, we included in the report a complete list of running projects, published papers, and events organized in 2022-2023.

A strategic element of this two-year period has been the large participation of Cnr Nano researchers at several Next Generation EU PNRR projects: NQSTI, RESTART, THE, EcosistER, 3A-ITALY, INF-ACT, NEST, MOST, and ICSC. This large involvement of the Cnr Nano researchers has allowed recruiting several fixed-term researchers and has offered the possibility to renew and acquire state-of-the-art scientific equipment and to develop novel collaborations. Another important achievement to highlight is the large number of granted PRIN2020 (20) and PRIN-PNRR (3) projects from Italian Ministry of University and Research (MUR), indicating the large activity of the Cnr Nano researchers in project submission and in fund raising. Moreover, the European Centre of Excellence MaX, coordinated by Cnr Nano, has been granted by EuroHPC JU its third grant, ensuring its activity until 2026.

The large number of publications in high impact Journals, e.g., Nature Portfolio Journals, demonstrates the excellence of the Cnr Nano activities in the international context.

The staff of Cnr Nano enlarged in this span of time, and at present consists of 71 researchers and technologists, 29 postdocs, and 16 administrative and technical personnel. Moreover, with the Generation EU PNRR projects, seven fixed-term researchers have been recruited.

I would like to acknowledge Stefania Benedetti, Claudia M. Cardoso, Luisa Neri, Maddalena Scandola, Antonella Sgarbossa, Fabio Taddei, and Simone Zanotto for their contribution to drafting this report.

Since this report will be my last as director of Cnr Nano, I would like to acknowledge the Institute staff (administration and technical staff, researchers, technologists, and postdocs) and associates for their extensive and excellent work carried out during the 12 years of my direction of the Cnr Nano Institute.

Lucia Sorba
Director of Cnr Nano

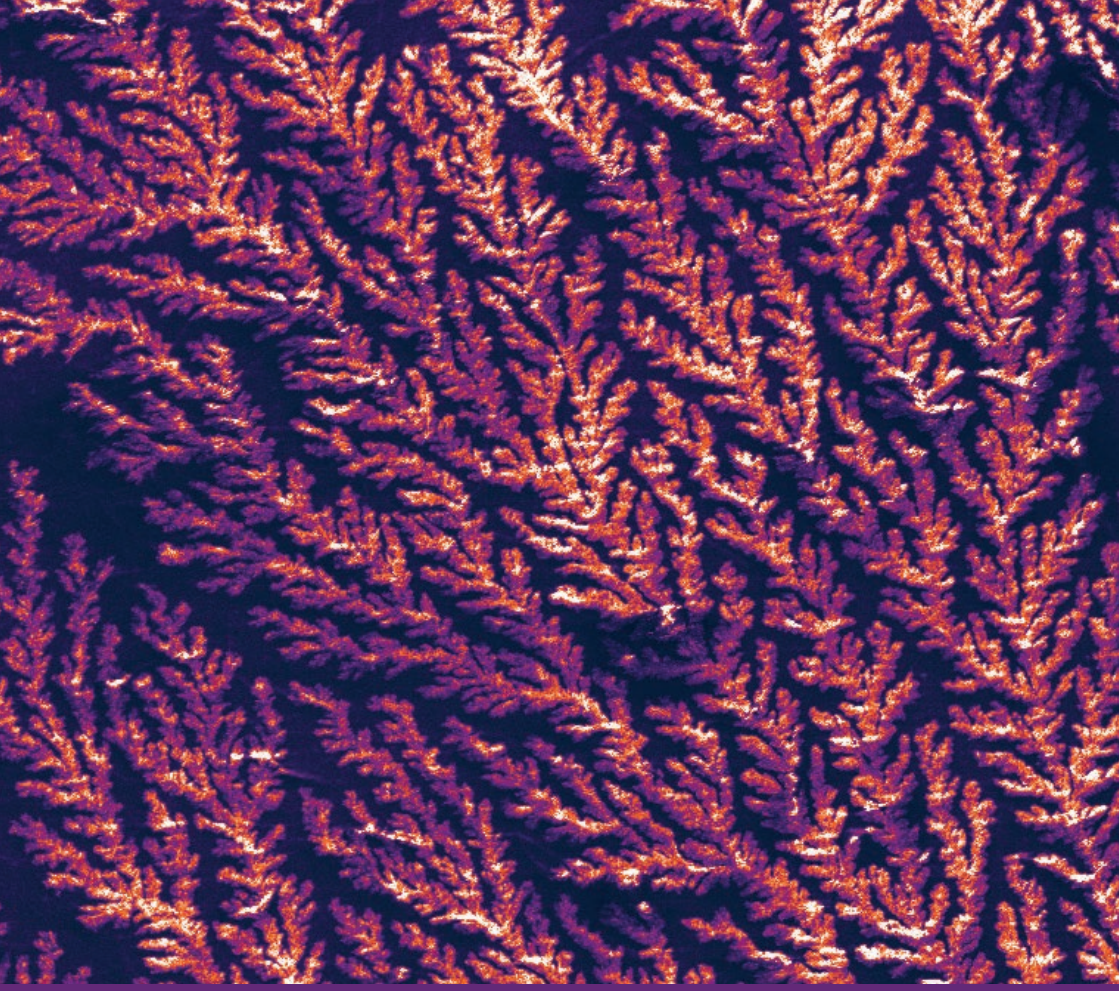

Highlights - Fundamental and translational nanobiophysics

Nanobiophysics research employs a variety of multidisciplinary skills from different disciplines, including biology, biotechnology, physics, chemistry, and nanotechnology. Biological systems and processes can be tackled at a nanoscale resolution by combining theoretical-computational methodologies and experimental techniques. The research activities encompass a variety of topics ranging from nanomaterials and supramolecular recognition for biomedical applications and drug delivery to biosensing devices, neuroscience, and pathological protein aggregation. Here are the recent key highlights of the Institute's research:

Novel nanomaterials for biomedical and sensing applications. Gold nanoparticles (NPs) with functionalized surfaces can be used for a variety of applications in biotechnology and biomedicine, including biosensing and theranostic purposes. Coarse-grained and mesoscale models for NPs that account for electrostatics at various ionic strengths have been created through the combination of bottom-up strategies and knowledge-based information. The use of this methodology enabled a detailed analysis of the electrostatic behaviour at variable ionic strengths of gold NPs functionalized with different biomolecules or functional groups resulting in different global size, shape, and charge.

By combining multiscale computational studies with experiments, the binding mechanism of protein-nanoparticles has been deeply investigated at an atomistic level. The interfacial forces that determine the recognition between nanoscale particle-protein complexes have been identified through computational atomistic studies, while the experiments demonstrated their robustness even when subjected to high ionic strength conditions that completely disrupt normal electrostatic NP-protein interactions. The strategy is suitable to a wide range of applications and has the potential to develop novel nanomaterials that are valuable for biomedical and sensing applications.

Chitosan nanoparticles (CHI-NPs) for intranasal drug delivery have been developed, characterized for the size, the surface charge, and their stability, and finally tested *in vitro* for their biocompatibility. Through a novel synthetic scheme, CHI-NPs with improved cytocompatibility and mucoadhesion potential, good physicochemical features and an optimal safety profile *in vitro* were found to have the potential to be used as a drug carrier for intranasal administration.

Lab-on-a-chip device for biosensing. Even though an effective vaccine is available, the number of deaths for measles virus is still high, especially in developing countries. Therefore, a rapid, handy, and low-cost diagnostic test may help to contain the infection. A surface-acoustic-wave (SAW) device based on a lab-on-a-chip (LOC) - that is smaller than a €1-cent coin and can detect measles in human saliva - has been realized and characterized. This is the first point-of-care biosensing device for measles detection that can be used in conditions where conventional testing is not possible, as in airports, trains, bus stations, war, and emergency zones. The synergic combination of SAW-mixing and SAW-sensing has been shown to be promising for realizing a POC diagnostic platform for measles diagnosis and these findings may serve as a guideline for designing new microfluidics-based biosensing systems.

Neuroscience. A novel mechanism that links brain functions to the time of the day has been proposed. The balance between excitatory and inhibitory neuronal activities is crucial in stabilizing the cortical network. Various brain pathologies are caused by changes in inhibition. Inhibitory currents are highly influenced by the concentration of intracellular chloride ([Cl-]i) at the synaptic site. By means of 2-photon microscopy studies with a novel generation of ratiometric chloride sensor, a two-fold increase in baseline [Cl_{in} has been observed during the night, when the mouse, a nocturnal animal, is active, compared to daytime causing a drastic reduction of the inhibition at night. Its loss has a significant impact on the way the brain processes visual stimuli and can lead to seizure susceptibility.

Pathological protein aggregation. Molecular chaperones, such as small Heat Shock Proteins (sHSPs), are key components of cellular Protein Quality Control system. They can suppress the aggregation of misfolded/unfolded proteins and assist the folding or assembly of other proteins. Among them, HSPB8 is highly expressed in striated and smooth muscles, as well as in motoneurons of the spinal cord. Its mutated form HSPB8-K141E has been linked to motor neuropathies and other muscular and neuronal disorders. By means of optical tweezers, the mechanism of how HSPB8 and its disease-causing mutant HSPB8-K141E affect the aggregation process of the Maltose Binding Protein (MBP) has been elucidated. Unlike other chaperones, HSPB8i interacts with misfolded conformers formed at the early stages of aggregation, preventing them from growing into larger aggregated structures.

Development of coarse-grained models for functionalized gold nanoparticles

A methodological development to perform detailed analysis of the electrostatics of gold nanoparticles (NPs) with different core and different functionalization is reported. The procedure allows building coarse-grained and meso-scale models for the NPs accurately accounting from the electrostatics at different ionic strengths, based on the knowledge of a few parameters extracted from atomistic molecular dynamics simulations, and shows the importance of combining bottom-up strategies with knowledge-based information to build models for NPs with controlled interactions with biomolecules, for sensing, delivery, and imaging applications.

In silico modeling of gold NPs functionalized with different biomolecules or functional groups selectively favouring interactions with proteins or other specific component of the cell milieu can be conveniently addressed with low resolution models with implicit solvent representation. We have explored the structural and electrostatic properties of four gold NPs with different core and different functionalization, resulting in different global size, shape, and charge, thoroughly analyzing data from atomistic molecular dynamics simulations performed at different ionic strength.

Specifically, we developed a method to perform detailed analyses of the electrostatics of gold NPs functionalized with different organic ligands, based on atomistic molecular dynamics simulations performed at increasing ionic strength [1]. The approach can disclose the role of the different features of the NP and of the ionic strength in determining the details of the inter-particle interactions occurring between common core-shell NPs used in wide range of applications in biotechnology and precision nanomedicine. On one side, our findings offer the basis to aid the interpretation of experimental data on the aggregation properties of these NPs [2], on the other side, they lay the foundation to build colloidal-like inter-particle potential to be used in coarse grained simulations, able to account for varying ionic strength (Fig. 1). In addition, the approach can be generalized to develop more refined models where NP's functionalization is represented by means of smaller beads distributed on the NP surface, which can allow a more accurate description of the specific interactions with proteins represented with residue-based coarse-grained models.

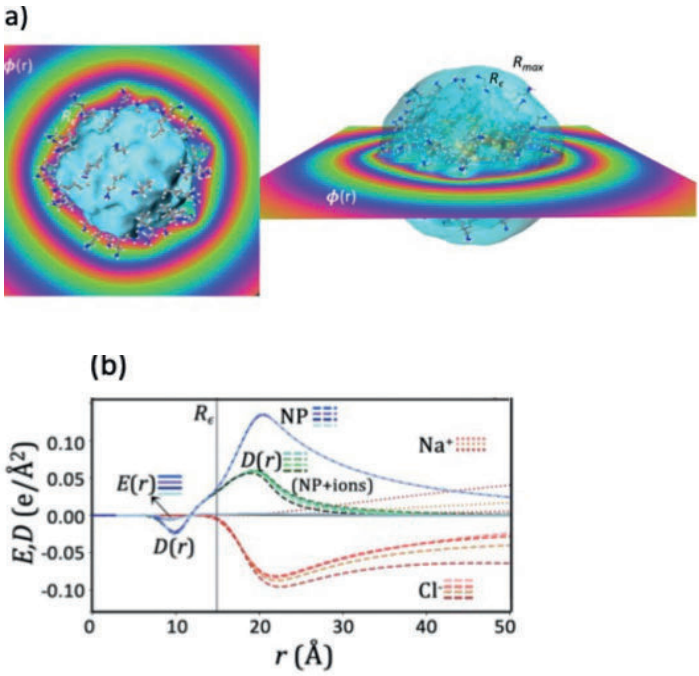

Fig. 1
(a) Contour plots of the total electrostatic potentials of NP-NH3 with cut on different orthogonal planes.
(b) Radial electrostatic fields (Electric E and Electric Displacement D) separated in the NP and ionic components, at different ionic strength.

Contact persons
Giorgia Brancolini (giorgia.brancolini@nano.cnr.it)
Valentina Tozzini (valentina.tozzini@nano.cnr.it)

References
[1] Deconstructing Electrostatics of Functionalized Metal Nanoparticles from Molecular Dynamics Simulations. M. Bini, V. Tozzini, and G. Brancolini. Journal Physical Chemistry B 127, 8226 (2023).
[2] Aggregation behavior of nanoparticles: Revisiting the phase diagram of colloids. M. Bini, G. Brancolini, and V. Tozzini. Frontiers in Molecular Biosciences 9, 986223 (2022).

Surface functionalization with peptides to design biosensors

The report illustrates how modelling and experiments can be brought together to provide key insight into supramolecular binding and complexation between engineered proteins and complementarily charged nanoparticles (NPs). Computational atomistic studies elucidated the interfacial forces responsible for the recognition between nanoscale particle-protein complexes, while experiments assessed their robustness even under conditions of high ionic strength that totally disrupt normal electrostatic NP-protein interactions. The strategy is highly generalizable and has potential for development of novel nanomaterials invaluable to biomedical and sensing applications.

Supramolecular recognition between proteins and NPs is highly significant to the development of sensors and platforms for therapeutics delivery. Most NP-protein binding approaches use 'tags', such as biotin, or His-tags to provide high affinity; protein surface recognition provides a versatile alternative strategy. Generating high-affinity NP-protein interactions is challenging however, due to dielectric screening at physiological ionic strengths. We report the co-engineering of NPs and protein to provide high-affinity binding. In this strategy, 'supercharged' proteins provided enhanced interfacial electrostatic interactions with complementarily charged NPs, generating high affinity complexes. Significantly, the co-engineered protein-nanoparticle assemblies featured high binding affinity even under high ionic strength conditions. By combining multiscale computational studies with experiments, the fundamental forces involved in binding were disclosed. At first, dynamic light scattering characterization were carried out to validate discrete nanoparticle-protein assembly formation. Thus, to further support these data, docking simulations were performed which have elucidated the electrostatic and hydrophobic forces responsible for interfacial recognition between binding partners. Additionally, multiple parallel atomistic simulations were performed at different ionic strengths to disclose the role of the ionic environment on the binding. The computational pipeline allowed to achieve a deep understanding of the protein-nanoparticle binding mechanism at an atomistic level, suggesting a rational approach to modify effectively the experimental protocols of nanoparticles formulations [1,2].

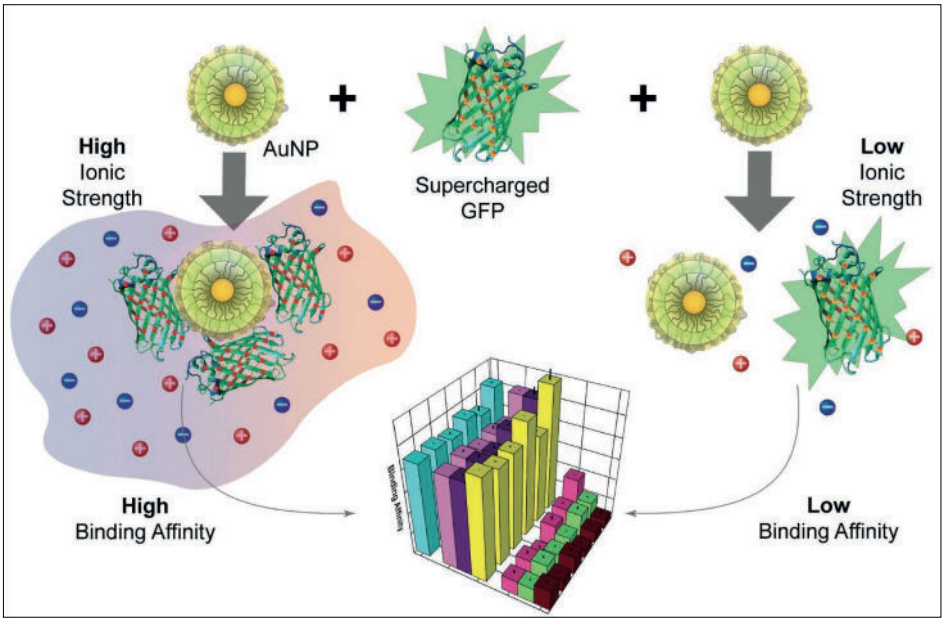

Fig. 1
Supercharged proteins provide a strategy for high-affinity nanoparticle-protein binding at high ionic strength.

Contact persons
Giorgia Brancolini (giorgia.brancolini@nano.cnr.it)
Stefano Corni (stefano.corni@unipd.it)

References
[1] High affinity protein surface binding through co-engineering of nanoparticles and proteins. M. Ray, G. Brancolini, D. C. Luther, Z. Jiang, R. Cao-Milán, A. M. Cuadros, A. Burden, V. Clark, S. Rana, R. Mout, R. F. Landis, S. Corni, and V. M. Rotello. Nanoscale 14, 2411 (2022).
[2] Role of Ionic Strength in the Formation of Stable Supramolecular Nanoparticle–Protein Conjugates for Biosensing. G. Brancolini, V. M. Rotello, and S. Corni. Internal Journal of Molecular Sciences 23, 2368 (2022).

Surface-Acoustic-Wave (SAW) induced mixing enhances the detection of viruses: application to measles sensing in whole human saliva with a SAW Lab-On-a-Chip

Even though an effective vaccine is available, measles is still common in developing countries. This work presents a point-of-care (POC) biosensing device that can detect measles in human saliva. The device is a surface-acoustic-wave (SAW) based lab-on-a-chip (LOC), smaller than a €1-cent coin, in which SAWs are used for sensing and fluid recirculation. The results highlight a crucial aspect of the biosensing process: the interactions between probing and target species during incubation with or without fluid mixing. Our findings are promising for realizing a POC diagnostic platform for measles diagnosis and may serve as a guideline for designing new microfluidics-based biosensing systems.

The measles virus is six and twelve times more infectious than most SARS-CoV-2 variants and influenza, respectively, and is among the most contagious pathogen worldwide. Even though a cheap and effective vaccine is available, measles is still common in developing countries. In 2018 the number of deaths was still 140 000 globally, with sporadic outbreaks even in developed countries.

Diagnosis of the disease is mostly clinical. At this stage, the patient is already highly contagious. Therefore, it is not surprising that, in the last decade, several technologies have been proposed to facilitate and reduce the costs of the diagnosis of measles. A handy solution is the point-of-care (POC) device, often referred to as lab-on-a-chip (LOC).

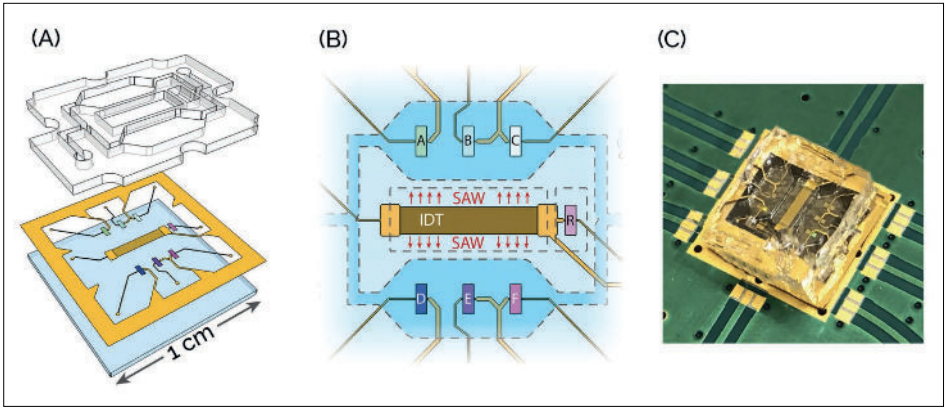

Fig. 1
SAW-LOC scheme and mounting. A) The SAW-LOC comprised a Lithium Niobate substrate, a patterned gold metallization, and a PDMS microfluidic network. B) Six one-port SAW resonators were used as biosensors (three for each microchamber), while one resonator was kept as a reference. The central interdigital transducer (IDT) launched a bi-directional SAW to generate acoustic streaming inside the incubation microchambers. C) Photo of a representative device mounted on a printed circuit board.

POCs require minimal or no sample pre-processing and can be used in difficult conditions for performing conventional tests, such as airports, trains, bus stations, war settings, and emergency zones.

This work presents the first POC biosensor capable of detecting Measles virions (MV) in human saliva. The device is a surface-acoustic-wave (SAW) based LOC smaller than a €1-cent coin. SAW devices are microelectromechanical systems (MEMS) that exploit a piezoelectric substrate to generate surface traveling or standing waves. The synergic combination of SAW-mixing and SAW-sensing is here shown and characterized for the first time, with an application to detect MV in clean buffers and loaded in healthy, whole human saliva. Indeed, SAWs are a unique means for liquid manipulation and analysis. As a result, the LOD in the SAW-mixing case was 209 U/mL, while without SAW-mixing was 741 U/mL. We finally validated the SAW-LOC with whole human saliva with an MV concentration of 2400 U/mL. The presented highlights have demonstrated the high potential of the effect provided by liquid mixing during sample incubation in overcoming restraints related to the surface heterogenicity. The findings here presented are promising for realizing a POC platform for measles diagnosis and might serve as a guideline for designing new microfluidic biosensing systems.

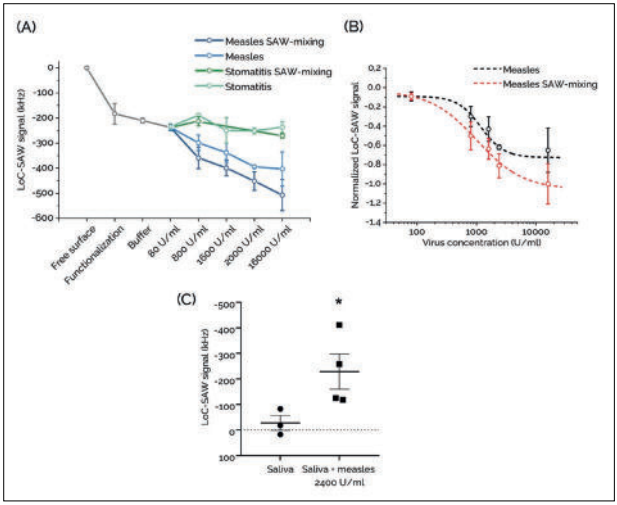

Fig. 2
MV detection in clean buffer and saliva with the SAW-LOC. A) Whole experimental dataset created by measuring the functionalization, buffer injection, MV, and Stomatitis Virions (VSV) with and without SAW-mixing. Blue curves refer to MV (light = no mixing, dark = with mixing), green curves refer to VSV (light = no mixing, dark = with mixing). Grey data is shared among the experiments. B) Calibration curves with increasing concentrations of MV with (red) and without (black) SAW-mixing. C) MV detection in whole human saliva and negative control.

Contact persons
Marco Cecchini (marco.cecchini@nano.cnr.it)

References
[1] Surface-Acoustic-Wave (SAW) Induced Mixing Enhances the Detection of Viruses: Application to Measles Sensing in Whole Human Saliva with a SAW Lab-On-a-Chip. M. Agostini, F. Lunardelli, M. Gagliardi, A. Miranda, L. Lamanna, A. G. Luminare, F. Gambineri, M. Lai, M. Pistello, and M. Cecchini. Advanced Functional Materials 32, 2201958 (2022).

Human small Heat Shock Protein B8 inhibits protein aggregation without affecting the native folding process

Small Heat Shock Proteins (sHSPs) are key components of our Protein Quality Control system. Here, we employ optical tweezers to explore the mechanisms of action of the human small heat shock protein HSPB8 and its pathogenic mutant K141E, which is associated with neuromuscular disease. Through single-molecule manipulation experiments, we studied how HSPB8 and its K141E mutant affect the refolding and aggregation processes of the maltose binding protein. Our data show that HSPB8 selectively suppresses protein aggregation without affecting the native folding process. This anti-aggregation mechanism is distinct from previous models that have been reported for other chaperones.

Molecular chaperones are an evolutionarily conserved family of proteins that form an integral component of Protein Quality Control system, and play a key role in maintaining cellular proteostasis. One major group of molecular chaperones are the Heat Shock Proteins (HSP), which are upregulated under stressful conditions that promote protein denaturation and misfolding, and are known to counter protein aggregation in the cellular environment. HSPB8, also known as

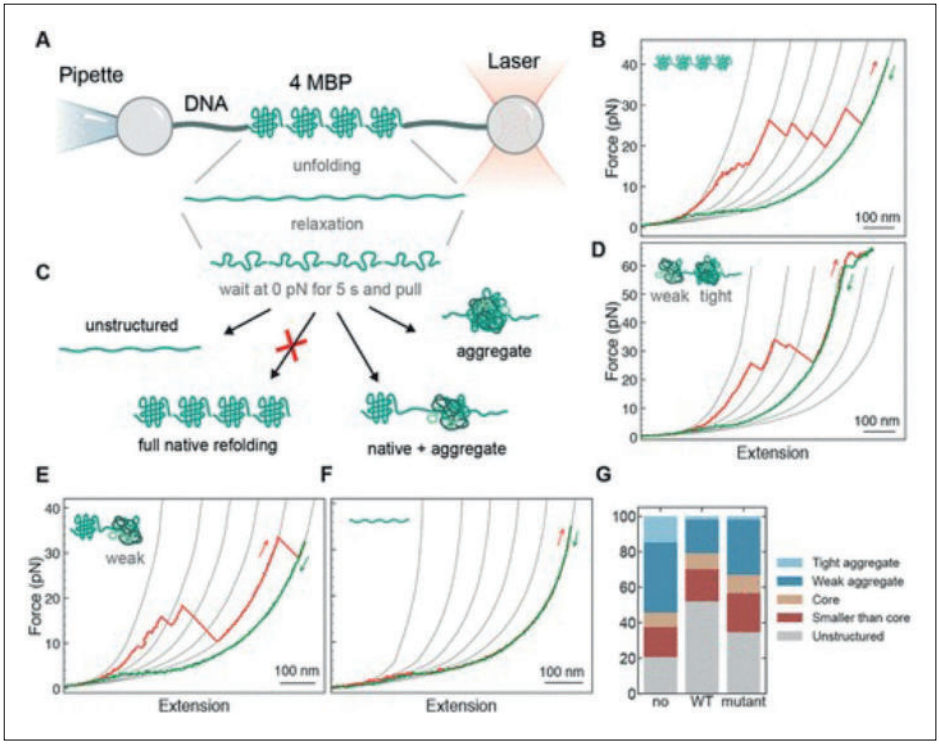

HSP22, is one of the ten members of the human small HSP (HSPB) family and is expressed widely in striated and smooth muscles, as well as in motoneurons in the spinal cord. One missense mutation in the α-crystallin domain of HSPB8, namely HSPB8-K141E, has been linked to motor neuropathies and other muscular and neuronal disorders. How exactly HSPB8 exerts its chaperone-like activity has been yet only in part understood.

In this work, we use optical tweezers to study how HSPB8 and its disease-causing mutant HSPB8-K141E affect the aggregation process of the Maltose Binding Protein (MBP). Our results reveal a peculiar chaperone activity of HSPB8: it suppresses MBP aggregation without affecting its native folding. Unlike other chaperones tested in ensemble averaged and single-molecule experiments, HSPB8 does not limit aggregation by stabilizing unfolded polypeptide chains or near-native states of the substrate protein. Rather, it prevents the growth of misfolded conformations into larger structures, likely by interacting with misfolded conformers formed at the onset of aggregation. This interpretation is further supported by the experimental evidence that the K141E mutation directly affects the anti-aggregation activity, but has no effect on the probability of native folding.

Fig. 1

Mechanical manipulation of 4MBP with and without the presence of chaperones. (A) Four maltose binding proteins arranged in tandem (4MBP) are mechanically manipulated with polystyrene beads by means of DNA molecular handles. (B) When stretched for the first time, 4MBP starts losing its structure when external α helices unzip from each monomer and unfold. These structural changes generate a 4MBP lengthening of 100 nm that gives rise to a gradual discontinuity in the stretching trace at ~10 pN (B). At higher forces (~25 pN), the remaining core structures unfold sequentially giving rise to a sawtooth-like pattern where each rip corresponds to the unfolding of 250–290 aa. (C) After complete denaturation of the 4MBP molecule, the applied force is relaxed and held at 0 pN for 5 s before the molecule is pulled again. During this relaxation period, amino acids from adjacent domains can interact and end up in different molecular states, as depicted in (C). An analysis of the unfolding jumps observed in the second or subsequent stretching traces allowed us to distinguish 5 molecular states: (i) “tight aggregates”, i.e., compact structures that survive at forces larger than 63 pN (D), (ii) “weak aggregates”, related to jumps that involve more than 290 aa ((D) and (E)), (iii) “core-like structures”, related to jumps that involve between 250 and 290 aa (E), (iv) “small structures”, related to jumps that involve less than 250 aa ((D) and (E)), and (v) “unstructured”, all of the amino acids that do not end up into any of the previous categories (F). (G) Percentage of aa that ends up in each of these molecular states in the presence of no chaperone (107 traces; 3 individual molecules), HSPB8 (5 μM) (132 traces; 4 molecules), or HSPB8-K141E (5 μM) (190 traces; 11 molecules).

Contact persons
Ciro Cecconi (ciro.cecconi@unimore.it)

References

[1] Human Small Heat Shock Protein B8 Inhibits Protein Aggregation without Affecting the Native Folding Process. D. Choudhary, L. Mediani, M. J. Avellaneda, S. Bjarnason, S. Alberti, E. E. Boczek, P. O. Heidarsson, A. Mossa, S. Carra, S. J. Tans, and C. Cecconi. J. Am. Chem. Soc. 145, 15188 (2023).

A novel mechanism that links brain functions with the time of the day

Brain processing relies on dynamic electrical potentials within neurons. Excitatory neurons foster positive feedback, while inhibitory neurons provide negative feedback by injecting chloride (Cl) ions in target neurons. Thus, effective inhibition requires low intracellular Cl $[Cl]_{in}$ and, for this reason, it has always been assumed to be stably set at less than 10 mM. By 2-photon microscopy with a novel generation of Cl sensors, we discovered a two-fold increase in baseline $[Cl]_{in}$ in neurons at night, during mouse active phase. This change strongly impacts cortical processing and network stability. These novel findings transform our understanding of Cl dynamics and brain network stability.

Neurons encode information through changes of the electrical potential across their membrane, with a resting potential of approximately -70 mV that becomes more positive upon activation. The brain computation heavily relies on modulating electrical activity during sensory input and signal processing. The cortical network, consisting mostly of excitatory neurons, exhibits recurrent activation that increases membrane potential, creating positive feedback. This positive feedback is balanced by inhibitory neurons, which open chloride-permeable channels, leading to inward chloride currents and a more negative membrane potential, thus countering excitation. Inhibitory function is crucial in stabilizing the cortical network, regulating gain adaptation and brain state transitions. Alterations in inhibition underlie various brain pathologies. In particular, the concentration of intracellular chloride ($[Cl^-]_i$) at the synaptic site crucially influences inhibitory currents. Using the ratiometric chloride sensor, LSSmClophensor, we investigated $[Cl^-]_i$ stability in

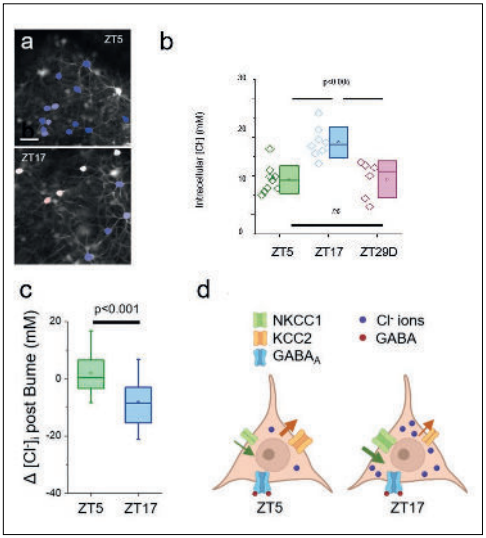

Fig. 1
Change of intracellular Chloride in cortical pyramidal neurons. a) Representative fields of view, showing pyramidal cells expressing LSSmClopHensor, in layers 2/3 of visual cortex, in mice. b) $[Cl]_i$ depends on the time of the day. ZT5 correspond to 12:00, 5 hours after light on. ZT17 to midnight. ZT29D represent Cl concentration in mice imaged at 12:00 after 5 hours of complete darkness. The decrement of Cl does not require light. Each symbol represent a single mouse. c) Change of $[Cl^-]_i$ measured in the same neurons before and after superfusion of the cortex with Bumetanide (a modulator of $[Cl^-]_i$). d) Representative scheme of receptor activation and $[Cl^-]_i$ at different time points.

the neocortex of adult mice via *in vivo* two-photon imaging. We observed that $[Cl^-]_i$ doubled during the night compared to daytime causing a drastic reduction of the inhibition at night when the mouse, a nocturnal animal, is active. This loss of inhibition strongly affects cortical processing of visual stimuli and seizure susceptibility [1]. This discovery prompted the development of a more sensitive ratiometric chloride sensor, characterized by higher affinity for Cl (~4.5 mM at pH 7.2) and a higher pKa (7.8). Compared to LSSmClopHensor, this sensor provides improved accuracy in measuring $[Cl^-]_i$ under physiological intracellular pH conditions. *In vivo* experiments demonstrated its utility in monitoring $[Cl^-]_i$ fluctuations during pharmacologically induced epileptic activity in cortical pyramidal neurons. This sensor is a valuable tool for exploring $[Cl^-]_i$ dynamics across cellular compartments under diverse physiological and pathological conditions, enhancing our understanding of GABAergic inhibition in cortical circuits.

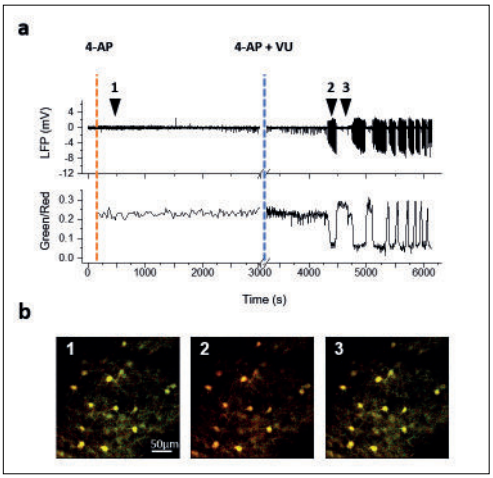

Fig. 2
Dynamic Chloride Measurements with an improved version of LSSmClopHensor. a) Acute *in vivo* LFP recording with 2P microscope (top). Green over red fluorescence ratio (bottom). B) Images taken with 2P microscope at three different time points.

Contact persons
Gian Michele Ratto (gianmichele.ratto@cnr.it)
Melissa Santi (melissa.santi@nano.cnr.it)

References
[1] Daily rhythm in cortical chloride homeostasis underpins functional changes in visual cortex excitability. E. Pracucci, R. T. Graham, L. Alberio, G. Nardi, O. Cozzolino, V. Pillai, G. Pasquini, L. Saieva, D. Walsh, S. Landi, J. Zhang, A. J. Trevelyan, and G. M. Ratto. Nature Communications 14, 7108 (2023).

Projects
DECODE-EE: Developmental and epileptic encephalopathies: epidemiology, comorbidities, molecular diagnosis, personalized management, and costs analysis. Bando Ricerca Salute 2018 -DD15397/2018 Regione Toscana.
DEM-AGING: Neurodegenerative disorders throughout the lifespan. Regione Toscana. Bando Salute 2018.

Crosslinked chitosan nanoparticles with muco-adhesive potential for intranasal delivery applications

Intranasal drug delivery is convenient and provides a high bioavailability but requires the use of mucoadhesive nanocarriers. Chitosan is a well-established polymer for mucoadhesive applications but can suffer from poor cytocompatibility and stability upon administration. In this work, we present a method to obtain stable and cytocompatible crosslinked chitosan nanoparticles (CHI-NPs). NPs were developed, characterized for the size, the surface charge as well as their stability, and finally tested *in vitro* for their biocompatibility. The proposed synthetic system shows an interesting potential as a drug carrier for intranasal delivery.

We developed a novel synthetic scheme to obtain CHI-NPs with improved cytocompatibility and mucoadhesion potential. We used 2,6-pyridinedicarboxylic acid (DA), a biologically derived and non-toxic dicarboxylic acid, as a biocompatible crosslinker (with an EDCl/NHS chemistry): we compared the obtained NPs (CHI-DA-NPs) with those prepared by ionotropic gelation using sodium tripolyphosphate (CHI-TPP-NPs), which were selected as a reference formulation.
The size of CHI-DA-NPs was dependent on the DA concentration (1- 20 mg/mL) used for the synthesis: after preliminary screening, we selected the formulation obtained with 1.25 mg/mL DA concentration. CHI-DA-NPs-1.25 showed optimal characteristics at physicochemical level: a size around 150 nm and a mild surface charge of 10.3 mV ± 0.9 mV, both compatible with the intranasal drug administration. Size and surface

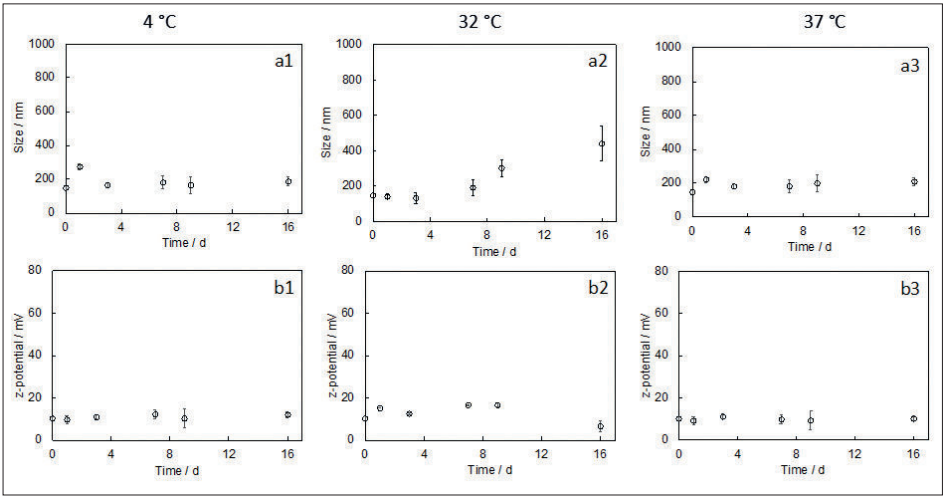

Fig. 1
Evaluation of size (a1-a3) and z-potential (b1-b3) values for CHI-DA-NPs-1.25, measured during stability tests at different temperatures (4 °C, 32 °C, and 37 °C) up to 16 days. Values are reported as mean ± SEM.

charge parameters did not significantly vary over time (Fig. 1), indicating the good stability of CHI-DA-NPs-1.25, due to the covalent crosslinking. The stability of the system at 4 °C ensures that NPs can be safely stored after their preparation. Moreover, the stability at 32 °C and at 37 °C at early times (nasal cavity and body temperature) indicates that the system could control the potential release of the cargo *in vivo*, avoiding drug leakage or massive release for their disaggregation.

We finally tested *in vitro* their cytocompatibility using SHSY5Y human neuroblastoma and RPMI-2650 human nasal epithelial cells, the cell types primarily involved in the nose-to-brain delivery process. CHI-DA-NPs-1.25 slightly reduce both neuronal and nasal cell proliferation only at the higher doses (≥ 2 mg/mL) but with low-to-null effects on cell vitality (Fig. 2). RPMI-2650 cells showed standard spreading and morphological features also exposed to the higher doses of CHI-DA-NPs-1.25.

In conclusion, the proposed synthetic system shows good physicochemical and an optimal safety profile *in vitro*, with an overall interesting potential as a drug carrier for intranasal delivery.

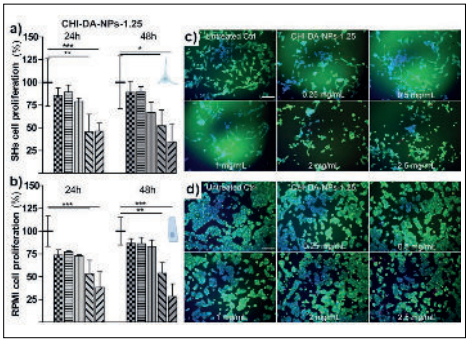

Fig. 2
Biocompatibility tests on neuronal and nasal ephitelial cells. (a,b) The proliferation rate of SH or RPMI-2650 cells treated with CHI-DA-NPs-1.25 at different concentrations (0.25-2.5 mg/mL) for 24 and 48h, reported in % over untreated conditions (Ctrl). Data = mean ± SEM, n ≥ 3; only Ctrl is reported as mean ± SD, to show the intra-assay variability. */*** P<0.05/0.001, Oneway ANOVA, Dunnett's test. (c-d) Vitality test: adherent vital cells are visible in green (calcein-positive), all cell nuclei in blue (Hoechst), and the level of necrotic/dying cells in red (Propidium Iodide-positive). Fluoresence microscopy images of SHs or RPMI-2650 cells (t=24h) untreated and after CHI-DA-NP treatments. Scale bar = 100 µm.

Contact persons
Ilaria Tonazzini (ilaria.tonazzini@nano.cnr.it)
Marco Cecchini (marco.cecchini@nano.cnr.it)

References
[1] Crosslinked chitosan nanoparticles with muco-adhesive potential for intranasal delivery applications. M. Gagliardi, S. Chiarugi, C. De Cesari, G. Di Gregorio, A. Diodati, L. Baroncelli, M. Cecchini, and I. Tonazzini. International Journal of Molecular Sciences 24, 6590 (2023).

Projects
InnovAS. Innovative brain-targeting nano-tools and imaging methods for therapeutic development in Angelman Syndrome. International Angelman Syndrome Alliance (ASA) - call 2021.
END. Isolamento e caratterizzazione molecolare di esosomi neurali in modelli di disturbi del neurosviluppo. Regione Toscana Bando Assegni di ricerca 2021 & Fondazione Pisana per la Scienza.

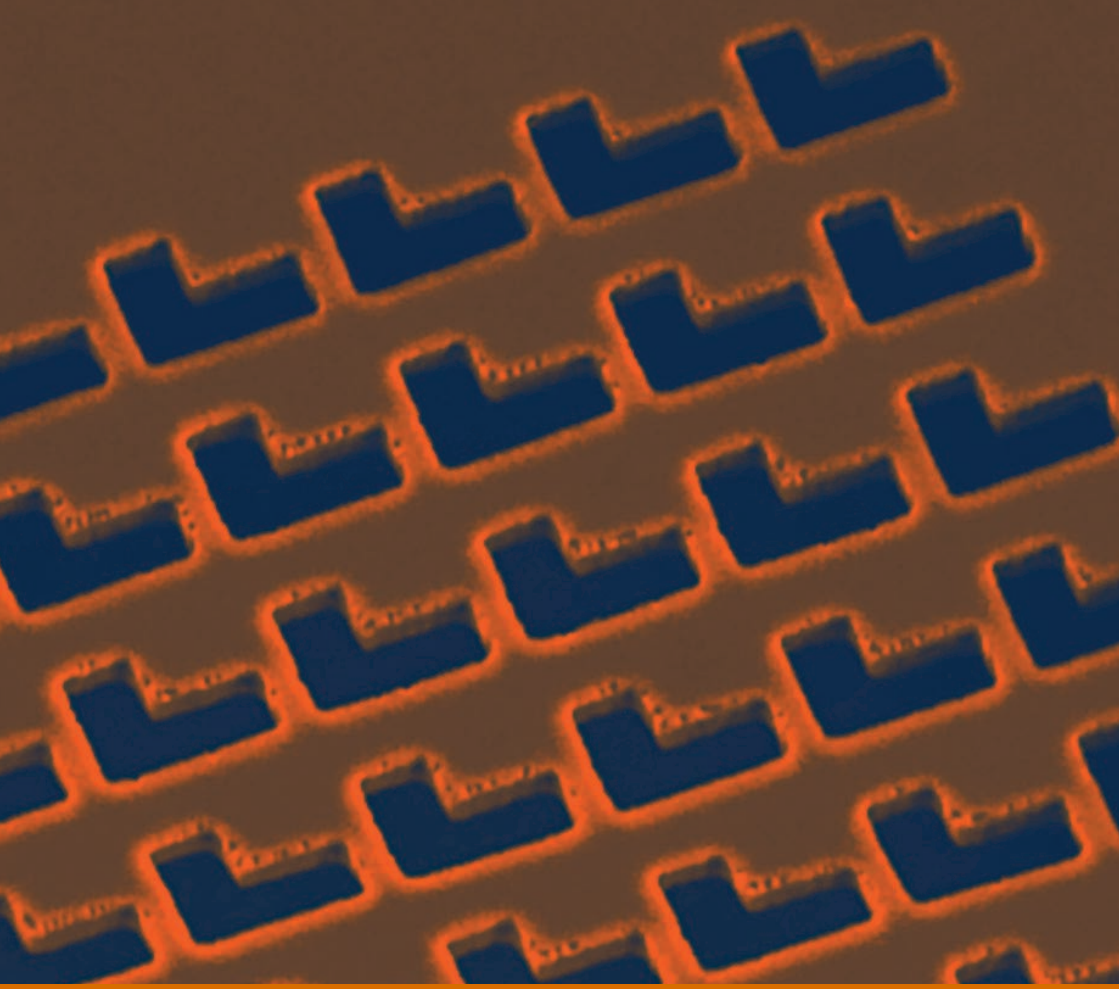

Highlights
-
Physics and technology of light at the nanoscale

It is hard to overestimate the role of light in our lives. Besides visual perception, indeed, mankind has mastered the use of lasers and optical fibers to communicate at global scale, the development of powerful microscopes to diagnose the tiniest elements of life, and the engineering of delicate mechanisms to exploit the quantum nature of photons. Those are just a few among all advanced application of light – or better, of electromagnetic radiation – in an ever-evolving technological environment. Basically, in all the aforementioned frameworks, it is crucial to deploy a precise control of the interaction between light and nanostructured materials. It is indeed when the substances are shaped in forms like few-atom thick layers, nanofibers, or nanohole arrays, that light-matter interactions follow unusual rules, which can be cleverly exploited for powerful applications.

In the following, we report on the most representative activities developed at Cnr Nano on this theme. Such activities cover a broad range of the electromagnetic spectrum – from Terahertz to ultraviolet – leveraging on the properties of polymeric, crystalline, and amorphous materials.

In particular, contributes from Andrea Camposeo and coworkers report on polymeric nanofibres containing light-emitting molecules that enable a lasing action dependent upon humidity and temperature. Moreover, they report on polymeric “magic windows”, that are optical components which project different images depending on the applied strain. This research line opens thus

important perspectives for smarter sensors and for criptographic labels.

The works by Miriam Vitiello and coworkers deal with the generation, manipulation and detection of Terahertz radiation through two-dimensional materials and semiconductor heterostructures. In a first contribute, they demonstrated a laser able to emit short pulses of Terahertz radiation, and a Terahertz frequency comb source – a kind of "ruler" with key applications in metrology and quantum sensing. In a second contribute, they illustrate how a two-dimensional material (bismuth selenide) unconventionally molds the flow of Terahertz radiation. In a third contribute, they outline a fast Terahertz photodetector, of interest for future high-speed telecommunications.

Last but not least, Antonella Battisti and colleagues show that a careful engineering of emitting molecules enables high-performance luminescent solar concentrators, which could play a key role as cheap energy harvester enabling the non-delayable green transition. Simone Zanotto and colleagues study artificially structured materials, known as metamaterials, where light-matter interaction takes unusual forms, with possible applications as radiation detectors or radiation shields. Arrigo Calzolari and coworkers demonstrated, by advanced numerical simulations followed by experimental investigation, that certain amorphous carbides support a plasmonic resonance – of interest for creating light "hotspots" – that is robust to very high temperatures.

Luminescent solar concentrators for sunlight harvesting

Luminescent solar concentrators (LSCs) are colored polymeric materials loaded with high quantum yield luminophores able to absorb natural sunlight and to direct it to the sides of the device where photovoltaic cells convert it to electricity. These devices can be produced on a large scale and integrated in architectural transparent elements for new-generation buildings. Here, a set of flexible LSCs were prepared by covalent immobilization of a red-fluorescent dye on polysiloxane-based polymers. The photochemical properties of these LSCs were investigated to select the best performances in terms of stability and quantum efficiency. A superior power conversion efficiency was achieved if compared with literature data about flexible LSCs.

The recent events linked to climate changes and geopolitical crises clearly showed how the transition to renewable energies is becoming urgent. Among the several renewable sources, solar energy is considered reliable and relatively cheap in terms of maintenance. In this context, luminescent solar concentrators (LSCs) gained increasing attention because of their ability to absorb the solar light and to re-emit a radiation along specific directions according to the waveguide principle, making it

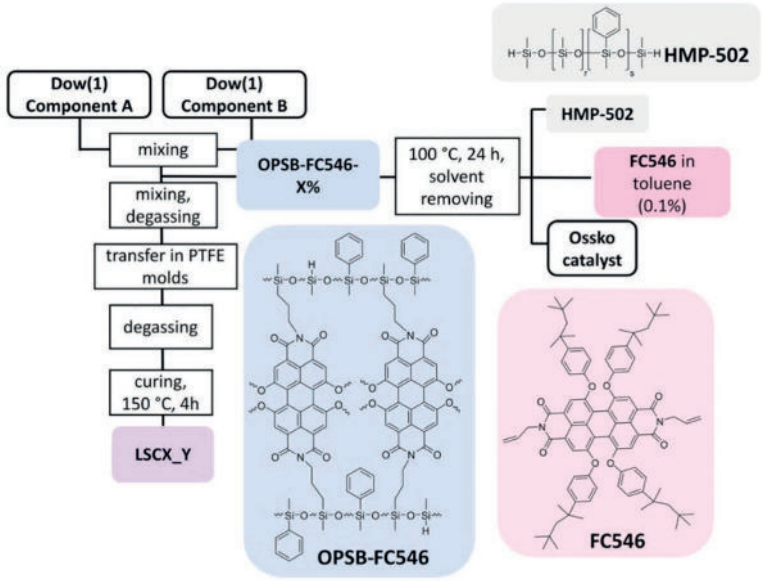

Fig. 1
Scheme of the synthesis of the two LSCs series (LCSX_Y), including the structures of the fluorescent dye (FC546), copolymer (HMP-502) and covalent bonded FC546 in HMP-502 (OPSB-FC546).

possible to collect this radiation with photovoltaic cells placed in strategic points. When the device is designed to be flexible, it can be exploited not only for building-integrated photovoltaics, but also for portable electronics or wearable devices.
In this work, generated from the international collaboration between Saarland University (DE), University of Pisa and Cnr Nano, two series of LSCs were obtained by incorporation of the perylene bisimide dye FC546 (characterized by red fluorescence, high quantum yield, and reactive peripheral allyl moieties) chemically bounded to a phenyl-substituted polysiloxane (HMP-502) in a two-component polysiloxane resin (Dow(1) A+B), containing Si–H and Si–vinyl components (Fig. 1). First, FC546 was covalently linked to the linear polysiloxane HMP-502 via a hydrosilylation reaction to obtain the adduct OPSB-FC546. Then, OPSB-FC546 was added to the pre-mixed components A and B of the Dow(1) curable resin. After processing and curing, two sets of LSC sets were obtained containing different concentration ratios between the resin and HMP-502 or FC546. The optical, structural, and thermal stability properties of the final 5x5 cm transparent and flexible devices were studied, and their photonic performance was characterized in terms of the internal and external photon efficiencies (η_{int} and η_{ext}, Fig. 2). Remarkably, a power conversion efficiency n_{dev} of about 0.5% was obtained for these flexible devices, a value that gets over the recently reported values for other comparable flexible LSC systems.

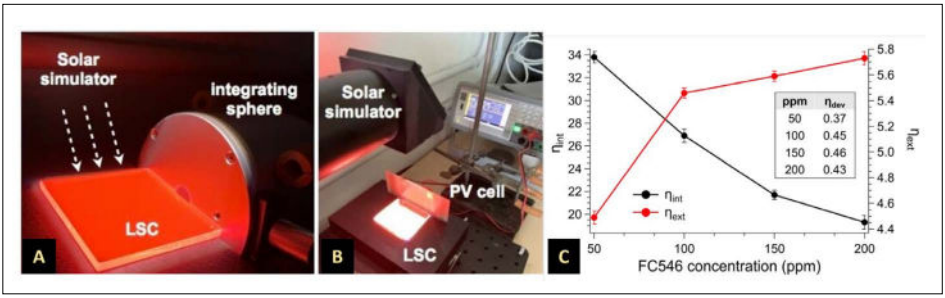

Fig. 2
Experimental setups for the determination of photonic performances (A) ηint, ηext, and (B) ηdev. (C) Photon efficiencies ηint (%, black circles), ηext (%, red circles), and ηdev (inset) as a function of the FC546 fluorophore content (ppm).

Contact persons
Antonella Battisti (antonella.battisti@nano.cnr.it)

References
[1] Performant flexible luminescent solar concentrators of phenylpolysiloxanes crosslinked with perylene bisimide fluorophores. E. Della Latta, F. Sabatini, C. Micheletti, F. Carlotti, F. Martini, F. Nardelli, A. Battisti, I. Degano, M. Geppi, A. Pucci, S. Pohl, and G. Kickelbick. Polymer Chemistry 14, 1602 (2023).

Projects
University of Pisa, grant PRA_2020_21. MIUR-PRIN 20179BJNA2.

Plasmonic high-entropy carbides

By integrating computational thermodynamic modeling and time-dependent density functional theory characterization, we discovered plasmonic high-entropy carbides: a class of disordered materials with extreme thermal, chemical, and mechanical resistance and a plasmonic resonance in the infrared and visible range, exploitable for plasmonics. Their plasmonic response can be largely tuned when changing the transition metal components and the concentration. By monitoring the electronic structures, we suggest rules for optimizing optical properties and designing tailored high- entropy ceramics. Experiments performed on HfTa4C5 yielded plasmonic properties from room temperature to 1500K.

Plasmonic systems have been profitably proposed for a variety of applications that encompass telecommunications, antennas, sensor, and heat engineering. This heterogeneity of applications demands for an extended tunability of the active materials which cannot be restricted to the traditional class of plasmonic noble metals. In particular, the research for materials that are simultaneously plasmonic, compositional tunable, mechanically resistant, chemically and thermally stable still remains a challenge. Here, we proposed transition-metal high-entropy carbides (HECs), which exhibit extraordinary thermal stability, hardness, strength, toughness, as well as wear and oxidation resistance. We demonstrated that some HECs have plasmonic properties in the near-IR/vis range, whose characteristics can be tuned by controlling the chemical composition and the stoichiometry [1].
By integrating computational thermodynamic modeling and TDDFT characterization, we first investigated the optical properties of the archetype HfTa4C5 carbide, which has exceptional thermal and mechanical properties. Simulations predicted a plasmonic resonance in the visible range which remains extremely stable even at ultra-high temperature. Direct measurements confirmed the theoretical results over a wide temperature range T=300-1500K (Fig. 1a), well above the melting point of noble metals. Then, we propose a set of 14 high-entropy carbides that are six element alloys: C and a combination of 5 different transition metals among {Ti, Zr, Hf, V, Nb, Ta, Cr, Mo, and W}. These compounds exhibit a crossover energy E0 in IR- visible range, whose value can be tuned with composition (Fig. 1b). For a few systems this corresponds to the excitation of a low-loss plasmonic resonance, which is expected to remain stable at ultra-high temperature.
The combination of plasmonic activity, high-hardness, and extraordinary thermal stability, makes HECs the first example of multifunctional plasmo-mechanical materials for high-temperature plasmonics.

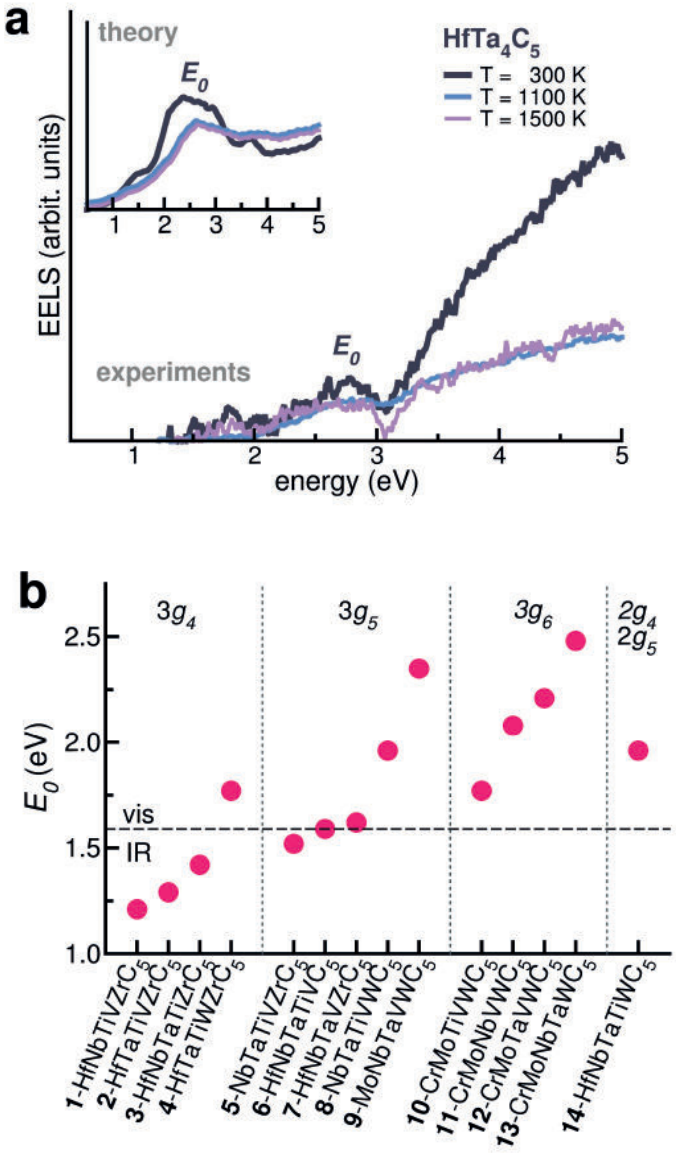

Fig. 1
a) Experimental EELS spectra of HfTa4C5 as a function of temperature. Inset reports the corresponding theoretical spectra, evaluated at the same temperatures.
b) Trend of the crossover energy E0 (i.e., the energy at which the real part of the dielectric function switches sign upon incoming electromagnetic field) in the simulated plasmonic HECs. Properties of simulated HECs, ordered in classes according to the group number g_x (X = 4, 5, 6) of transition metals included in the compound. Images adapted from Ref. [1].

Contact persons
Arrigo Calzolari (arrigo.calzolari@nano.cnr.it)

References
[1] Plasmonic high-entropy carbides. A. Calzolari, C. Oses, C. Toher, M. Esters, X. Campilongo, S. P. Stepanoff, D. E. Wolfe, and S. Curtarolo. Nature Communications 13, 5993 (2022).

Polymer nanofibers and networks with tunable lasing properties

We report on electrospun nanofibers with lasing properties tunable by composition, optical excitation features, and ambient parameters. The increase in the content of the light-emitting dye in polymer nanofibers is effective for decreasing the lasing threshold and varying the laser emission wavelength. Moreover, in planar networks of electrospun nanofibers, the high sensitivity of the lasing modes to external perturbations was exploited to change the lasing spectrum by shaping the spatial profile of the pumping beam. Finally, switchable optical gain was reported in complex arrays of nanofibers made of a thermo-responsive polymer doped with a blue-emitting dye.

Polymer nanofibers have recently gained interest for the realization of complex laser devices [F. Matino et al., Adv. Opt. Mater. 7, 1900192 (2019)]. For some applications such as spectroscopy, imaging, and optical sensing, nanofibers with tunable emission and optical gain are needed. Here, we have investigated various approaches for controlling the spectral and intensity properties of lasers based on arrays of electrospun nanofibers. Typically, nanofibers for lasing applications are made by doping optically transparent polymer with light-emitting dyes. By varying the weight ratio of a blue-emitting dye compared to the polymer matrix, a variation of the wavelength of the optical gain band and of random lasing peaks by about 10 nm was achieved [1]. The emission properties of planar arrays of nanofibers turned out to be highly sensitive to minimal perturbations of the spatial intensity distribution of the pumping beam [2]. This effect was used for controlling and reversibly varying the emission wavelengths of nanofiber networks by tailoring the shape of the pumping beam [2]. Finally, nanofiber with optical gain tunable by environmental parameters (temperature and humidity) were introduced by utilizing a thermo-responsive polymer as matrix, poly(2-*n*-propyl-2-oxazoline) (P*n*PrOx), and a blue-emitting dye (S420) for light emission (Fig. 1a). An example of the nanofiber samples realized by electrospinning is shown in Fig. 1b-d. Upon optical pumping the samples featured a line narrowing process with well-defined excitation threshold due to light amplification (Fig. 1e). In these samples, the excitation threshold for light amplification was found to be dependent on temperature and humidity (Fig. 1f). These findings were attributed to changes in the morphology of the nanofibers as a consequence of the moisture sorption/desorption occurring by varying temperature and humidity [3]. Overall, the tunable and responsive light-emitting nanofibers here developed may find application as novel complex laser devices for imaging, spectroscopy, and smart sensors, and for light-emitting devices with dynamically-controlled properties.

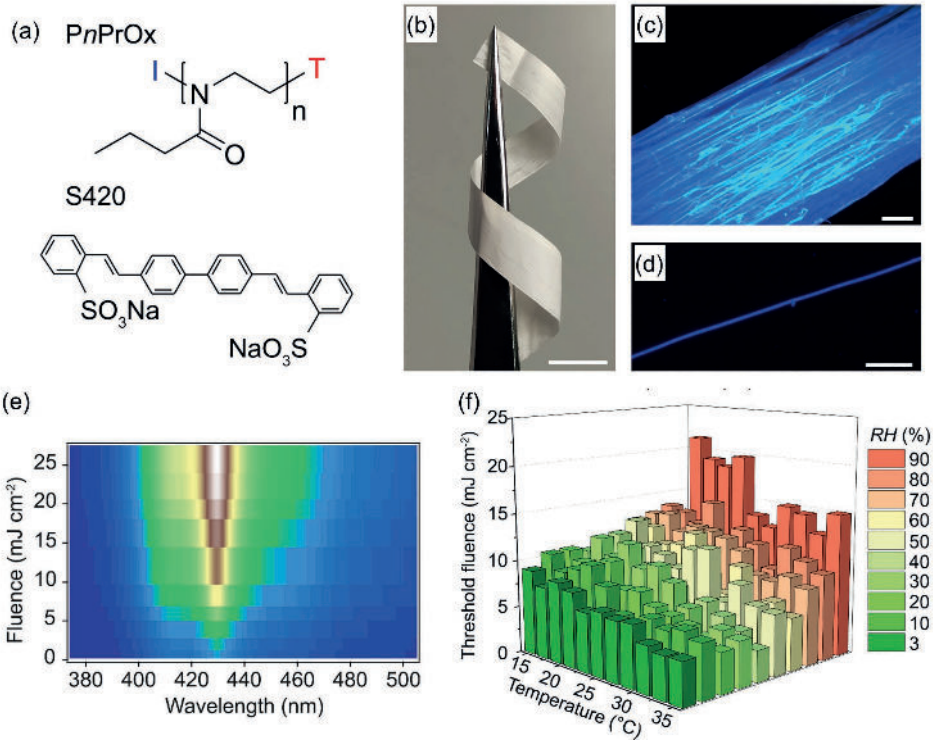

Fig. 1
(a) Chemical structures of P*n*PrOx and S420. (b) Photograph of a sample of aligned electrospun NFs. Scale bar: 1 cm. Fluorescence images of (c) the sample and (d) an isolated nanofiber. Scale bars: 1 mm (c), 10 µm (d). (e) Dependence of the emission spectra on the excitation fluence. (f) Dependence of the excitation threshold on temperature and relative humidity (RH). Reproduced under the terms of the Creative Commons Attribution License from [3]. © 2023 The Authors. Published by Wiley-VCH GmbH.

Contact persons
Andrea Camposeo (andrea.camposeo@nano.cnr.it)
Francesca Matino (francesca.matino@nano.cnr.it)

References
[1] Tuneable optical gain and broadband lasing driven in electrospun polymer fibers by high dye concentration. L. Morello, M. Moffa, M. Montinaro, A. Albanese, K. Kazlauskas, S. Jursenas, A. Tomkeviciene, J. V. Grazulevicius, A. Camposeo, and D. Pisignano. Journal of Materials Chemistry C 10, 2042 (2022).
[2] Sensitivity and spectral control of network lasers. D. Saxena, A. Arnaudon, O. Cipollato, M. Gaio, A. Quentel, S. Yaliraki, D. Pisignano, A. Camposeo, M. Barahona, and R. Sapienza. Nature Communications 13, 6493 (2022).
[3] Optical Gain Switching by Thermo-Responsive Light-Emitting Nanofibers through Moisture Sorption Swelling. M. Archimi, E. Schoolaert, J. Becelaere, R. Hoogenboom, A. Camposeo, K. De Clerck, and D. Pisignano. Advanced Optical Materials 11, 2202056 (2023).

3D printing of optical components with tailorable optical properties

We report on optical elements made by additive manufacturing. An experimental method to monitor in-situ and in real time the vat-photopolymerization processes was developed by exploiting the light diffused by the UV-polymerized volume. Novel optical components with 3D surface reliefs that generate complex light patterns tailorable by uniaxial strain were realized. Cryptographic optical components were designed and realized by combing 3D printing and replica molding. Optical devices capable of generating light patterns, including micro-QR-codes, were realized. These may be correctly projected and recognized upon either combination of two printed components or controlled uniaxial strain, while remain cryptic for as-produced devices.

Additive manufacturing (AM) and 3D printing technologies have emerged as a powerful fabrication platform for objects with complex geometrical features, typically not accessible to conventional manufacturing processes. The opportunities opened by AM technologies are also changing the way optical components and devices are designed and realized [A. Camposeo et al., Adv. Opt. Mater. 7, 1800419 (2019)]. To meet the requirements of optical systems in terms of uniformity of the printed devices and properties of the embedded materials, suitable process monitoring systems are needed. We have implemented a real-time and in-situ monitoring of vat photopolymerization processes based on the measurement of the intensity of light backscattered by the UV-cured volumes [1]. This method allows for effectively monitoring photopolymerization processes and for unveiling the dependence of the curing time on the size of the volume of the photopolymerized material [1]. Moreover, the possibility of realizing optical components with complex 3D surface textures by AM processes was used for making novel freeform optical components, known as magic windows (MW), capable of generating complex light intensity patterns [2]. These optical systems are schematized in Fig. 1a: light rays from a visible light source are refracted by the MW, whose surface profile is designed to generate the target pattern on a screen placed at pre-defined distance. Examples are shown in Fig. 1b-d, showing various intensity patterns projected by MW realized by 3D printing. MW were also utilized as cryptographic components as shown in Fig. 1e-j. In particular, two MWs were coupled together so that the encrypted light pattern (here a micro-QR code) can be read only if the two MWs are placed in series. It remains undecipherable if only one of them is used. Other encryption mechanisms were demonstrated, by using deformable MW made by 3D printing and replica molding [2]. These results are relevant for application in smart labels, illumination design, and anti-counterfeiting systems.

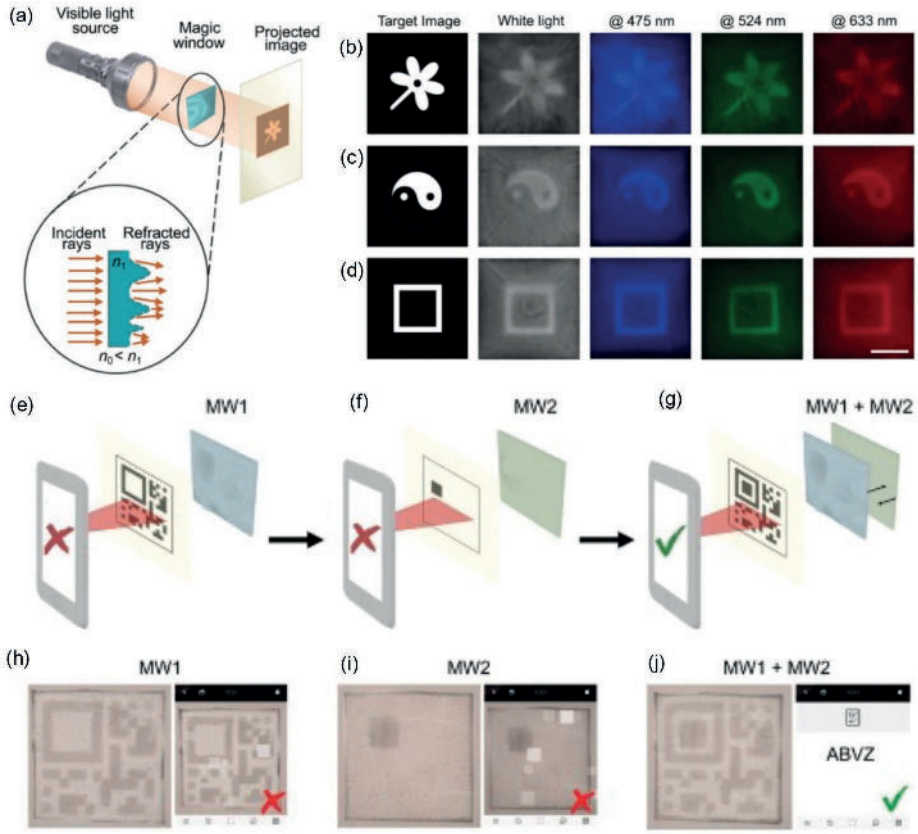

Fig. 1
(a) Scheme of the MW working principle. (b)-(d) Cast images with different visible light sources: target images (left side), and photographs of the images cast by the MWs when illuminated with different light sources. (e)-(g) Schematic illustration of the operation of two coupled cryptographic MWs (MW1 and MW2). Photographs (left side of each panel) of the patterns projected by the cryptographic (h) MW1, (i) MW2, and (j) the combination of the two. On the right side of (h)–(j) the screenshot of the QR scanner is shown. Reproduced under the terms of the Creative Commons Attribution License from [2]. © 2021 The Authors. Published by Wiley-VCH GmbH.

Contact persons
Andrea Camposeo (andrea.camposeo@nano.cnr.it)
Luana Persano (luana.persano@nano.cnr.it)

References
[1] Impact of size effects on photopolymerization and its optical monitoring in-situ. A. Camposeo, A. Arkadii, L. Romano, F. D'Elia, F. Fabbri, E. Zussman, and D. Pisignano. Additive Manufacturing 58, 103020 (2022).
[2] Cryptographic Strain-Dependent Light Pattern Generators. F. D'Elia, F. Pisani, A. Tredicucci, D. Pisignano, and A. Camposeo. Advanced Materials Technologies 7, 2101129 (2022).

Fast and scalable terahertz photodetectors based on graphene and related heterostructures

We devise fast and sensitive room-temperature receivers based on large area single layer graphene (SLG), embedded in different layered material heterostructures. We provide the first demonstration of an integrated THz photonic device comprising a multi-layer graphene thermometer patterned over the bottom part of a quantum cascade laser waveguide, transportable THz free-space optical communications system, comprising the QCL and the SLG receiver, providing 1 Mbaud error-free data transmission.

The unique optoelectronic properties of single layer graphene (SLG) are ideal for the development of photonic devices across a broad range of frequencies, from X-rays to microwaves. In the terahertz (THz) frequency range (0.1-10 THz frequency) this has led to the development of optical modulators, non-linear sources, and photodetectors, with state-of-the-art performances. A key challenge is the integration of SLG-based active elements with pre-existing technological platforms in a scalable way, while maintaining performance level unperturbed.
Recently, we reported on the development of fast (< ns response times) room temperature THz detection in large-area SLG. These were grown by chemical vapor deposition (CVD) and integrated in antenna-coupled field effect transistors. We then studied different dielectric environments for SLG to investigate their effect on SLG thermoelectric properties underpinning photodetection. Specifically, we employed different dielectric configurations of SLG on Al_2O_3 with and without large-area CVD hexagonal boron nitride capping. With these scalable architectures, response times ~5 ns and noise equivalent powers (NEPs) ~1 nW $Hz^{-1/2}$ are achieved under zero-bias operation [1]. We also reported the first scalable photodetectors comprising large area graphene embedded between two layers of large area hBN.
Furthermore, we conceive and devise an integrated photonic system comprising a SLG micro-thermometer, lithographically patterned on the bottom contact of a single-plasmon-waveguide THz quantum cascade laser (Fig. 1) [2]. We aim to monitor, in real-time, its local lattice temperature during operation, with mayor implications for the optimization of the device thermal management.
Finally, we devise a cryogen-free, transportable, THz free-space optical communications system, relying on a directly-modulated 2.83 THz QCL transmitter, hosted in a closed-cycle Stirling cryocooler, and a room-temperature SLG receiver, implementing a binary on-off keying (OOK) modulation scheme with Manchester encoding, enabling 1 Mbaud error-free data transmission (Fig. 1a, b). Our approach, reduced in complexity and costs with respect to state-of-the-art THz systems, paves the way for the deployment of optical wireless communication (OWC) links exploiting the 1-5 THz frequency range.

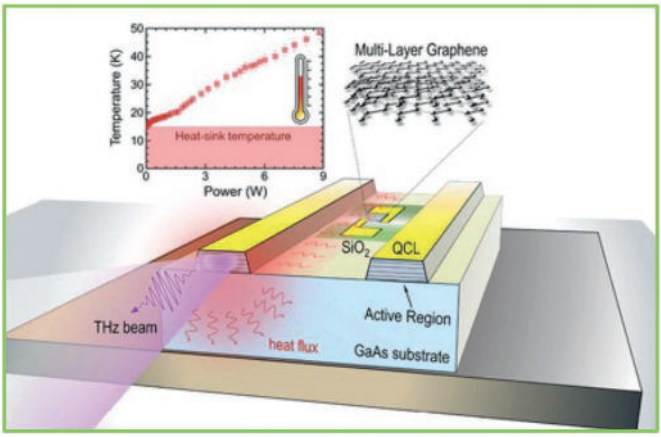

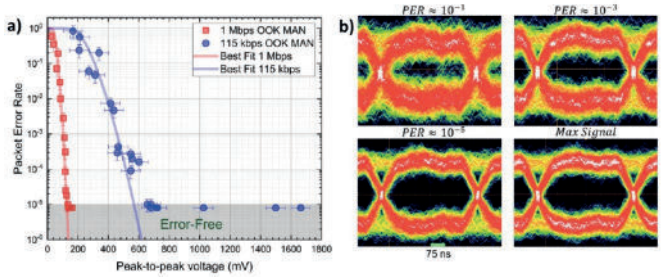

Fig. 1
a) multi-layer-graphene thermometer, integrated on-chip with a terahertz quantum cascade laser, allows to measure the laser lattice temperature during operation. a) Packet error rate measured with the devised optical communication system vs peak-to-peak amplitude for 1 Mbps and 115 kbps OOK Manchester (MAN). b) Eye Diagrams at 1 Mbps for different Packet Error Rates (PERs).

Contact persons
Leonardo Viti (leonardo.viti@nano.cnr.it)
Miriam Serena Vitiello (miriam.vitiello@nano.cnr.it)

References
[1] Terahertz photodetection in scalable single-layer-graphene and hexagonal boron nitride heterostructures. M. Asgari, L. Viti, O. Balci, S. M. Shinde, J. Zhang, H. Ramezani, S. Sharma, A. Meersha, G. Menichetti, C. McAleese, B. Conran, X. Wang, A. Tomadin, A. C. Ferrari, and M. S. Vitiello. Applied Physical Letters 3, 031103 (2022).
[2] Real-Time Measure of the Lattice Temperature of a Semiconductor Heterostructure Laser via an On-Chip Integrated Graphene Thermometer. L. Viti, E. Riccardi, H. E. Beere, D. A. Ritchie, and M. S. Vitiello. ACS nano 17, 6103 (2023).

Projects
EU ERC-2015-CoG SPRINT (GA 681379). Graphene Flagship core 3. PNRR Next Generation EU partnership on “Telecommunications of the Future” (PE00000001 - program “RESTART”, Structural Project DREAMS).

Passively mode-locked THz micro-lasers and metrological quantum sources and components

By integrating graphene or graphene saturable absorbers with semiconductor heterostructure lasers, in different architectures/configurations we demonstrate: i) a self-starting miniaturized ultra-short pulse THz laser, emitting 4.0-ps-long pulses across the 2.3-3.6 THz range in a compact, all-electronic, all-passive, and inexpensive configuration; ii) mode-locking in surface-emitting electrically-pumped random THz quantum cascade lasers (QCLs), providing an important milestone in the physics of disordered systems; iii) frequency modulated THz frequency combs, showing a proliferation of emitted modes over the entire gain bandwidth and across more than 60% of its operational range, with ~ 0.18 mW/mode optical power.

In solid-state electrically pumped lasers, the primary route to generate short pulses is through passive mode-locking; however, this has not yet been achieved in the terahertz (THz) frequency range, defining one of the longest standing goals over the past two decades. In fact, the realization of passive mode-locking has long been assumed to be inherently hindered by the fast recovery times associated with the intersubband gain of the terahertz semiconductor heterostructure quantum cascade lasers (QCLs). We recently demonstrated a self-starting miniaturized short pulse terahertz laser, exploiting an original device architecture that includes the surface patterning of multilayer-graphene saturable absorbers distributed along the entire cavity of a double-metal semiconductor 2.30–3.55 THz wire laser. Self-starting pulsed emission with 4.0-ps-long pulses is demonstrated in a compact, all-electronic, all-passive, and inexpensive configuration. Furthermore, we also prove mode-locking in surface-emitting electrically pumped THz random quantum cascade lasers. This is achieved by either lithographically patterning a multilayer graphene film to define a surface random pattern of light scatterers, or by coupling on chip a saturable absorber graphene reflector, acting simultaneously as saturable absorber, amplitude modulator and frequency tuner.
Finally, we devise metrological-grade THz frequency combs (FCs) operating over the entire available gain bandwidth of a QCL. The intracavity light intensity of a multistack QCL, inherently showing a giant Kerr nonlinearity, is altered by increasing the mirror losses of its Fabry-Perot cavity through coating the back facet with an epitaxially-grown multilayer graphene film. This enables a frequency modulated THz FC showing a proliferation of emitted modes over the entire gain bandwidth and across more than 60% of its operational range, with a record ≈0.18 mW per mode optical power and an exceptional phase coherence.

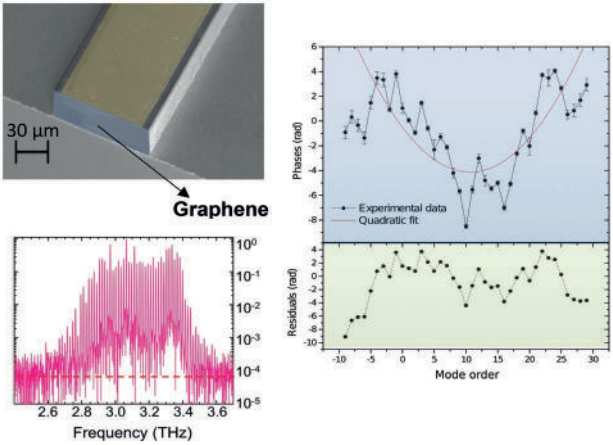

Fig. 1
Top: SEM image of a graphene-coated QCL frequency comb with measured emission spectrum (pink), phase of the individual modes and related residuals. Bottom: Passively mode-locked, short pulse THz laser. Center. Mode-locked surface-emitting random THz laser.

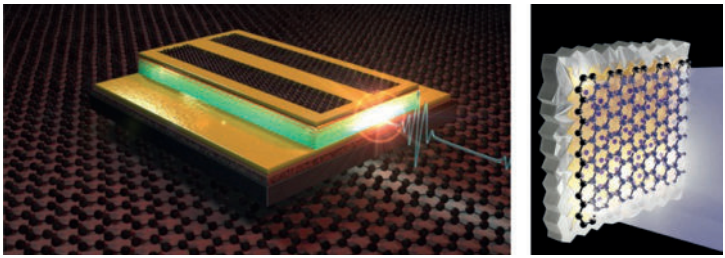

Contact persons
Miriam Serena Vitiello (miriam.vitiello@nano.cnr.it)
Alessandra Di Gaspare (alessandra.digaspare@nano.cnr.it)

References
[1] Short pulse generation from a graphene-coupled passively mode-locked terahertz laser. E. Riccardi, V. Pistore, S. Kang, L. Seitner, A. De Vetter, C. Jirauschek, J. Mangeney, L. Li, A.G. Davies, E. H. Linfield, A. C. Ferrari, S. S. Dhillon, and M. S. Vitiello. Nature Photonics 17, 607 (2023).
[2] Self-Induced Mode-Locking in Electrically Pumped Far-Infrared Random Lasers. A. Di Gaspare, V. Pistore, E. Riccardi, E. A. A. Pogna, H. E. Beere, D. A. Ritchie, L. Li, A. Giles Davies, E. H. Linfield, A. C. Ferrari, and M. S. Vitiello. Advanced Science 10, 2206824 (2023).
[3] Terahertz Sources Based on Metrological-Grade Frequency Combs. E. Riccardi, V. Pistore, L. Consolino, A. Sorgi, F. Cappelli, R. Eramo, P. De Natale, L. Li, A. Giles Davies, E. H. Linfield, and M. S. Vitiello. Laser & Photonics Reviews 17, 2200412 (2023).
[4] Terahertz quantum cascade lasers as enabling quantum technology. M. S. Vitiello and P. De Natale. Advanced Quantum Technologies 5, 2100082 (2022).
[5] All in One-Chip, Electrolyte-Gated Graphene Amplitude Modulator, Saturable Absorber Mirror and Metrological Frequency-Tuner in the 2–5 THz Range. A. Di Gaspare, E. A. A. Pogna, E. Riccardi, S. M. A. Sarfraz, G. Scamarcio, and M. S. Vitiello. Advanced Optical Materials 10, 2200819 (2022).

Projects
EU ERC-2015-CoG SPRINT (GA 681379). HORIZON-CL4-2021-DIGITAL-EMERGING-01 Muquabis (GA 101070546). QuantERA II project QATACOMB (GA 491801597).

Phase-sensitive, hyperspectral, terahertz near-field nanoscopy

We devise the first self-mixing intermode-beatnote spectroscopy system, based on THz quantum cascade laser frequency combs, in which light is back-scattered from the tip of a scanning near-field optical-microscope (SNOM) and the intracavity reinjection is simultaneously monitored. We then collect near-field images of topological insulator (TI) thin films grown by molecular beam epitaxy (MBE), or TI flakes of Bi_2Se_3 and Bi_2Te_3. By applying synthetic optical holography, we provide spectroscopic characterization on a >1 THz optical bandwidth and extract information on the material optical contrast and on the excitation of collective excitations launched by the s-SNOM tip on the investigated two-dimensional materials. The proposed technique is versatile and enables phase-sensitive imaging with sub-wavelength spatial resolution, opening the possibility for hyperspectral near-field optical microscopy of classical and quantum nano-systems.

We demonstrate a hyperspectral terahertz near-field optical microscope comprising a miniaturized quantum cascade laser frequency comb, acting simultaneously as a source and as a detector. This scattering type near-field optical microscope (s-SNOM) imaging system provides 160nm spatial resolution, coherent detection of multiple phase-locked modes and allows mapping the THz optical response of nanoscale materials in the 2.29-3.60 THz range with noise-equivalent-power ~400 pW/$\sqrt{\text{Hz}}$, relying on a 6 mW comb-emitting THz QCL [1].
The technique has been then employed for a set of applications, also experimentally compare the performances of different s-SNOM tips, such as traditional conical tips, or tips with unconventional shapes, such as elephant-trunk and pyramidal probes.
We investigate thin (14–19 nm) films of Bi_2Se_3 (Fig. 1), a well-known topological insulator (TI), experimentally, through a combination of X-ray diffraction, Hall-bar magneto-transport, and near-field synthetic optical holography at THz frequencies, from 2 to 4.3 THz [2]. We determine the dispersion of surface plasmon polaritons for different Bi_2Se_3 film thicknesses, proving the presence of massless surface carriers. Our results open intriguing opportunities in THz nano-plasmonics and topological nano-photonics exploiting plasmon polaritons, including the development of superlenses and metasurfaces.

We also trace the propagation of Dirac plasmon polaritons (DPPs) at terahertz (THz) frequencies, where the DPP wavelength becomes over one order of magnitude shorter than the free space photon wavelength, in TI-based devices [3]. Bi_2Se_3 rectangular antennas (Fig. 1a, b) can efficiently confine the propagation of DPPs to a single dimension and, as a result, enhance the DPPs visibility despite the strong intrinsic attenuation. We experimentally determine the plasmon dispersion (Fig. 1c) and loss properties from plasmon phase profiles acquired along the antennas, using holographic near-field nanoimaging in a wide range of THz frequencies, from 2.05 THz to 4.3 THz. The reported detailed investigation of the optical and electronic properties of these structures can guide the design of novel topological quantum devices exploiting the directional propagation of the unveiled DPPs.

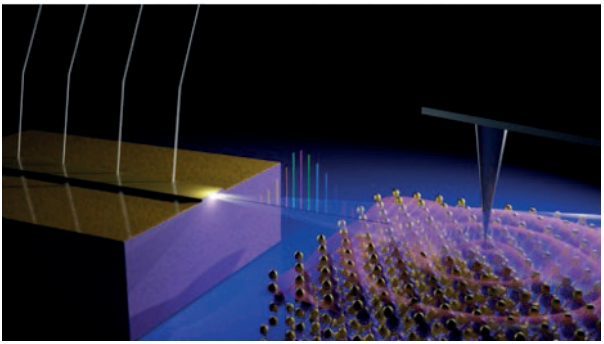

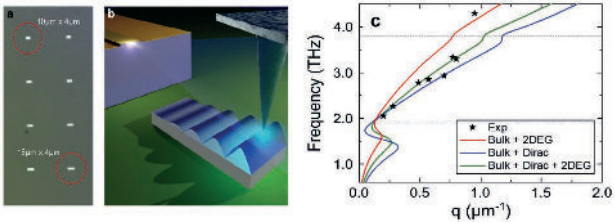

Fig. 1
Top. Graphic representation the frequency comb based hyperspectral s-SNOM. Right. a) Optical image of the Bi2Se3 antennas fabricated on a sapphire substrate. b) Artistic representation of the THz Dirac plasmon polaritons (DPPs), in blue, launched by the AFM probe of the s-SNOM system illuminated by a THz QCL. c) Dispersion of surface plasmon polaritons in Bi2Se3 as obtained by fitting of phase profiles along antennas (symbols). Colored solid lines show dispersion calculations based on the analytical conductivity model and including the contributions of bulk carriers, Dirac carriers and massive surface carriers (2DEG). The optical phonon contribution to the conductivity is included for each model.

Contact persons
Miriam Serena Vitiello (miriam.vitiello@nano.cnr.it)
Leonardo Viti (leonardo.viti@nano.cnr.it)

References
[1] Self-Induced Phase Locking of Terahertz Frequency Combs in a Phase-Sensitive Hyperspectral Near-Field Nanoscope. V. Pistore, L. Viti, C. Schiattarella, Z. Wang, S. Law, O. Mitrofanov, and M. S. Vitiello. Small 2308116 (2023).
[2] Terahertz plasmon polaritons in large area Bi2Se3 topological insulators. V. Pistore, L. Viti, C. Schiattarella, E. Riccardi, C. S. Knox, A. Yagmur, J. J. Burton, S. Sasaki, A. G. Davies, E. H. Linfield, J. R. Freeman, and M. S. Vitiello. Advanced Optical Materials 2301673 (2023).
[3] Holographic nano imaging of terahertz Dirac plasmon polaritons in topological insulator antenna resonators. V. Pistore, L. Viti, C. Schiattarella, Z. Wang, S. Law, O. Mitrofanov, and M. S. Vitiello. Small 2308116 (2023)

Projects
EU ERC-2015-CoG SPRINT (GA 681379). ERC-2022-POC2 STAR (GA 101081567). Balzan Research Project.

Optomechanics of symmetry-engineered metamaterials

Thin membranes made of semiconductors or dielectrics have in the last decades emerged as a key technological platform in the framework of microelectromechanical systems (MEMS). Importantly, such systems can be endowed with further functional features by exploiting appropriate submicrometer patterning, i.e., metamaterials and metasurfaces. Moreover, the efficient coupling between vibrational and electromagnetic degrees of freedom allows for new device concepts such as mechanical bolometric detection of far-infrared radiation, that could in the future benefit from extreme wave-matter interaction such as synthetic symmetry engineering and asymmetric negative refraction.

The last decades have witnessed the integration of mechanical microdevices into electronic platforms – MEMS – with enormous technological breakthroughs such as the advent of compact accelerometers, a key component of today's smartphones. Meanwhile, photonics has also experienced successful marriage with nanomechanics, giving rise to the optomechanics research field. In parallel to key results in quantum optomechanics, devices operating in the classical regime have proved to play a unique role in view of specific applications.
In recent years, we have been working on this class of systems, including micromechanical bolometers (MB). In a MB, one measures the natural oscillation frequency of a SiN membrane (Fig. 1). Interestingly, such resonance frequency depends upon the membrane temperature, that in turn depends on the presence of impinging electromagnetic radiation. Sensitivity measurements revealed that this mechanism is competitive with other state-of-the-art techniques for detecting terahertz (THz) radiation at room temperature [1]. What is more, MB can be fashioned in multi-pixel arrays, leading to strongly sought-after uncooled THz cameras; in perspective, the integration of electromagnetic metamaterials will also add multispectral functionality to the sensor.
As optomechanical systems rely on the precise control of both optical and mechanical degrees of freedom, a powerful strategy for the development of advanced devices exploits the metamaterial concept also applied to the mechanical wave propagation. In this view, we have studied perforated SiN membranes, where the hole shape is tuned from circular to elongated (Fig. 2a-e). The geometric asymmetry translates into a wave speed asymmetry, thus converting an isotropic material into an artificially anisotropic one [2]. An even stronger degree of asymmetry was studied in the system of Fig. 2f-h, where L-shaped holes were considered. Here, wave propagation at an interface experiences either ordinary or negative refraction, depending on the incident direction [3].

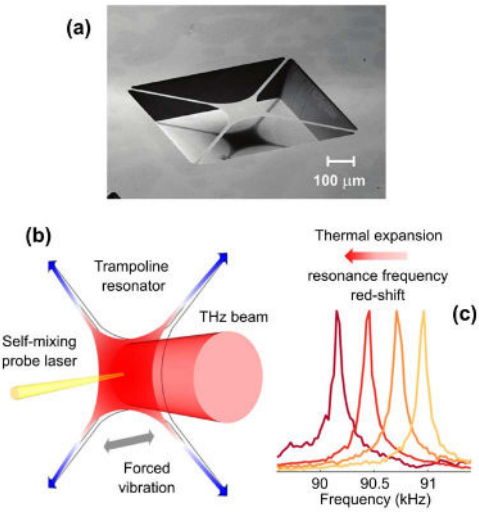

Fig. 1
A SiN membrane (a) operates as a micromechanical bolometer (b). When terahertz (THz) radiation impinges on the oscillating membrane, its mechanical eigenfrequency is shifted (c). Here, the read-out is performed through self-mixing interferometry; current work focuses on electronical readout techniques.

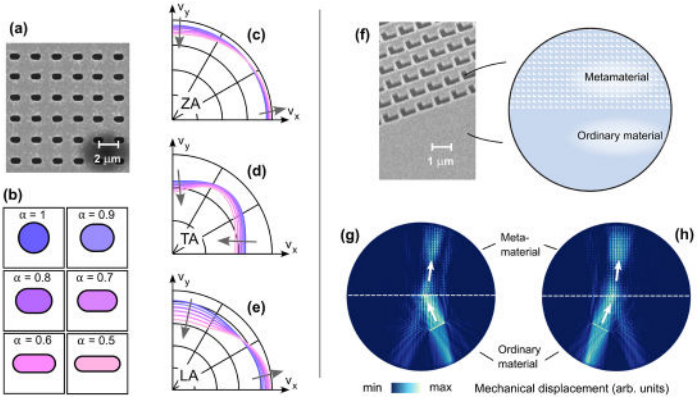

Fig. 2
A membrane perforated with holes (a) acts as a mechanical metamaterial where the wave speed anisotropy can be engineered by controlling the hole shape (b-e). Here, ZA, TA and LA label the three fundamental wave modes in an effective orthotropic plate. If L-shaped holes are instead considered (f), additional wave anisotropies exist, leading to the coexistence of negative refraction (g) and ordinary refraction (h).

Contact persons
Simone Zanotto (simone.zanotto@nano.cnr.it)
Alessandro Pitanti (alessandro.pitanti@unipi.it)

References
[1] Micromechanical bolometers for subterahertz detection at room temperature. L. Vicarelli, A. Tredicucci, and A. Pitanti. ACS Photonics 9, 360 (2022).
[2] Mechanical Mode Engineering with Orthotropic Metamaterial Membranes. G. Conte, L. Vicarelli, S. Zanotto, and A. Pitanti. Advanced Materials Technologies 7, 2200337 (2022).
[3] Metamaterial-enabled asymmetric negative refraction of GHz mechanical waves. S. Zanotto, G. Biasiol, P. V. Santos, and A. Pitanti. Nature Communications 13, 5939 (2022).

Projects
H2020 EU ATTRACT II H-CUBE (GA 101004462).

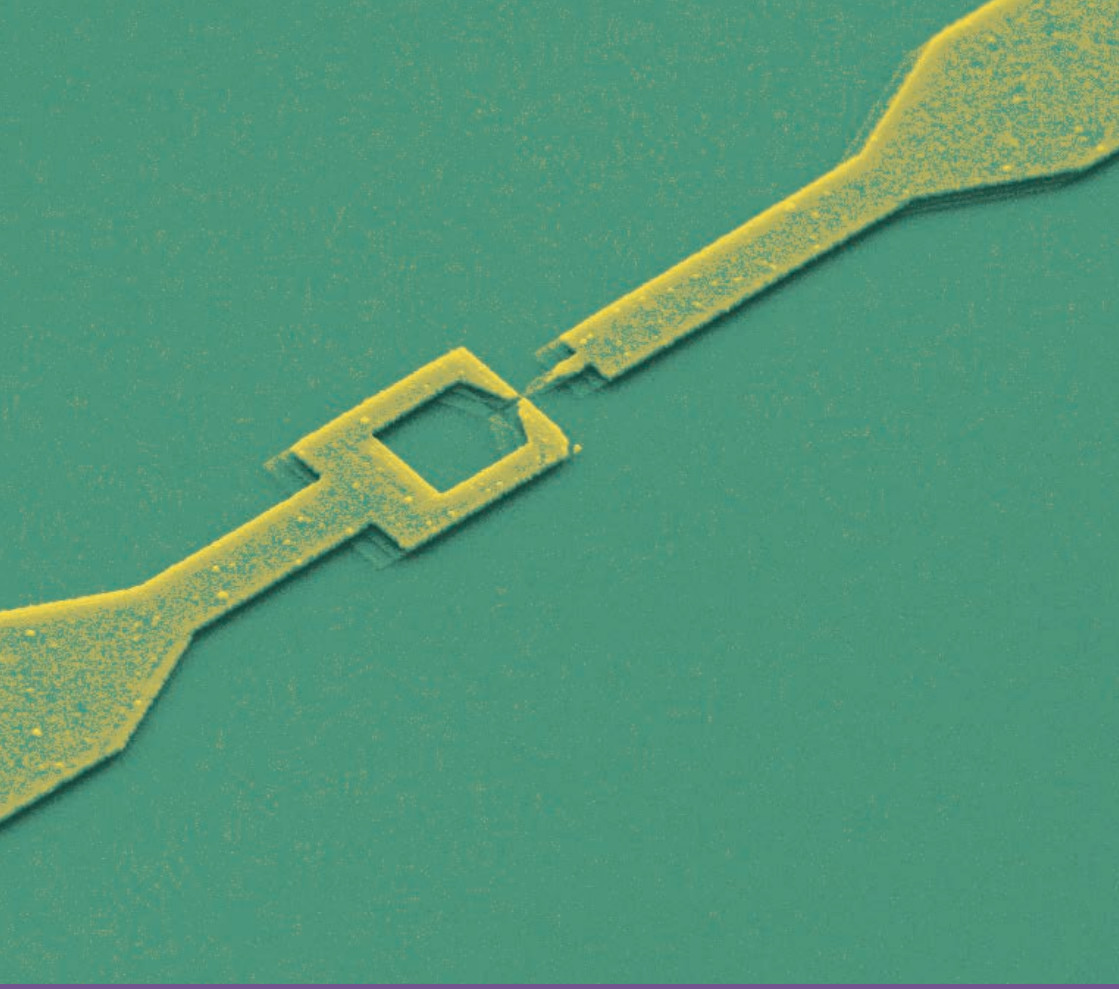

Highlights
-
Solid-state quantum technology

Research in solid-state quantum technology focuses on the **fabrication, investigation, and implementation of novel quantum nanodevices** both for fundamental science and for applications. Joint experimental and theoretical activity is devoted to the study of quantum systems and phenomena, and aims at developing novel concepts and ideas, with potential impact on future applications. Advanced fabrication techniques, low-temperature measurements, and theoretical approaches are developed along **the following main research lines.**

Quantum transport and superconducting devices. The precise control of charge and heat fluxes at the nanoscale is at the heart of new technological advances, including quantum technologies. Moreover, phase-coherent control and harvesting of heat are fundamental for the development of new functionalities for superconducting circuits. Our research comprises quantum transport and quantum thermoelectricity in nanoscale structures, superconducting devices, and topological matter. As far as superconducting systems are concerned, we have demonstrated the existence of non-equilibrium-induced bipolar thermoelectricity due to a spontaneous symmetry breaking, and we have studied the implementation of non-reciprocal superconducting elements and linear-response mesoscopic superconducting interferometers. Josephson junctions are important superconducting devices. In this context, we have investigated ballistic InSb nanoflag-based Josephson junctions showing quantum transport phenomena such as the diode effect and the occurrence of half-integer Shapiro steps under microwave irradiation. We have also shown that hybrid quantum Hall superconducting systems can be used to implement robust and electrically tunable topological Josephson junctions. Regarding quantum Hall systems, we have studied the role of correlation effects in the heat transport between quantum Hall edge states and we have shown that nonlocal thermoelectricity can probe interaction phenomena. We have also shown that

the quantum Hall phase can be realized in graphene encapsulated in hexagonal boron nitride at close-to-room temperatures, where dissipation is governed predominantly by electron-phonon scattering. Finally, we have investigated in detail the the finite-size effects occurring in different types of topological insulators, including second-order ones.

Quantum information and quantum thermodynamics. With the advent of the quantum technology revolution, mastering of quantum states has become a reality. Our pioneering cross-fertilized research combines quantum theory, information theory, thermodynamics, and solid-state physics to achieve a deeper understanding of energy and information management in quantum systems and devices. Regarding energy management, our major results span from methods to effectively extract energy from a quantum battery to methods to rectify heat flow in quantum dot systems. As far as quantum information is concerned, we have demonstrated new methods to effectively erase information in quantum computers and discovered new methods to enable communication along long optical fibers. Furthermore, we have considered the multidimensional generalization of the quantum capacitance to maximize the response of a quantum system to arbitrary signals, and we have investigated the implementation of remote charge sensing, where the state of a target dot is inferred from its effect on a coherently manipulated hole-spin based sensor. We have implemented the coupling of microwave resonators with a reduced number of molecular spins and improved the readout of spin signals through machine learning approaches. Microwave resonators have been also used to investigate the excitation of spin wave modes and to demonstrate that they are very strongly coupled to microwave photons. Finally, foundational results have been developed to fully describe the open quantum system evolution of coherent systems, such as micromasers and collision models.

Coherent manipulation and readout of spin ensembles at the sub-nanoliter scale

Molecular spins have shown large potential for quantum technologies when integrated into planar microwave (MW) superconducting resonant device. Along this line, the most ambitious and challenging goal is achieving the magnetic coupling with single molecules placed in proximity of a suitable resonant device. This comes along with the development of resonant geometries having high sensitivity to reduced spin numbers as well as of novel techniques to improve the readout of vanishingly small signals. Here we report our recent results on coupling MW resonators with reduced number of spins and on improving the readout of the spin signals through machine learning approaches.

We first consider a new type of resonant geometry, an Inverse Anapole Resonator (IAR, Fig. 1.a) made of superconducting Yttrium Barium Copper Oxide (YBCO). Such geometries can host three different resonant modes in the 5-15 GHz frequency range, which are designed to highly suppress radiative losses, enhancing the MW field at their constrictions. We investigate the coupling between IARs and a diluted ensemble of α-γ-bisdiphenylene-β-phenylally (BDPA) organic radical [1], and we then compare our results with the ones obtained for the same sample coupled to a linear coplanar resonator [C. Bonizzoni et al., npj Quantum Inf. 6, 68 (2020); Bonizzoni et al., Sci. Rep. 7, 13096 (2017)]. We show that it is possible to address BDPA with MW pulses and to coherently manipulate it, as demonstrated by the measure of its Hahn's echo and of its memory time (Fig. 1.c,d). Our analysis reveals that the effective sample volume is at sub-nanoliter scale [1]. Finally, IAR are found to improve the spin sensitivity by up to 3 orders of magnitude with respect to linear coplanar resonators, both in continuous wave and in pulsed wave regime, reaching a maximum value of $5 \cdot 10^7$ spin/$\sqrt{\text{Hz}}$ at 13 GHz and 2 K [1].

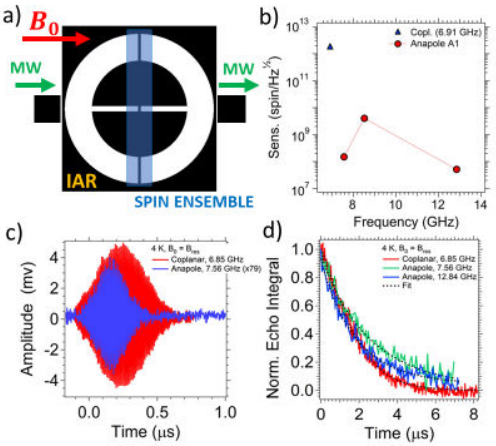

Fig. 1
a) Sketch of an Inverse Anapole Resonator (IAR). Black rectangle on the back is the feeding transmission line. Green arrows and red arrow represent the microwave signal and the static magnetic field, respectively. Blue rectangle shows the sample position. b) Spin sensitivity achieved for all resonant modes of IAR in pulsed-wave regime. c) Hahn's echo signal obtained for BDPA using a IAR (blue). d) Decay of the Hahn's echo signal in c) as a function of time. In b), c), and d) data obtained for a linear coplanar resonator are added for comparison.

We then show that the readout of the amplitude or of the phase of molecular spin qubits through the resonators can be assisted by means of machine learning methods (Fig. 2) [2]. The amplitude readout is performed with an artificial neural network (ANN) combined with a post-selection method based on clusterization, which is tested on experimental data obtained from a storage-retrieval protocol performed on an oxovanadium tetraphenyl porphirin (VO(TPP)) [C. Bonizzoni et al., al, npj Quantum Inf. 6, 68 (2020)]. The output echo signals are recognized from raw data without any prior information on their number or position, and then the initial input sequence is successfully inferred. The phase readout is performed using a similar ANN on the experimental raw data obtained from a Hahn's echo sequence. The ANN can successfully infer the echo phase and can also recognize possible additional manipulations introduced during its initialization or its refocusing [2].

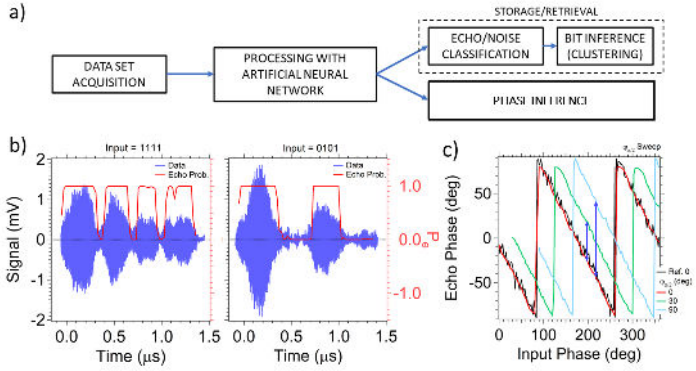

Fig. 2
a) Experimental workflow implemented for machine learning-assisted readout of spin echo signals. The topology of the Artificial Neural Network (ANN) depends upon the task to be performed. b) Examples of recognition (red probability traces, P_e) of echo signals (blue traces) from noise baseline done with an ANN on experimental raw data obtained from a Storage-Retrieval protocol with two different input sequences (1111 and 0101, where 1 = pulse ON and 0 = pulse OFF). c) Example of recognition of the phase of a Hanh's echo from raw data (red trace). Different initializations introduced changing the phase of the first pulse (green and blue traces) can be detected. Data reported in b) and c) were obtained for a VO(TPP) sample embedded into a coplanar resonator.

Contact persons
Marco Affronte (marco.affronte@unimore.it)
Claudio Bonizzoni (claudio.bonizzoni@unimore.it)

References
[1] Coupling Sub-nanoliter BDPA Organic Radical Spin Ensembles with YBCO Inverse Anapole Resonators. C. Bonizzoni, M. Maksutoglu, A. Ghirri, J. van Tol, B. Rameev, and M. Affronte. Appl. Magn. Res. 54, 143 (2023).
[2] Machine-Learning-Assisted Manipulation and Readout of Molecular Spin Qubits. C. Bonizzoni, M. Tincani, F. Santanni, and M. Affronte. Phys. Rev. Appl. 18, 064074 (2022).

Projects
H2020-FETOPEN Supergalax (GA 863313).

Transport and quantum dynamics in topological and coherent nanodevices

Topological and hybrid superconducting materials have unique physics as far as charge and heat transport are concerned. In particular, topological insulators and integer quantum Hall (IQH) systems combined with superconductors represent unique platforms where quantum and coherent dynamics affect transport properties in an exceptional manner. Furthermore, topological corner states in polygon-shaped flakes of second-order topological insulators promise novel topological features. Finally, foundational results have been developed to fully describe the open quantum system evolution of coherent systems, such as micromasers and collision models.

Over the last years the interest in topological order in condensed matter systems has exploded: many different classes of topological materials have been discovered and many possible experimental implementations have been proposed. Topological insulators (TI), for example, are characterised by an insulating bulk and gapless conducting surface states at the interface between the system and the vacuum which consist, at low energy, of single Dirac fermions. The research at Cnr Nano in this field comprises quantum transport properties, quantum thermodynamics and confinement effects, even aiming to propose new quantum technological applications. In our first research line we have studied quantum transport in order to investigate how hybrid topological quantum Hall superconducting nanodevices can be used to implement robust and electrically tunable topological Josephson junctions (TJJ) (Fig. 1). We have derived the Josephson current and have investigated the Andreev bound state (ABS) spectrum, which can be conveniently used to implement Andreev qubits [1]. Furthermore, we have shown, using bosonization techniques, that nonlocal thermoelectricity can probe the interaction phenomena and the role of correlation effects in heat transport between quantum Hall edge states for an experimentally measurable setup.

In our second research line we have investigated in detail the the finite-size effects occurring in different types of topological insulators (TI). On the one hand, we have studied the spectral properties and the optical absorption of surface states in 3DTI nano-cylinders [2]. On the other hand, we have studied the occurrence and features of corner states, in second-order two-dimensional TIs, inside convex polygon-shaped flakes [3]. Finally, in the last years, we have developed a set of foundational results and general theoretical tools [4] for investigating the quantum evolution, dynamics, and transport in open quantum systems, such as micromasers (Fig. 2). We have also organized those results in a pedagogical review [5].

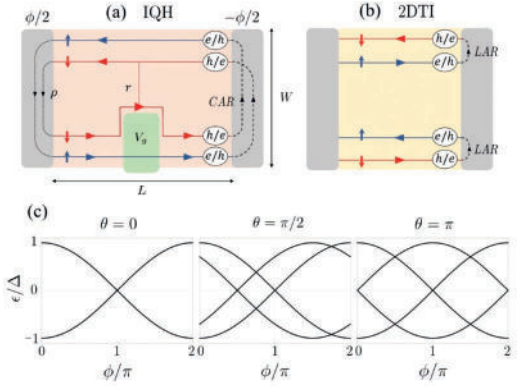

Fig. 1
Sketch of IQH TJJ proposal and associated ABS spectrum. (a) IQH bar of dimensions W ×L at filling factor ν = 2, coupled to two superconducting electrodes with phase difference φ. Opposite spin-polarized chiral upper and lower edge states are coupled through CAR processes. Nonideal interfaces allowing for normal reflections are characterized by an amplitude ρ. The gate voltage V_g electrostatically controls the effective phase θ between the two different ABS sectors. A tunneling amplitude r allows a coupling between right and left propagating edge states. (b) Comparison model for 2DTI TJJ, based on local Andreev reflection (LAR) processes between opposite counter-propagating spin-polarized edge states. (c) ABS spectrum as a function of φ at different gates θ = {0,π/2,π} in the IQH TJJ for r = 0 and ρ = 0. For θ = 0, both 2DTI and IQH TJJ feature exactly the same doubly-degenerate ABS spectrum. A value of theta different from 0 lifts the degeneracy in the IQH TJJ spectrum, demonstrating full electrostatic control of the topological properties of the IQH TJJ [1].

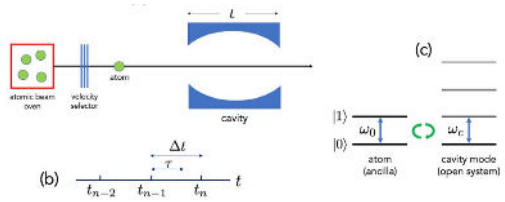

Fig. 2
Micromaser. (a) Basic micromaser setup. Atoms are heated in an oven (on the left). As atoms are ejected from the oven, a velocity selector filters only those of desired velocity v. Each selected atom then travels at speed v towards the cavity (of length L) until it crosses it. (b) Characteristic times. If L is the cavity length, each atom interacts with the cavity mode for a time τ = v/L. Since τ ≤ Δt, where Δt is the time between two consecutive atomic injections, there are never two atoms in the cavity at the same time meaning that the dynamics is naturally described by a basic cavity mode (atoms interact with the cavity mode one at a time). In the interaction picture, during the interval [tn−1 + τ, tn] when the nth atom is out of the cavity, the system does not change its state. (c) Atomic and cavity-mode levels involved the interaction [5].

Contact persons
Alessandro Braggio (alessandro.braggio@nano.cnr.it)
Fabio Taddei (fabio.taddei@nano.cnr.it)

References

[1] Topological Josephson junctions in the integer quantum Hall regime. G. Blasi, G. Haack, V. Giovannetti, F. Taddei, and A. Braggio. Phys. Rev. Research 5, 033142 (2023).
[2] Topological-insulator nanocylinders. M. Governale and F. Taddei. SciPost Phys, Core 6, 032 (2023).
[3] Corner states of two-dimensional second-order topological insulators with a chiral symmetry and broken time-reversal and charge conjugation. J. Poata, F. Taddei, and M. Governale. Phys. Rev. B 108, 115405 (2023).
[4] Entanglement-assisted, noise-assisted, and monitoring-enhanced quantum bath tagging. D. Farina, V. Cavina, M. G. Genoni, and V. Giovannetti. Phys. Rev. A 106, 042609 (2022).
[5] Quantum collision models: Open system dynamics from repeated interactions. F. Ciccarello, S. Lorenzo, V. Giovannetti, and G. M. Palma. Phys. Rep. 954, 1 (2022).

Projects

Royal Society through the International Exchanges between the UK and Italy: “The mechanics in quantum mechanics: nano-electromechanical Josephson junctions” (IEC R2 192166); “Topological Thermal Machines” (IEC R2 212041).
MIUR-PRIN2022 NEThEQS. Non-equilibrium coherent thermal effects in quantum systems (2022B9P8LN).

Caloritronics and bipolar thermoelectricity in quantum nanodevices

Phase-coherent control and harvesting of heat are fundamental for the development of superconducting-based quantum technologies. We investigated different strategies to control and harvest in a phase coherent fashion the heat current in quantum devices. We demonstrated the existence of non-equilibrium-induced spontaneous symmetry breaking bipolar thermoelectricity in gap asymmetric superconducting tunnel junctions, and we applied the new research finding to new devices and technologies.

Coherent management of heat transfer opens unique capabilities in heat control, heat harvesting and heat-based logic (caloritronics) for quantum technology applications. Heat management is crucial to fully realize the first scalable solid-state quantum computing platforms or to reach the promised performances of many different quantum machines or sensors. We recently realized the first thermal superconducting quantum interference proximity transistor where the phase control of heat currents is exploited by using the superconducting proximity effect [1] (Fig. 1). We also reported the first experimental demonstration of the existence of the bipolar thermoelectricity as induced by the spontaneous symmetry breaking of the electron-hole symmetry in an asymmetric superconductor-insulator-superconductor (SIS') junction under a temperature gradient [2] (Fig. 2). After the experimental confirmation we further developed this research line creating new devices and technologies and deepening the theoretical analysis. We demonstrated a current-controlled thermoelectrical cryogenic memory, which can be phase-controlled, in a SQUID-like device [3]. At the same time, we also discussed alternative electrically tunable nanodevices based on a hybrid bilayer graphene setup [4] or in a superconductor quantum dot setup thereby clarifying better what happens in the presence of a moderate breaking of the particle-hole symmetry and the important role of the electron-electron interactions. We identified the unique interplay between photon-assisted tunnelling and the bipolar thermoelectricity generation in SIS' tunnel junctions envisioning applications in microwave physics [5]. We have also considered all the diffusive effects [6]. Finally, we also investigated the possible application as a broadband superconducting single-photon detector which may find applications in quantum communication or astrophysics [7].

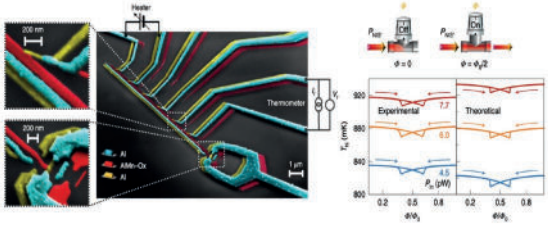

Fig. 1
Thermal superconducting quantum interference proximity transistor (T-SQUIPT) [1]. On the left, false-color scanning electron micrograph of a typical T-SQUIPT. An Al nanowire (S'; yellow) is inserted in an Al ring (SR; blue), whereas an Al0.98Mn0.02 normal metal electrode (N; red) is tunnel coupled through a thin Al oxide layer (Ox) to the middle of the nanowire. A set of superconducting Al tunnel probes (yellow) are coupled to N and serve as local heaters and thermometers. On the top right, one finds the schematic of the magnetic-flux control of the heat current

(PNIS') flowing through the T-SQUIPT. On the bottom right, comparison between experimental and theoretical electronic temperatures of N versus magnetic flux [TN(Φ)] for different values of *P*in.

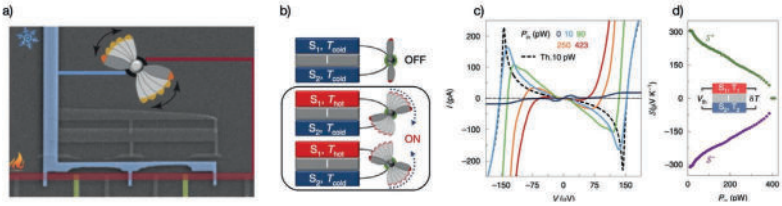

Fig. 2

Bipolar thermoelectric Josephson engine (BTJE) [2]. a) Pseudo-color scanning electron micrograph of a typical BTJE. An aluminum island (S1, red) is tunnel coupled through three AlOx barriers to a Cu/Al bilayer (S2, blue) thus realizing a double-loop SQUID. Additional tunnel-coupled Al electrodes (green) serve as Joule heaters for S1. b) Scheme of the BTJE: two different superconductors S1 and S2 (with zero-temperature energy gaps Δ0,1 > Δ0,2) are tunnel coupled through a thin insulating layer (grey, I). The S1IS2 junction is predicted to generate power when S1 is kept at a higher temperature (Thot) than S2 (that is, T1 = Thot > T2 = Tcold). Remarkably, this structure can produce both positive and negative thermovoltages for the *same* thermal gradient imposed across the junction (bipolar thermoelectric effect). c) Subgap current (I) versus voltage (V) characteristics of the SQUID measured at Φ = 0.33Φ0 for different values of the input power (Pin) injected in S1. In the presence of a thermal bias, the BTJE shows an absolute negative conductance for both polarities of V. The black dashed line is the result from the theory (Th.) for a single junction calculated at 10 pW. The temperature bias across the BTJE is deduced by fitting the experimental IV curves with the theory. d) Bipolar Seebeck coefficient S= Vth/ δT versus Pin extracted from the data shown in c). In the presence of thermoelectricity, the value of S monotonically decreases, in module, by increasing Pin. Inset: scheme of the thermoelectric element generating Vth in the presence of a temperature gradient (δT).

Contact persons

Alessandro Braggio (alessandro.braggio@nano.cnr.it)
Francesco Giazotto (francesco.giazotto@nano.cnr.it)

References

[1] Thermal superconducting quantum interference proximity transistor. N. Ligato, F. Paolucci, E. Strambini, and F. Giazotto. Nature Phys. 18, 627 (2022).
[2] Bipolar thermoelectric Josephson engine. G. Germanese, F. Paolucci, G. Marchegiani, A. Braggio, and F. Giazotto. Nature Nanotech. 17, 1084 (2022).
[3] Phase Control of Bipolar Thermoelectricity in Josephson Tunnel Junctions. G. Germanese, F. Paolucci, G. Marchegiani, A. Braggio, and F. Giazotto. Phys. Rev. Applied 19, 014074 (2023).
[4] Bipolar Thermoelectricity in Bilayer-Graphene–Superconductor Tunnel Junctions. L. Bernazzani, G. Marchegiani, F. Giazotto, S. Roddaro, and A Braggio. Phys. Rev. Applied 19, 044017 (2023).
[5] Microwave-Assisted Thermoelectricity in SIS' Tunnel Junctions. A. Hijano, F. S. Bergeret, F. Giazotto, and A. Braggio. Phys. Rev. Applied 19, 044024 (2023).
[6] Bipolar thermoelectricity in S/I/NS and S/I/SN superconducting tunnel junctions. A. Hijano, F. S. Bergeret, F. Giazotto, and A. Braggio. Appl. Phys. Lett. 122, 242603 (2023).
[7] Broadband passive superconducting thermoelectric single photon-detector. G. Germanese, F. Paolucci, A. Braggio, and F. Giazotto. Patent (2023).

Quantum information and quantum thermodynamics

With the advent of the quantum technology revolution, mastering of quantum states has become a reality. Our pioneering cross-fertilized research combines quantum theory, information theory, thermodynamics, and solid-state physics to achieve a deeper understanding of energy and information management in quantum systems and devices. Our major results span from the discovery of new methods to enable communication along long optical fibers, to the discovery and demonstration of new methods to effectively erase information in quantum computers; from methods to effectively extract energy from a quantum battery to methods to rectify heat flow in a quantum dot.

Among our main results in quantum information, we demonstrate the possibility to devise schemes that enable unassisted quantum communication across arbitrarily long optical fibres at a fixed positive qubit transmission rate [1] (Fig. 1).
At the crossroad between quantum information and quantum thermodynamics are the works in Refs. [2,3]. In Ref. [2] we have reported the discovery and experimental implementation (performed on a quantum computer) of a novel method to erase information based on quantum cooperative effects. The method achieves the best erasure performance ever reported in the literature in terms of (energy-cost)×(execution-time), while operating nearly at the Landauer limit and with an exceptional erasure success rate of 99,9% (Fig. 2). In Ref. [3] we have exploited the control on the dynamics of an open spin qutrit implemented as a nitrogen-vacancy centre in diamond to experimentally realize an Autonomous Dissipative Maxwell's Demon, that is a microscopic quantum device that inverts the natural flow of heat from hot to cold regions.
Further discoveries and original results in the field of quantum thermodynamics are reported in Refs. [4-7]. In Ref. [4], we have introduced a new set of quantum channels: resonant multilevel amplitude damping (ReMAD) channels, which can describe energy dissipation effects in multilevel atomic systems induced by the interaction with a zero-temperature bosonic environment. In Ref. [5], we have demonstrated an asymmetry between the beneficial effects one can obtain using nonlocal operations and nonlocal states to mitigate the detrimental effects of environmental noise in the work extraction process from quantum battery models. Thermoelectric quantum effects are investigated in Refs. [6,7]. First, we have studied heat rectification through quantum dots in the Coulomb blockade regime using a master equation approach. In Ref. [7], we have derived bounds to the thermodynamic uncertainty relations in two-terminal systems when time reversal symmetry is broken.

Fig. 1
Steps 2 and 3 of the noise attenuation protocol in a long communication optical fibre. At the beginning of step 2, the environment is initialised in τ_ν. By sending the signals S1, S2, . . . , Sk, Alice aims to turn the environment into a state σ, where the latter is such that $\Phi_{\lambda,\sigma}$ is less noisy than $\Phi_{\lambda,\tau}$. Right after the environment ν has transformed into σ, step 3 starts with Alice sending the information-carrying signal S.

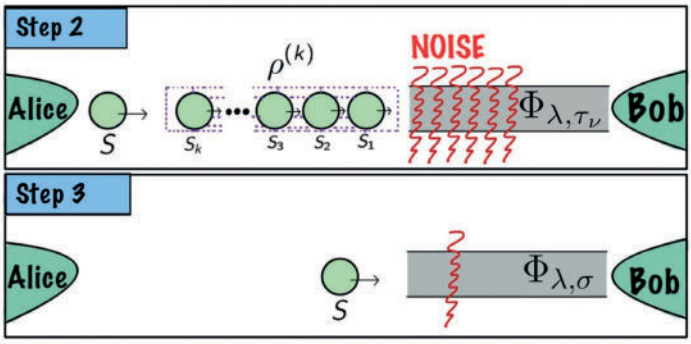

Fig. 2
Information erasure of an ensemble of N qubits [2]. The qubits are initially each in a random state (up or down each with 50% probability), corresponding to a null average polarization <mz>=0. The plot shows the time evolution of the polarization probability density p(mz,t). The classical erasure process (left) can reset only about 80% of the qubits to the up state while the quantum erasure process (right) resets about 99,9% of them.

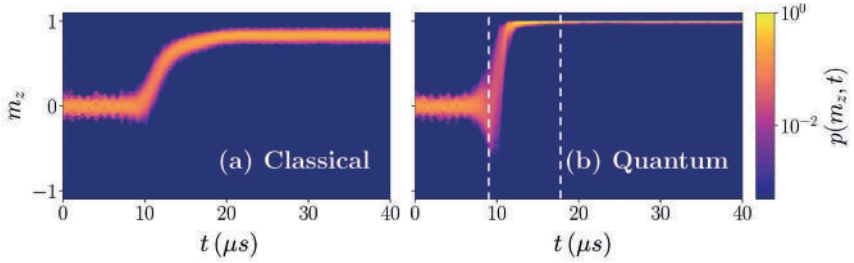

Contact persons
Michele Campisi (michele.campisi@nano.cnr.it)
Vittorio Giovannetti (vittorio.giovannetti@sns.it)

References
[1] Restoring quantum communication efficiency over high loss optical fibres. F. A. Mele, L. Lami, and V. Giovannetti. Phys. Rev. Lett. 129, 180501 (2022).
[2] Cooperative quantum information erasure. L. Buffoni and M. Campisi. Quantum 7, 961 (2023).
[3] Autonomous Dissipative Maxwell's Demon in a Diamond Spin Qutrit. S. Hernández-Gómez, S. Gherardini, N. Staudenmaier, F. Poggiali, M. Campisi, A. Trombettoni, F. S. Cataliotti, P. Cappellaro, and N. Fabbri. PRX Quantum 3, 020329 (2022).
[4] Resonant Multilevel Amplitude Damping Channels. S. Chessa, and V. Giovannetti. Quantum 7, 902 (2023).
[5] Work extraction processes from noisy quantum batteries: the role of non local resources. S. Tirone, R. Salvia, S. Chessa, and V. Giovannetti. Phys. Rev. Lett. 131, 060402 (2023).
[6] Heat rectification through single and coupled quantum dots. L. Tesser, B. Bhandari, P. A. Erdman, E. Paladino, R. Fazio, and F. Taddei. New J. Phys. 24, 035001 (2022).
[7] Thermodynamic uncertainty relations for systems with broken time reversal symmetry: The case of superconducting hybrid systems. F. Taddei and R. Fazio. Phys. Rev. B 108, 115422 (2023).

Non-reciprocal transport in superconducting devices

Non-reciprocal charge transport is an essential element in modern electronics as a building block for multiple applications such as rectifiers, photodetectors, and logic circuits. Aiming at the creation of a new class of electronics - superconducting and thus dissipationless -, we have studied the implementation of non-reciprocal superconducting elements for both quantum and classical applications. In analogy with conventional diodes based on semiconductors, in supercurrent diodes some transport features depend on the charge flow direction, thus potentially providing new functionalities for superconducting circuits.

A wide analysis on different materials and layouts has been carried out by the SQEL group in Pisa. In [1], the diode is a ferromagnetic tunnel barrier where the quasi-particle dissipative current flows preferentially from the Al layer to the Cu layer through a EuS thin film (Fig. 1), while the reverse flow is inhibited. Such a spintronic device is now at the base of cryogenics diodes [2] and ultrasensitive detectors [3].
In dissipationless supercurrent diodes the switching current, i.e., the maximal supercurrent that a weak link can sustain, depends on the current bias polarity. This has been reported in “hybrids”, i.e., Josephson junctions out of ballistic InSb nanoflag (see Highlight “Highly transmissive InSb nanoflag Josephson junctions” pag. 62): they show unequal supercurrents for the two opposite current propagation directions thanks to the Rashba spin–orbit coupling that imposes an “anomalous” shift in the current-phase relation of the junction. Also, metallic constrictions of superconducting Nb thin films, e.g., the ones in Fig. 2, offer similar functionalities; they realize a good rectification (~30%) with a fairly simple fab process [4]. Another strategy to obtain diodes relies on quantum interference. In dc SQUIDs, when a magnetic flux is applied, both spatial and time-reversal symmetry, i.e., the two ingredients to realize rectification, can be broken simultaneously. The two junctions can be tuned to be maximally different by a gate electrode (see Highlight "Superconducting quantum interferometers for new generation superconducting electronics" pag. 58) or thanks to the high harmonic content of the current phase relation of 3D metallic bridges [5].

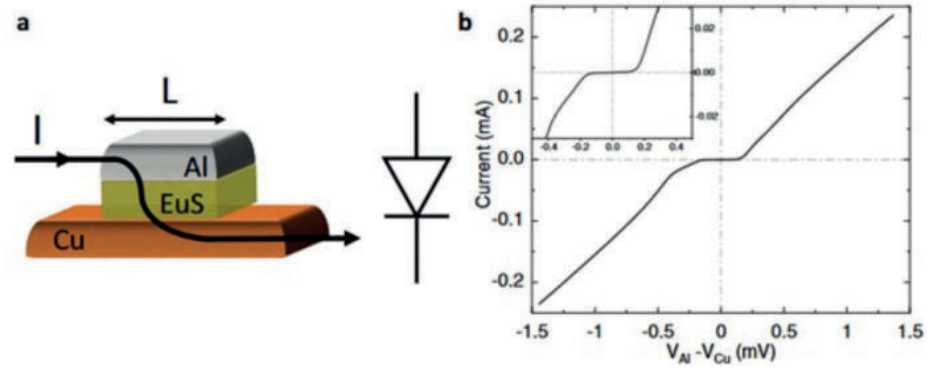

Fig. 1
Superconducting tunnel diode. a) Schematic of the N/FI/S tunnel junction. The path of the tunneling current is indicated by the black line and its arrows. In terms of electronic circuit elements this junction behaves like the indicated diode: the current flows preferentially from the Al layer to the Cu layer while the reverse flow is inhibited. b) Current-to-Voltage I(V) characteristics of the junction measured at T ≃ 50 mK, B = 0.1 T showing a preferential flow for positive voltage bias respect to the negative one.

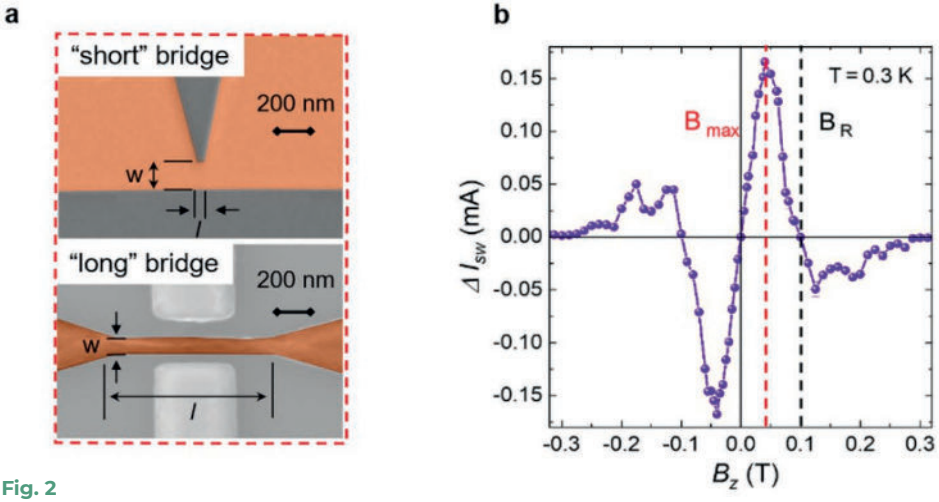

Fig. 2
a) Scanning Electron Micrograph of Dayem nanobridge of different layout obtained from a thin Nb micrometric stripe. b) ΔIsw defines the asymmetry between positive and negative critical currents. This quantity can be tuned by applying an out-of-plane B field and shows sign reversal without changing the sign of magnetic field.

Contact persons
Alessandro Crippa (alessandro.crippa@nano.cnr.it)
Elia Strambini (elia.strambini@nano.cnr.it)

References

[1] Superconducting spintronic tunnel diode. E. Strambini, M. Spies, N. Ligato, S. Ilic, M. Ruoco, C. Gonzalez-Orellana, M. Ilyn, C. Rogero, F. Bergeret, J. S. Moodera, P. Virtanen, T. T. Heikkila, and F. Giazotto. Nat. Commun. 13, 2431 (2022).
[2] Apparatus and method for superconducting diode. S. Ilic, F. S. Bergeret, P. Virtanen, T. Heikkila, E. Strambini, F. Giazotto, and M. Spies. Patent WO2023002513A1 (2023).
[3] Superconductor-ferromagnet hybrids for non-reciprocal electronics and detectors. Z. Geng, A. Hijano, S. Ilić, M. Ilyn, I. Maasilta, A. Monfardini, M. Spies, E. Strambini, P. Virtanen, M. Calvo, C. González-Orellána, A. P. Helenius, S. Khorshidian, C. I. L. de Araujo, F. Levy-Bertrand, C. Rogero, F. Giazotto, F. S. Bergeret, and T. T. Heikkilä. Supercond. Sci. Technol. 36, 123001 (2023).
[4] Sign reversal diode effect in superconducting Dayem nanobridges. D. Margineda, A. Crippa, E. Strambini, Y. Fukaya, M. T. Mercaldo, M. Cuoco, and F. Giazotto. Communications Physics 6, 343 (2023).
[5] Josephson diode effect in monolithic dc-SQUIDs based on 3D Dayem nanobridges. A. Greco, Q. Pichard, and F. Giazotto. Appl. Phys. Lett. 123, 092601 (2023).

Superconducting quantum interferometers for new generation superconducting electronics

Superconducting quantum interference device (SQUID) outperform classical magnetometers. Here, we discuss linear-response mesoscopic superconducting interferometers that maintain the signal integrity, crucial for high-sensitivity cryogenic current amplifiers. Our approaches, using proximity-based superconducting transistors and multi-looped SQUIDs, match state-of-the-art linear-response interferometers. Additionally, we leverage the gating effect demonstrated on all-metallic mesoscopic superconducting devices to tailor phase-coherent responses for specific needs, like gate-tunable non-reciprocal supercurrent transport or controlling the linearity of superconducting interferometer responses.

Superconducting quantum interference devices outperform their classical counterparts. Indeed, they have long been employed as ultra-high precision magnetic flux transducer sensors across several applications spanning from medical imaging to quantum metrology. Yet, a large room exists to further tailor their behavior to needs emerging from the impetuous development of quantum technologies. On this premises, we present the activities - carried out by the Superconducting Quantum Electronic Laboratory Group of this institute - aimed at the demonstration of coherent quantum devices to be integrated in quantum electronics.

In the first place, we focus on the realization of linear-response superconducting interferometers, which possess the ability not to distort the electromagnetic signals they sense. Although lacking in conventional SQUIDs, this characteristic is highly desirable to implement high-sensitivity cryogenic current amplifiers. We tackled this issue through different approaches based on proximity-based superconducting transistors [1] and on multi-looped all-metallic SQUIDs [2]. In terms of linearity, the performances of these devices are at least on par with those of state-of-the-art superconducting linear-response interferometers.

It is also worth noting that, as recently demonstrated by us on all-metallic mesoscopic superconducting devices [3], by electrostatically gating the weak-links of our interferometers, it is possible to tailor their response, e.g., to tune their linearity or to ad-hoc introduce a non-reciprocity of the supercurrent transport. The latter is a manifestation of the so-called supercurrent diode effect, an issue that has been recently polarizing a growing interest for its potential applications in superconducting electronics. Thus, we developed superconducting interferometers based on gate-controlled Dayem nanobridges [4] that, not relying on exotic nonreciprocal superconductors, are still able to implement a voltage and magnetic-flux tunable rectification efficiency as large as 6%.

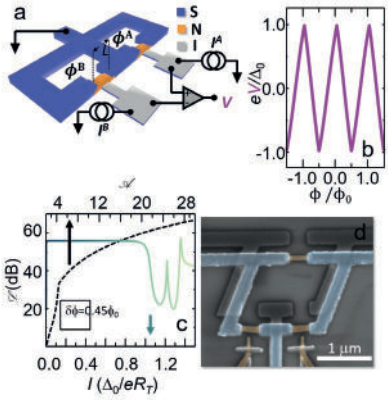

Fig. 1
a) Double superconducting quantum interference proximity transistor: the bi-SQUIPT. Two superconducting rings (A and B, colored in blue), having the same area $A_A = A_B$, are closed on L-long normal-metal weak links (orange). A magnetic flux $\Phi_A = \Phi$ and $\Phi_B = \Phi + \delta\Phi$ is threaded to loop A and B, respectively. A probe (made of the same superconductor, blue) is tunnel-coupled to each weak-link through a thin insulating layer (grey) and is used to inject quasi-particle currents IA and IB and to measure the differential voltage drop $V = V_A - V_B$ with respect to the common ground terminal. b) V as a function of Φ for δ Φ=0.45. This curve was calculated at a temperature T = 0.01T_C, where T_C is the critical temperature of the superconductor. c) Evolution of the spur free dynamic range L vs. flux modulation amplitude A /Φ_0 (black dashed line, top axis) and vs. bias current I (aquamarine solid line, bottom axis). d) Proximity-based gated all-metallic bi-SQUID: false-color scanning electron micrograph of a representative double-loop DC superconducting quantum interference device (bi-SQUID) based on superconductor/normal metal/superconductor (SNS) proximity Josephson junctions. The Al interferometer ring is colored in blue. The Cu Josephson weak links are colored in brown. The 4-wire electrical setup is also shown. This figure is adapted from references [1] and [2].

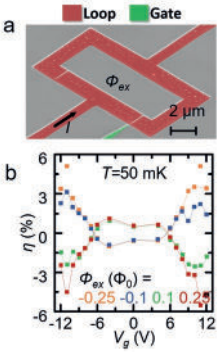

Fig. 2
a) False-color scanning electron micrograph of a magnetic-flux (Φex) and gate (Vg) controlled supercurrent diode (SD) realized by a SQUID based on weak-links equipped with a side gate (green) and with a large inductance of the loop made of 30-nm-thick Ti film (red). The SD is current biased (I), while the voltage is measured in a 4-terminal configuration. b) Rectification efficiency (η) of the device depicted in panel (a) versus the gate voltage (Vg) obtained for different values of Φex at T = 50 mK. The dashed lines are guides for the eye. This figure is adapted from reference [4].

Contact persons
Giorgio De Simoni (giorgio.desimoni@nano.cnr.it)
Francesco Giazotto (francesco.giazotto@nano.cnr.it)

References

[1] Ultralinear Magnetic-Flux-To-Voltage Conversion in Superconducting Quantum Interference Proximity Transistors. G. De Simoni and F. Giazotto. Phys. Rev. Applied 19, 054021 (2023).
[2] Ultrahigh Linearity of the Magnetic-Flux-to-Voltage Response of Proximity-Based Mesoscopic Bi-SQUIDs. G. De Simoni, L. Cassola, N. Ligato, G. C. Tettamanzi, and F. Giazotto. Phys. Rev. Applied 18, 014073 (2022).
[3] Effects of fabrication routes and material parameters on the control of superconducting currents by gate voltage. L. Ruf, T. Elalaily, C. Puglia, Y. P. Ivanov, F. Joint, M. Berke, A. Iorio, P. Makk, G. De Simoni, S. Gasparinetti, G. Divitini, S. Csonka, F. Giazotto, E. Scheer, and A. Di Bernardo. APL Mater. 11, 091113 (2023).
[4] A gate- and flux-controlled supercurrent diode effect. F. Paolucci, G. De Simoni, and F. Giazotto. Appl. Phys. Lett. 122, 042601 (2023).

Projects

H2020-FETOPEN-2018-2020 SUPERGATE (GA 964398), HORIZON-EIC-2021-TRANSITIONOPEN-01 SPECTRUM (GA 101057977). PNRR MUR project PE0000023-NQSTI.

Ultrastrong Coupling in Planar Magnon-Photon Hybrid Systems

Coherent coupling between spin wave modes (magnons) and microwave photons in a cavity may disclose new paths to unconventional phenomena as well as novel applications. Here, we present a systematic investigation of yttrium iron garnets (YIG) films on top of coplanar waveguide resonators made of superconducting $YBa_2Cu_3O_7$ (YBCO). We first investigate the excitation of spin wave modes by putting in direct contact a YIG film with the superconducting microwave resonator. With this bilayer configuration we obtain very large values of both collective coupling strength and cooperativity, and we demonstrate the achievement of the ultrastrong coupling regime [1].

The coherent interaction between magnons modes and microwave photons in a cavity can be described by the Dicke model and by its evolution in the Hopfield version, which holds for the description of a large variety of hybrid light-matter quantum systems. When the magnon-photon coupling strength reaches a non-negligible fraction of the cavity frequency, novel effects related to processes that do not conserve the number of excitations in the system are expected. In this so-called ultrastrong coupling regime, the coupling and decay rates of magnon and photon modes still needs to be tested on real magnetic materials. In particular, the effect of the diamagnetic coupling, which has been shown to inhibit the photon condensation and super-radiance, has yet to be clarified.

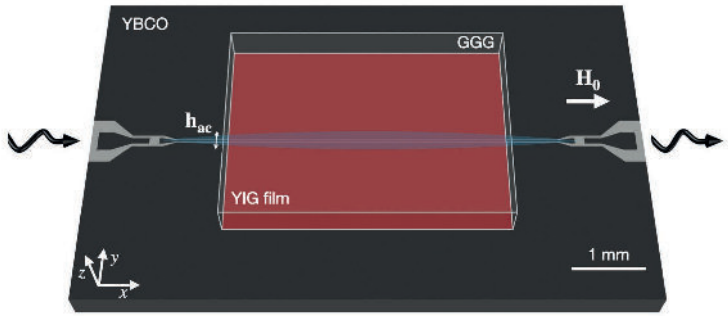

Fig. 1 (a) Sketch of the coplanar waveguide YBCO resonator with the YIG film positioned on top. The external magnetic field H_0, which is applied in the plane of the film along the x axis, allows the tuning of the magnon frequencies. The resonator field h_{ac} excites magnon modes with propagation direction perpendicular to H_0.

We fabricated a YBCO coplanar waveguide resonators and positioned an insulating YIG film (thickness 5 μm) in contact with the superconductor (Fig. 1). Transmission spectra were measured as a function of the microwave frequency in applied magnetic field. At low temperature, well-defined polaritonic branches emerge thanks to the enhanced spin-photon coupling in the low mode volume of the resonator (Fig. 2). Data analysis, carried out through the Hopfield Hamiltonian, allows for the estimation of the coupling strength, which results as high as 2 GHz. This value corresponds to about 0.2 times the cavity frequency and demonstrates the achievement of the ultrastrong coupling regime. From the measured linewidths of both spin wave and resonator modes, the cooperativity results ≈ 50000. The fits also indicate that the influence of the diamagnetic term is almost negligible, as expected for the vanishing orbital angular momentum of Fe^{3+} ions in YIG [1].
Our results show that the ultrastrong coupling regime can be achieved with a simple bilayer geometry in which the YIG film is positioned in contact with the YBCO resonator. The high coupling strength and cooperativity, together with the negligible diamagnetic coupling, open a path for the observation of the super-radiant phase transition with this architecture and materials.

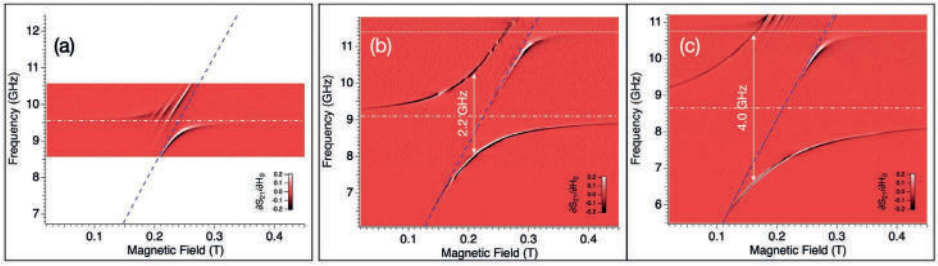

Fig. 2
Comparison between the spectral maps obtained with the YIG film and different planar resonators: (a) metallic microstrip resonator; (b) coplanar resonator with the YIG film installed at a separation of 10 μm from the YBCO surface; (c) YIG positioned in contact with the YBCO coplanar resonator. The coupling strength progressively increases from about 100 MHz in (a) to 1.1 GHz in (b) and 2 GHz in (c).

Contact persons
Alberto Ghirri (alberto.ghirri@nano.cnr.it)
Marco Affronte (marco.affronte@unimore.it)

References
[1] Ultrastrong Magnon-Photon Coupling Achieved by Magnetic Films in Contact with Superconducting Resonators. A. Ghirri, C. Bonizzoni, M. Maksutoglu, A. Mercurio, O. Di Stefano, S. Savasta, and M. Affronte. Phys. Rev. Appl. 20, 024039 (2023).

Projects
European Community FET Open SUPERGALAX project (GA 863313).

Highly transmissive InSb nanoflag Josephson junctions

We investigate ballistic InSb nanoflag-based Josephson junctions with superconducting contacts. The high mobility of the InSb nanoflags and the high transparency of the superconductor-semiconductor interfaces enables the exploration of quantum transport phenomena such as the Josephson diode effect. Under microwave irradiation, we observe half-integer Shapiro steps that are robust to temperature, suggesting their possible nonequilibrium origin. Our results demonstrate the potential of ballistic InSb nanoflag-based Josephson junctions as a valuable platform for understanding the physics of hybrid devices and investigating their nonequilibrium dynamics.

Low-dimensional InSb nanostructures have sparked interest in the past few years due to their potential applications in high-speed and low-power electronics, quantum electronics, and topological quantum computation. These applications stem from the outstanding intrinsic properties of InSb such as a narrow band gap, high bulk electron mobility, small effective mass, and a large Landé g-factor. Among the most influential developments are the topological superconducting quantum devices based on InSb nanowires. Besides one-dimensional nanowires, quasi two-dimensional InSb nanostructures, so-called nanoflags, also attracted great attention owing to their inherent design flexibility. These nanoflags have a defect-free zinc blend crystal structure, relaxed lattice parameters, and high electron mobility. Their size can be as large as 3 µm x 500 nm x 100

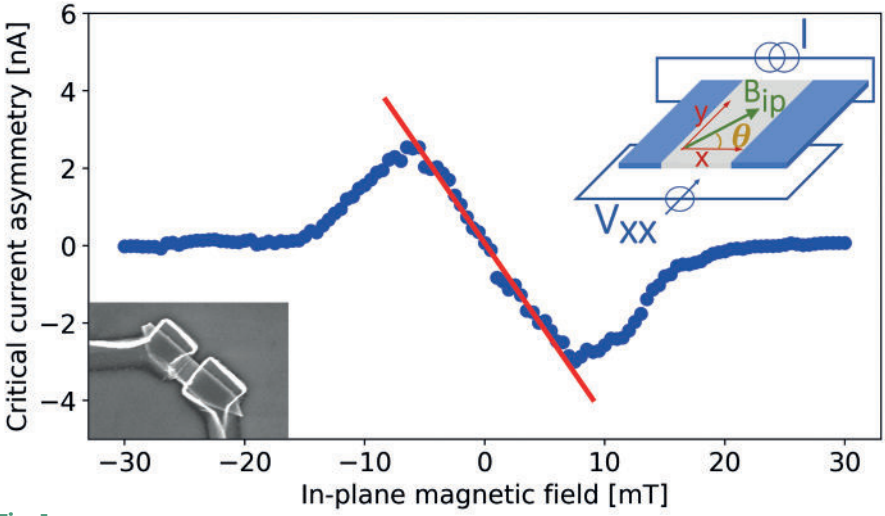

Fig. 1
Asymmetry in the critical current of the junction versus applied in-plane magnetic field. To highlight the linear behavior of the Josephson diode effect around zero field, we have added a linear best fit at the origin of the curve (red line). Upper right inset: Sketch of the measurement schematics. Lower left inset: Scanning electron microscopy image of the device structure.

nm. Our recent work has optimized the growth of InSb nanoflags and contributed to an improved understanding of the mechanisms governing their growth [1]. These nanoflags are important building blocks for state-of-the-art Josephson junction devices that show a gate-tunable proximity-induced supercurrent and clear signatures of subharmonic gap structures, indicating phase-coherent transport in the junction and a high transparency of the interfaces. Low-temperature magneto-transport has allowed us to observe nonreciprocal dissipation-less transport in single ballistic InSb nanoflag Josephson junctions [2]. Applying an in-plane magnetic field, we observed an inequality in critical current for the two opposite current propagation directions (Fig. 1). Thus, these devices work as Josephson diodes, with Rashba spin–orbit coupling as the main symmetry-breaking mechanism. Furthermore, we investigated InSb nanoflag-based Josephson junctions under microwave irradiation and observed strong half-integer Shapiro steps (Fig. 2), showing a nonmonotonic temperature evolution that points to nonequilibrium effects induced by the driving [3]. Our results place InSb nanoflags in the spotlight as a versatile and convenient 2D platform for advanced quantum technologies.

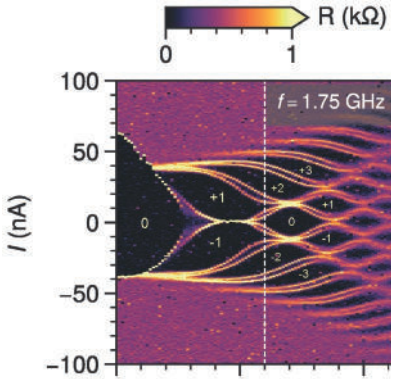

Fig. 2
Full evolution of the differential resistance R of the junction as a function of current bias I and microwave power P_{RF} at f = 1.75 GHz. Pairs of bright lines indicate the presence of half-integer Shapiro steps. Label numbers refer to the corresponding Shapiro step index n.

Contact persons
Stefan Heun (stefan.heun@nano.cnr.it)
Lucia Sorba (lucia.sorba@nano.cnr.it)

References
[1] Understanding the Morphological Evolution of InSb Nanoflags Synthesized in Regular Arrays by Chemical Beam Epitaxy. I. Verma, V. Zannier, V. G. Dubrovskii, F. Beltram, and L. Sorba. Nanomaterials 12, 1090 (2022).
[2] Josephson diode effect in high-mobility InSb nanoflags. B. Turini, S. Salimian, M. Carrega, A. Iorio, E. Strambini, F. Giazotto, V. Zannier, L. Sorba, and S. Heun. Nano Letters 22, 8502 (2022).
[3] Half-integer Shapiro steps in highly transmissive InSb nanoflag Josephson junctions. A. Iorio, A. Crippa, B. Turini, S. Salimian, M. Carrega, L. Chirolli, V. Zannier, L. Sorba, E. Strambini, F. Giazotto, and S. Heun. Phys. Rev. Res. 5, 033015 (2023).

Projects
H2020 QUANTERA ERA-NET Cofound in Quantum Technologies SUPERTOP (GA 731473). H2020 FET-OPEN AndQC (GA 828948). PNRR MUR NQSTI No. PE0000023-NQSTI. PRIN MUR (No. 2022PH852L). H2020-FETOPEN-2016-2017 SUPERTED EU (GA 800923). H2020-FETOPEN-2016-2017 SUPERGATE (GA 964398).

Phonon-mediated room-temperature quantum Hall transport in graphene

The quantum Hall effect in two-dimensional electron systems typically occurs only at very low temperature (few Kelvin). In these conditions, lattice vibrations are suppressed and thus play a marginal role in the electrical transport. Graphene stands out from its 2D peers due to a giant energy gap between its first two Landau levels, which enables the observation of quantum Hall states up to room temperature. In this work, we show that graphene encapsulated in hexagonal boron nitride realizes a novel transport regime, where dissipation in the close-to-room-temperature quantum Hall phase is governed predominantly by electron-phonon scattering.

Van der Waals (vdW) heterostructures of graphene and hexagonal boron nitride (hBN) have recently granted experimental access to novel phenomena in condensed matter, including transport regimes dominated by either electron-electron, electron-hole, or electron-phonon (e-ph) interactions. In Ref. [1], we address the fundamental question whether an e-ph mechanism could also govern the electrical transport in the quantum Hall (QH) regime at temperatures close to room temperature (RT, see sketches in Fig. 1a).

Figure 1b shows a representative measurement of the RT-QH effect, acquired at B = 30 T in one of our hBN-encapsulated devices. In addition to the pronounced maximum around the charge neutrality point (CNP), ϱ_{xx} (black curve) shows two sizable minima (Fig. 1b, inset), indicative of T-activated QH states. In Fig. 1c, we present a complete picture of the T-dependence of ϱ_{xx} at filling factor $\nu = 2$. In addition to our data, we show reference points from graphene on SiO_2 (black diamonds), and two theoretical calculations defining different dissipation limits (continuous lines). The upper line (yellow) assumes the universal conductivity pre-factor due to long-range disorder. The lower line (dark cyan) is the activated resistivity due to two-phonon scattering alone (as derived in Phys. Rev. B 92, 195431 (2015)), not including any free parameter. Strikingly, this limit is well approximated by our devices (while graphene on SiO_2 follows the long-range disorder limit), indicating that graphene/hBN heterostructures support e-ph-dominated transport in the RT-QH.

Considering different samples, we find deviations from the e-ph limit (quantified by the parameter ϱ_D, Fig. 1d) that correlate with the CNP broadening at zero magnetic field (n*, Fig. 1d inset). This behavior indicates that the random strain variations inducing the CNP broadening are also responsible for ϱ_{xx} exceeding the e-ph limit in the RT-QH. In conclusion, the use of an atomically flat vdW substrate results in essentially novel QH physics in graphene at high enough temperatures.

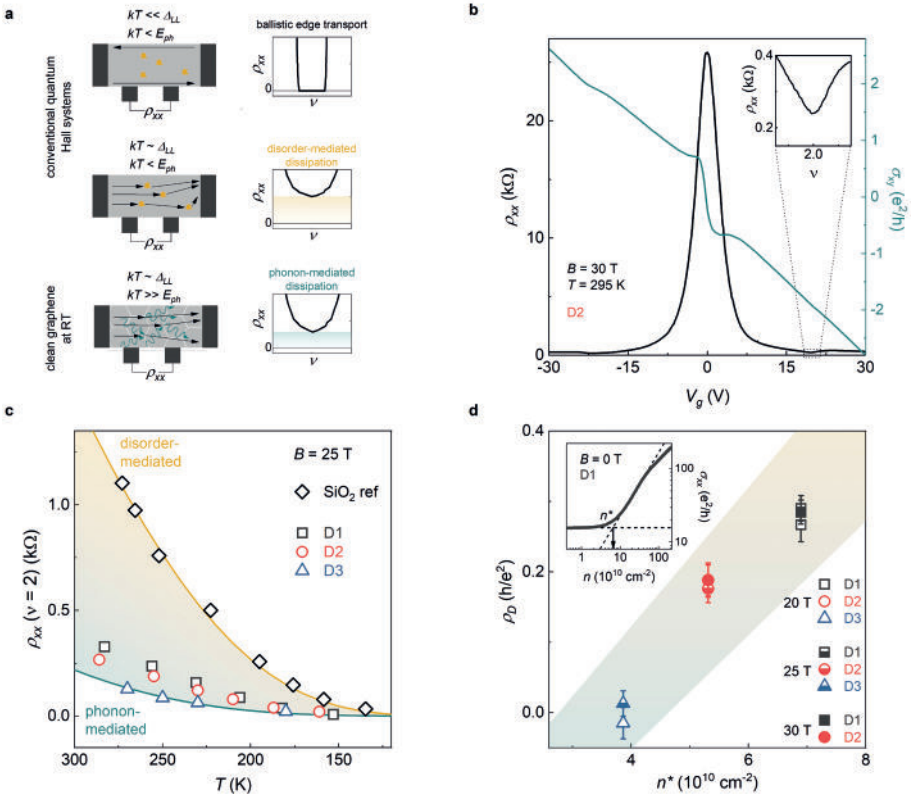

Fig. 1

(a) Schematics of T-dependent QH transport regimes: at low T (relative to the Landau level separation), the electrical current is carried by ballistic edge states; at higher T, in conventional 2D system thermally excited bulk states give a finite resistivity due to disorder scattering; at RT, graphene enables the realization of a QH regime with predominant phonon-mediated dissipation. (b) ρxx (black) and σxy (dark cyan) as a function of the back-gate voltage, measured in hBN-encapsulated device D2, at B = 30 T and T = 295 K. Inset: zoom-in of ρxx in the vicinity of ν = 2. (c) Minimum of ρxx at ν = 2 as a function of temperature, measured for different devices at B = 25 T. The reference data (black diamonds) are from graphene on SiO2. The continuous lines are theoretical calculations. (d) Correlation between the disorder-induced pre-factor to the activated resistivity and n*. Inset: zero-field conductivity of sample D1 as a function of the carrier density, measured at T = 220 K, exemplifying the extraction of n*.

Contact persons

Sergio Pezzini (sergio.pezzini@nano.cnr.it)

References

[1] Phonon-mediated room-temperature quantum Hall transport in graphene. D. Vaquero, V. Clericò, M. Schmitz, J. A. Delgado-Notario, A. Martín-Ramos, J. Salvador-Sánchez, C. S. A. Müller, K. Rubi, K. Watanabe, T. Taniguchi, B. Beschoten, C. Stampfer, E. Diez, M. I. Katsnelson, U. Zeitler, S. Wiedmann, and S. Pezzini. Nat. Commun. 14, 318 (2023).

Collective and remote readout of spin qubits in semiconductor quantum dots

The implementation of efficient and scalable approaches for qubit readout represents one of the key challenges in spin-based quantum computing. Here, we investigate two possible extensions of the schemes based on gate reflectometry. On the one hand, we consider the multidimensional generalization of the quantum capacitance, which allows one to maximize the response of the quantum system to arbitrary signals, simultaneously applied to multiple gates. On the other hand, we investigate the implementation of remote charge sensing, where the state of the target dot is inferred from its effect on a coherently manipulated hole-spin based sensor.

The multi-voltage generalization of the quantum capacitance (QC) leads to the introduction of the QC matrix (Fig. 1). Its calculation – based on the parametric dependence of the energy eigenvalues on the applied voltages – and diagonalization allow one to identify the optimal direction in the voltage space along which to apply the readout signal in order to maximize the fidelity of the reflectometry-based readout. The approach is applied to a representative model system, namely a Hubbard model of a linear quantum-dot array. Here, the QC matrix identifies the optimal regions in the voltage space for the charge and spin-state discrimination and provides the dependence of the QC on the specific processes responsible for the coupling between different charge configurations [1,2].
The suitability of hole-spin qubits for performing remote charge sensing (Fig. 2), resulting from the multiband character of the hole eigenstates, is quantified by figures of merit such as the discrimination probability and the Fisher information. Beyond the dependence of these quantities on the specific properties of the system, some general aspects emerge from our investigation. First, the use of double — rather than single — quantum dots allows for a significant enhancement of the precision in the estimate. In fact, the hole ground state in double dots is more polarizable, especially if

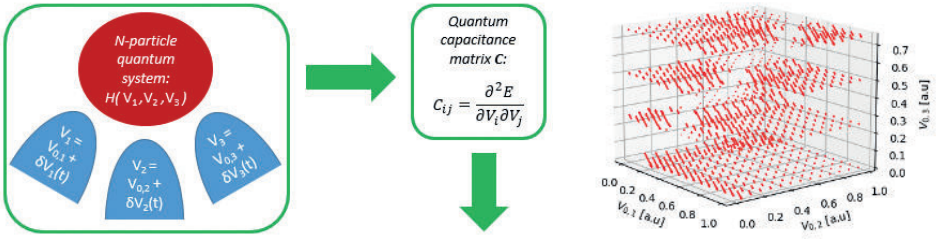

Fig. 1
Schematic view of the procedure based on the QC matrix. The system Hamiltonian (H) and energy (E) parametrically depend on the voltages Vk applied to the M metal gates (here, e.g., M = 3). The diagonalization of the resulting QC matrix Cij provides the optimal direction for the application of the signal δV and the corresponding value of the QC, here represented as a vector field in the voltage space.

the charge-induced bias is comparable to the interdot tunneling amplitude. Besides, its Larmor and Rabi frequencies – which determine the qubit coupling to external fields – are more sensitive to the position of the external charge. Second, a dynamic approach, where the value of D, the distance from the qubit to the charge, is encoded in the statistics of a Rabi or a Ramsey measurement, allows for better estimates than any possible static approach, where the distance of the charge determines the statistics of an arbitrary measurement performed on the hole ground state [3].

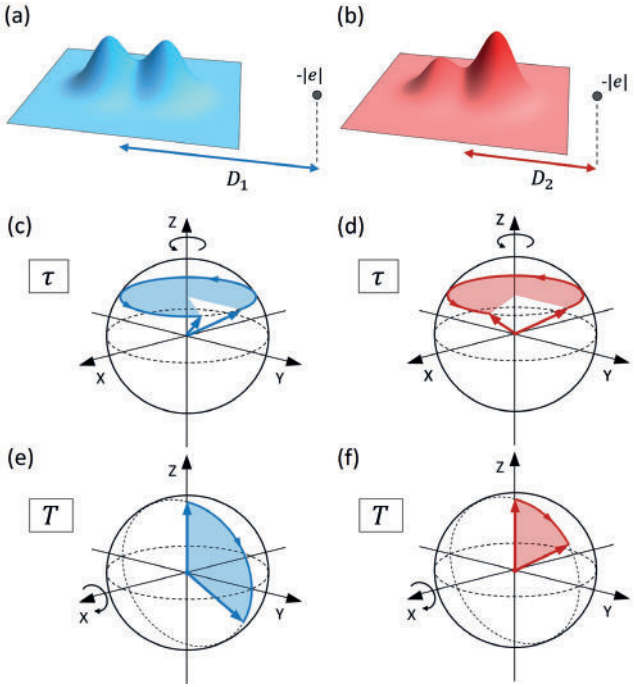

Fig. 2
Schematic representation of the effect induced by a negative charge on a hole-spin qubit, and specifically on its: charge density (a,b); Larmor frequency (c,d); Rabi frequency (e,f). These effects depend quantitatively on the distance between the remote charge and the hole-spin qubit (left vs. right panels).

Contact persons
Filippo Troiani (filippo.troiani@nano.cnr.it)
Andrea Secchi (andrea.secchi@nano.cnr.it)

References

[1] Theory of multidimensional quantum capacitance and its application to spin and charge discrimination in quantum dot arrays. A. Secchi and F. Troiani. Phys. Rev. B 107, 155411 (2023).
[2] Multi-dimensional quantum capacitance of the two-site Hubbard model: the role of tunable interdot tunneling. A. Secchi and F. Troiani. Entropy 25, 82 (2023).
[3] Quantum estimation and remote charge sensing with a hole-spin qubit in silicon. G. Forghieri, A. Secchi, A. Bertoni, P. Bordone, and F. Troiani. Phys. Rev. Research 5, 043159 (2023).

Projects

H2020–FETOPEN–2018–2019–2020–01 IQubits (GA 829005).

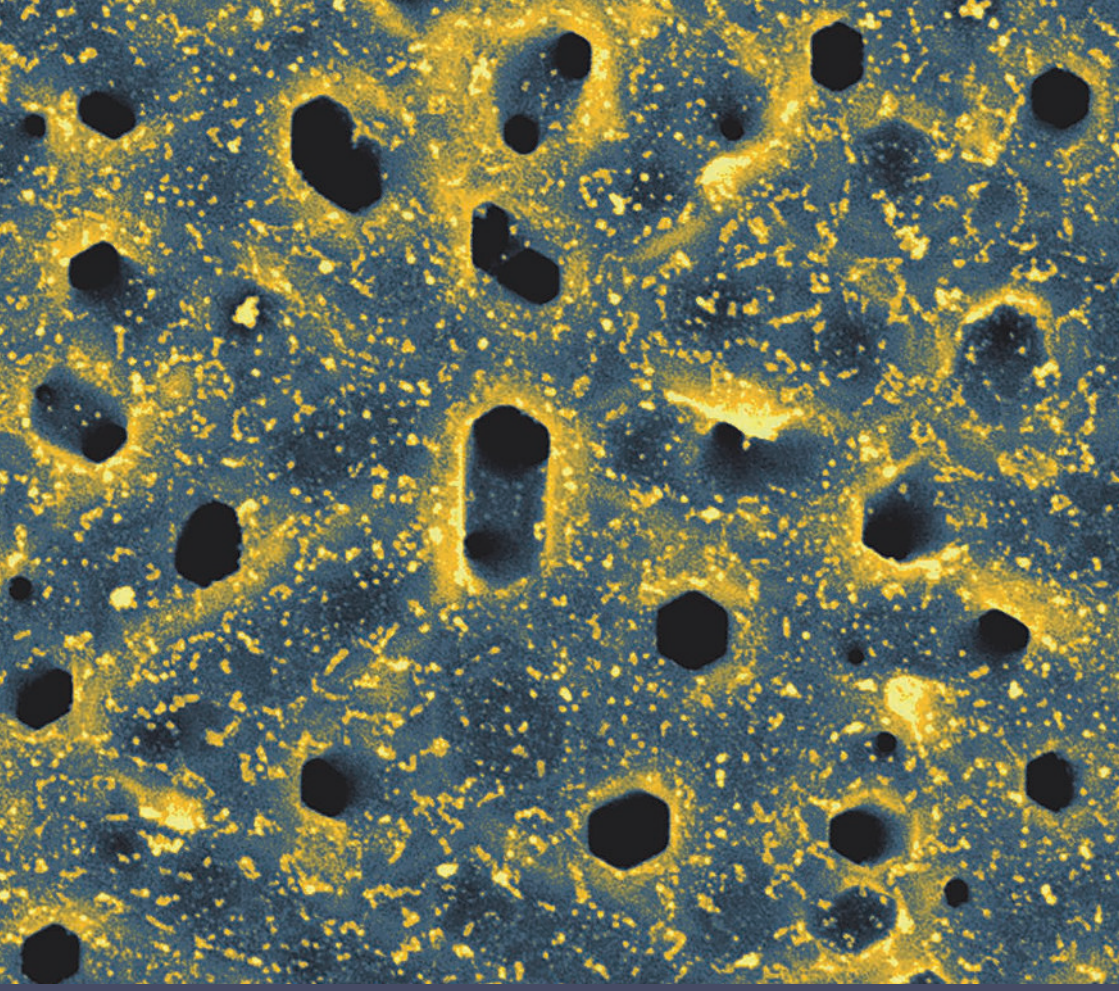

Highlights
-
Surfaces and interfaces: nanofabrication, imaging, and spectroscopy

The thematic area concerning "**Surfaces and Interfaces: nanofabrication, imaging, and spectroscopy**" is focused on the use of nanotechnologies to realize outperforming materials and devices for energy harvesting, storage, and sensing. The investigated materials are in most cases prepared in the laboratories of the Institute, exploiting facilities for physical and chemical deposition or for material treatments in controlled environment, like molecular beam epitaxy, sputter deposition also combined with inert gas-aggregation, or thermal treatments and irradiations, and employing advanced fabrication techniques like lithography and focused ion beam. The classes of materials investigated range from oxides to 2-dimensional materials, from semiconducting to plasmonic nanostructures. Material properties and devices are investigated with several advanced spectroscopic techniques in the laboratories and at synchrotron radiation facilities, with more and more attention given to the ability to actively tune the response of the materials and in combination with ab initio calculation. For the assessment of morphology at high resolution, scanning probe microscopes and transmission electron microscope are used. Furthermore, new MEMS-based electron optics for the TEM are realized in our labs to control the beam in space and time, exploiting artificial intelligence to efficiently control these non-standard optics. Time-resolved studies by ultrafast spectroscopies allow to follow the dynamics of electronic and plasmonic excitations at the femtosecond time scale and to identify the corresponding decay channels.

The search for improved materials for **energy harvesting and conversion** involves the **design of nanostructures and films with tunable properties**. In this direction, the coupling of metal plasmonic nanoparticles with reducible oxides has been explored as

one route to increase the reactivity of wide band gap materials in the visible range. The spectroscopic investigation of the time-resolved dynamics of energy and charge transfer will open the way to a better understanding of their electronic and optical properties and to a more efficient design of materials. Other routes involve the control of composition, superlattice periodicity and structure during the growth process to design tunable thermal, acoustic, and optoelectronic properties. The modification of superlattice periodicity and composition induces the appearance of new phonon modes in semiconducting nanowires, while the introduction of twins determines a reduction of thermal conductivity. In the same direction, the control of the crystalline order in transparent conducting oxide films allows to tune the electric properties and leads to the active control of the optical response of the system.

2D materials are largely investigated for **sensing and storage**. Different ways of defect engineering and structural modifications have been explored to implement the activity of several 2D materials, like graphene and boron nitride, and their responses have been assessed through spectroscopies in combination with ab initio calculations. The introduction of defects by irradiation or the modification of the stacking have dramatic consequences on luminescence that has been exploited to determine and control the material quality. The hydrogen uptake in graphene has been improved by the controlled hydrogenation of high-quality and high-specific area samples of nanoporous graphene. The combination of experimental techniques with ab initio simulations has led to the identification of well-defined hallmarks of the conversion from graphene to free-standing graphene. Furthermore, the realization of 3-dimensional graphene has brought to the possibility to store hydrogen even at room temperature.

Design and control of optoelectronic response of transparent conducting oxides

The control and improvement of the crystal quality of sputter deposited transparent conducting oxides like Al:ZnO allow to maintain a good mobility for exploitation in optoelectronic devices while reducing the thickness, when the presence of a high density of grain boundaries drastically degrades the electric properties. Furthermore, coupling metal nanoparticles with Al:ZnO is an interesting tool to tune the plasmonic response of the system. The induced modifications in the electronic properties of the Al:ZnO film induces a change in the plasmonic response of Au nanoparticles in contact with the oxide, providing a way to design the optical response of the entire system.

Transparent conducting oxides (TCO) like Al:ZnO (AZO) are used to obtain transparent films with a high conductivity for application in plasmonics and in optoelectronics. However, the requirement of thinner films determines the realization of materials with degraded electrical properties. To improve their quality one possibility is the growth of single crystalline layers exploiting epitaxy. By means of sputter deposition we have exploited perovskite $SrTiO_3$(110) substrates to guide the growth of AZO films of thickness down to 30 nm (Fig. 1a). Epitaxial films show a markedly improved resistivity compared to polycrystalline films of comparable thickness (Fig. 1b). By analyzing the resistivity and carrier mobility of the two classes of films, we have determined that the role of the grain boundaries is dominating scattering in polycrystalline films, while, on the contrary, in epitaxial AZO it is determined mainly by impurity scattering [1]. This leads to thin films with improved optoelectronic response that can be exploited for the active control (e.g., through electrical bias) of the optical response in simple devices [2].

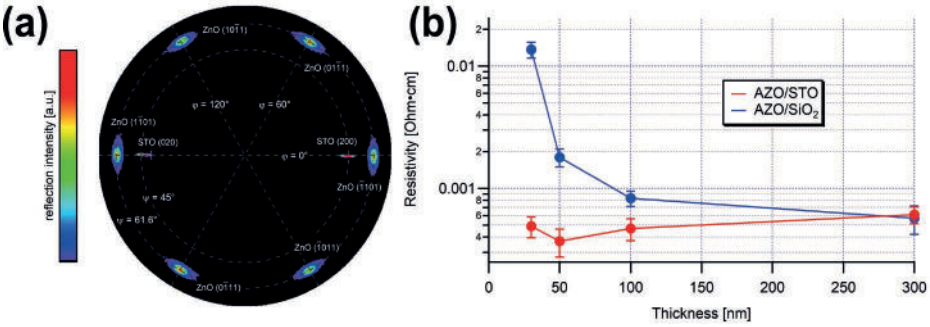

Fig. 1
(a) XRD pole figure of 300 nm AZO/SrTiO3(110) indicating the epitaxial growth of the oxide film with six-fold symmetry. (b) Electrical resistivity of the epitaxial AZO films on SrTiO3(110) (red) compared to that of polycrystalline films (blue). The resistivity of AZO increases with decreasing thickness in polycrystalline films, while it remains constant in epitaxial films.

Another route to act on the optoelectronic response is to couple TCO with plasmonic metal nanoparticles (NPs). Within a NP–TCO system, the TCO can tune the plasmon resonance of the NPs by modifying the TCO dielectric function via doping. We have shown by spectroscopic ellipsometry that localized surface plasmon resonance (LSPR) in Au NPs, occurring at around 2 eV, blue-shifts when the dopant concentration of Al in AZO increases from 0 to 4 at.% (Fig. 2) [3]. The reason is that the increase of chemical potential in AZO due to the doping promotes a charge accumulation in the Au NPs, which in turns leads to a blue-shift of the LSPR. From this shift we can obtain an estimation of the average charge transferred to the NPs of about 0.05 and 0.11 e/atom for 2 and 4 at. % AZO films, respectively. This could have interesting implications in terms of either passively or actively tuning the optical response of hybrid plasmonic/TCO systems, exploitable for a broad range of applications, such as in light harvesting and photocatalytic devices.

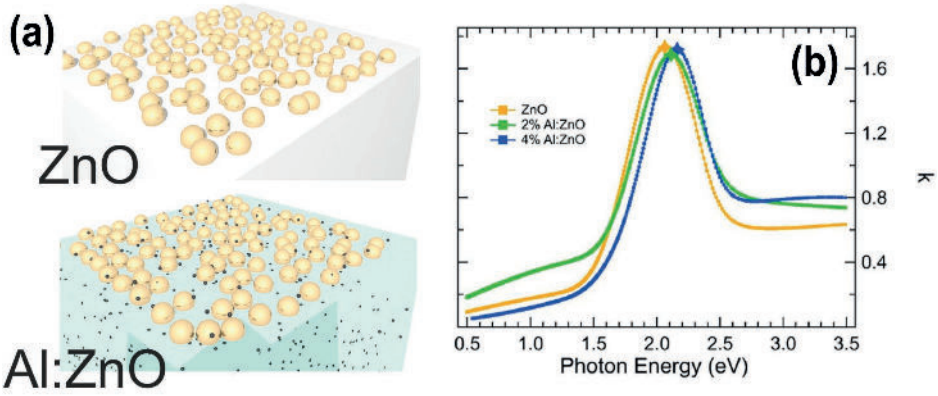

Fig. 2
(a) Schematic of the evolution of the optical properties of NPs on top of TCO films as a function of the TCO doping level. (b) Extinction coefficient of the effective Au-NP layer on bare ZnO and AZO films, as extracted by spectroscopic ellipsometry. Markers on the peak were placed to remark the LSPR blue-shift.

Contact persons
Stefania Benedetti (stefania.benedetti@nano.cnr.it)
Alessandro di Bona (alessandro.dibona@nano.cnr.it)

References
[1] Suppression of grain boundary contributions on carrier mobility in thin Al-doped ZnO epitaxial films. R. Magrin Maffei, A. di Bona, M. Sygletou, F. Bisio, S. D'Addato, and S. Benedetti. Appl. Surf. Sci 624, 157133 (2023).
[2] In-Operando Optical Spectroscopy of Field-Effect-Gated Al-Doped ZnO. M. Sygletou, S. Benedetti, A. di Bona, M. Canepa, F. Bisio, and E. Bellingeri. ACS Appl. Mater. Interfaces 15, 3112 (2023).
[3] Doping-dependent optical response of a hybrid transparent-conductive oxide/plasmonic medium. M. Sygletou, S. Benedetti, A. di Bona, F. Bisio, and M. Canepa. J. Phys. Chem. C. 126, 1881 (2022).

Development of 2D artificial systems via low-energy electron irradiation

Controlling the optical and the electronic properties of 2D materials by low-energy electron irradiation enables the creation of 2D artificial systems having functionalities that are not available in the material constituents and in nature. These systems largely contribute to the development of novel devices with applications in quantum optics and electronics, sensing, as well as in energy mastering and harvesting.

When irradiating the graphene lattice by electron beam, structural defects are efficiently generated [1-3]. These defects evolve with time until reaching a stable concentration after a partial reconstruction of the damaged lattice, as confirmed both experimentally and via molecular dynamics simulation techniques thanks to a specially developed computational protocol [1]. The defective sites are chemically reactive [2,3] and can be periodically patterned into the graphene sheet in a controlled manner with high lateral resolution (Fig. 1) [3]. Generally, defective graphene is a good candidate in energy harvesting and sensing devices thanks to the possible deterministic spatially-controlled functionalization. Instead, the periodical alteration of the crystalline structure can be exploited in electronics to tune the band structure, induce collective electron phenomena or manipulate the thermal properties of the graphene sheet for energy transport applications.

Among the other 2D materials, hexagonal boron nitride (hBN) is an interesting platform for quantum optics due to the peculiar defect-related luminescence properties. Indeed, defects into the hBN matrix are color centers acting as quantum sources. The energy of the emitted photons depends on the defect nature. Photon emission is observed from the defects created during the mechanical exfoliation, such as thickness steps with different crystallographic orientations, flake edges, and crystal deformation

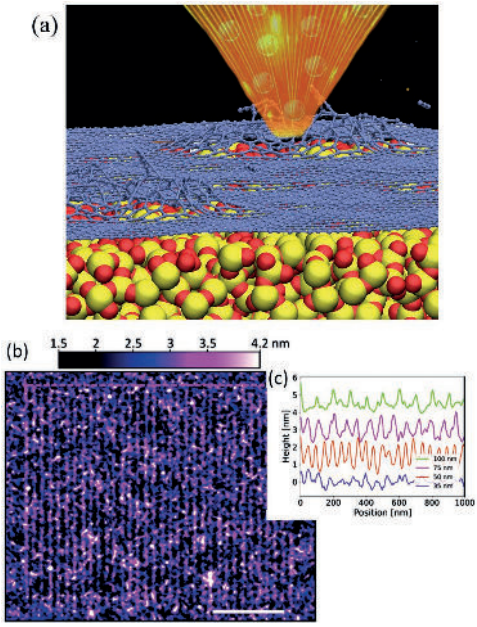

Fig. 1
a) Graphical representation of electron-irradiation of graphene sheet on silicon dioxide. b) Example of topographic height map of a pattern with a lattice with 50 nm-pitch. The patterned area is indicated by the dashed line. The scale bar is 500 nm. Adapted from [3]. c) Profile lines extracted from AFM scans of patterns with different pitches. Each line average is shifted of 1.5 nm. Adapted from [3].

[4]. On the other hand, color centers can be intentionally induced within the hBN matrix. By spatially-controlling the electron irradiation, color centers with multicolor photons emission in the green–red range can be generated [5]. This emission is strongly dependent on the electron energy and on the step-size of the irradiation pattern due to the interaction of the different irradiation spots (Fig. 2) [5]. In general, due to the multiple or single photon nature of its color centers, hBN represents the next generation of the on-demand quantum sources for quantum communication and quantum information.

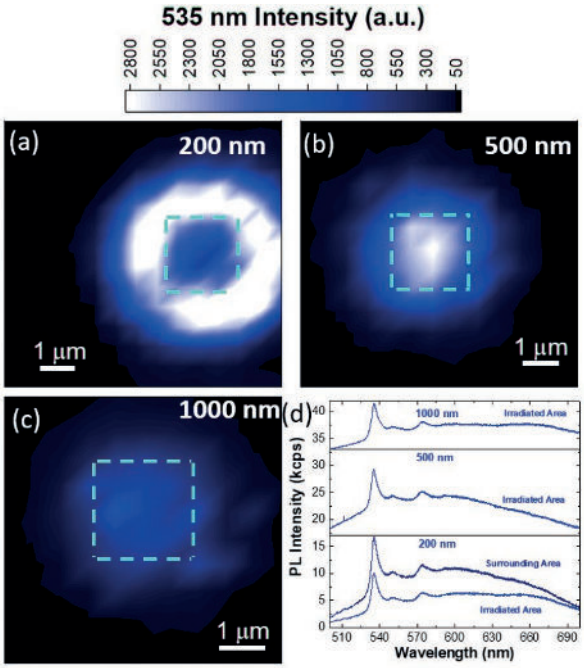

Fig. 2
Photoluminescence (PL) intensity map acquired at 535 nm for pattern spacing of 200 nm (a), 500 nm (b) and 1000 nm (c). The color bar is common to all maps. (d) PL spectra of the 15 keV electron-irradiated hBN with different pattern spacings. Adapted from [5].

Contact persons
Federica Bianco (federica.bianco@nano.cnr.it)
Filippo Fabbri (filippo.fabbri@nano.cnr.it)

References
[1] Operability timescale of defect-engineered graphene. N. Melchioni, L. Bellucci, A. Tredicucci, and F. Bianco. Surf. Interfaces 37, 102662 (2023).
[2] Deterministic organic functionalization of monolayer graphene via high resolution surface engineering. L. Basta, F. Bianco, A. Moscardini, F. Fabbri, L. Bellucci, V. Tozzini, S. Heun, and S. Veronesi. J. Mater. Chem. C 11, 2630 (2023).
[3] Periodic Structural Defects in Graphene Sheets Engineered via Electron Irradiation. N. Melchioni, F. Fabbri, A. Tredicucci, and F. Bianco. Micromachines 13, 1666 (2022).
[4] Light emission properties of mechanical exfoliation induced extended defects in hexagonal boron nitride flakes. G. Ciampalini, C. V. Blaga, N. Tappy, S. Pezzini, K. Watanabe, T. Taniguchi, F. Bianco, S. Roddaro, A. Fontcuberta i Morral, and F. Fabbri. 2D Materials 9, 035018 (2022).
[5] Engineering multicolor radiative centers in hBN flakes by varying the electron beam irradiation parameters. F. Bianco, E. Conte, S. Ditalia Tchernij, J. Forneris, and F. Fabbri. Nanomaterials 13, 739 (2023).

Projects
MIUR - PRIN 2020 q-LIMA (no. 2020JLZ52N). UE FETPROACT-EIC-05-201 LESGO (GA 952068).

Electron microscopy between artificial intelligence, novel imaging ideas, and quantum developments

Electron microscopy is a well-established method not only to image matter, but also to do spectroscopy and probe electron matter interaction at large. In this field, we try to expand this potentiality by creating new electron optics hardware [1] and control systems, and use them for new ideas of imaging and spectroscopy. We report here the progresses in the field.

The engine for creating innovative imaging and spectroscopy mode in a TEM is innovative electron optics: for this purpose, we work both on Micro Electronic Mechanical Systems (MEMS) based new electron-optics [2] and on electron-light interaction [3]. With advantages and drawbacks, both systems can be considered flexible new ways to control the beams in space and time. As these new technologies need a very accurate control system, we found that the fastest way to control a non-standard optics is by way of Artificial Intelligence (AI).
Fig. 1a shows the mechanism of beam shape control by light-electron interaction and the early experimental data showing the shape of the electron beam as controlled by the light that in turn is controlled by a Spatial Light Modulator [3].
Some results in the MEMS fabrication for the generation of caustics with a combination of vortex phases are shown in Fig. 1b. In this context we work on schemes for achieving more controllable contacts and on mathematical methods to extract and pre-

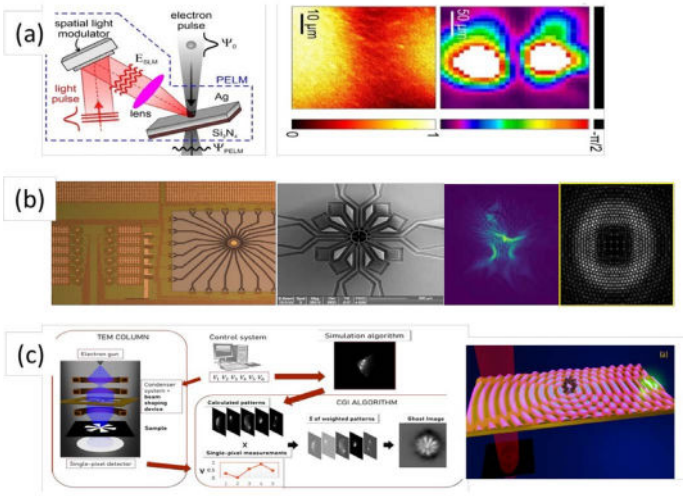

Fig. 1
(a) Schemes of light-based electron modulation (left) with first experimental data (right). (b) MEMS progresses: (left) integrated in-MEMS electronics allowing up to 24 electrodes. (centre left) new MEMS for ghost imaging. (right) example of generated caustics. (c) (left) scheme of the computational ghost imaging: recording intensity as a function of the probe shape allows image reconstruction. (right) the entanglement and the coincident collection of a bucket signal on the sample allows the imaging of the sample (here a protein on the metal plate).

dict in a precise way the wave-shape with atomic resolution. For the control of the MEMS, we also use Artificial Intelligence: e.g., a convolutional neural network with appropriate simulations as training was used to keep the alignment of the MEMS in the optical configuration of orbital angular momentum sorter we created [4,5].
Fig. 1c reports the schemes for computation [6,7] and real ghost imaging (GI) [8]. In the computational GI we correlate a series of probe with the detected intensity in a single pixel "bucket" detector. In real GI this is done by a real entanglement. Here the entanglement is between the electron and the collective excitation of the sample. In both cases by reversing the correlation and using the measured intensity at the bucket, it is possible to invert for the transmission function of the object. Computational GI can be used to beat the spherical aberration and potentially increase the resolution. The real GI can be used to reconstruct the shape and optical activity of objects on the sample without the electron beam directly investing the object.

Contact persons
Vincenzo Grillo (vincenzo.grillo@nano.cnr.it)

References
[1] Theoretical and practical aspects of the design and production of synthetic holograms or transmission electron microscopy. P. Rosi, F. Venturi, G. Medici, C. Menozzi, G. C. Gazzadi, E. Rotunno, S. Frabboni, R. Balboni, M. Rezaee, A. H. Tavabi, R. E. Dunin-Borkowski, E. Karimi, and V. Grillo. J. Appl. Phys 131, 031101 (2022).
[2] Generation of electron vortex beams with over 1000 angular momentum quanta using a tunable electrostatic spiral phase plate. A. H. Tavabi, P. Rosi, A. Roncaglia, E. Rotunno, M. Beleggia, P.-H. Lu, L. Belsito, G. Pozzi, S. Frabboni, P. Tiemeijer, R. E. Dunin-Borkowski, and V. Grillo. Appl. Phys. Lett. 121, 073506 (2023).
[3] Ultrafast transverse modulation of free electrons by interaction with shaped optical fields. I. Madan, V. Leccese, A. Mazur, F. Barantani, T. LaGrange, A. Sapozhnik, P. M. Tengdin, S. Gargiulo, E. Rotunno, J.-C. Olaya, I. Kaminer, V. Grillo, F. J. García de Abajo, F. Carbone, and G. M. Vanacore. ACS Photonics 9, 3215 (2022).
[4] Machine learning in scanning transmission electron microscopy. S. V. Kalinin, C. Ophus, P. M. Voyles, R. Erni, D. Kepaptsoglou, V. Grillo, A. R. Lupini, M. P. Oxley, E. Schwenker, M. K. Y. Chan, J. Etheridge, X. Li, G. G. D. Han, M. Ziatdinov, N. Shibata, and S. J. Pennycook. Nat. Rev. Methods Primers 2, 11 (2022).
[5] Near-real-time diagnosis of electron optical phase aberrations in scanning TEM using an artificial neural network. G. Bertoni, E. Rotunno, D. Marsmans, P. Tiemeijer, A. H. Tavabi, R. E. Dunin-Borkowski, and V. Grillo. Ultramicroscopy 245, 113663 (2022).
[6] Challenging point scanning across electron microscopy and optical imaging using computational imaging. A. Kallepalli, L. Viani, D. Stellinga, E. Rotunno, R. Bowman, G. M. Gibson, M.-J. Sun, P. Rosi, S. Frabboni, R. Balboni, A. Migliori, V. Grillo, and M. J. Padgett. Intelligent Computing 2022, 0001 (2022).
[7] Single-Pixel Imaging in Space and Time with Optically Modulated Free Electrons. A. Konečná, E. Rotunno, V. Grillo, F. J. García de Abajo, and G. M. Vanacore. ACS Photonics 10, 1463-1472 (2023).
[8] One-Dimensional "Ghost Imaging" in Electron Microscopy of Inelastically Scattered Electrons. E. Rotunno, S. Gargiulo, G. M. Vanacore, C. Mechel, A. H. Tavabi, R. E. Dunin-Borkowski, F. Carbone, I. Madan, S. Frabboni, T. Guner, E. Karimi, I. Kaminer, and V. Grillo. ACS Photonics 10, 1708 (2023).

Photoexcited states in oxide-based materials by ultrafast spectroscopies

We investigated the ultrafast dynamics of photoexcited states in systems composed of cerium oxide combined with plasmonic Au and Ag nanoparticles. The analysis of space and mirror charge effects in time-resolved photoemission spectra provided information on the characteristic reneutralization time of the positive charges generated by photoexcitation. Femtosecond transient absorption spectroscopy measurements demonstrated that the excitation of localized surface plasmon resonances in the nanoparticles leads to an ultrafast and efficient injection of electrons into the empty 4f states of the oxide, and that the injected charge undergoes a dynamic interaction with the matrix.

Oxides are abundant and stable materials, largely applied for solar to chemical energy conversion via photocatalysis. The optimization of their functionality requires a detailed dynamic description of excited carrier generation and decay. Cerium oxide is a material with wide application in catalysis and photocatalysis, although in its pure form it has a band gap in the UV. The coupling with plasmonic nanoparticles (NPs) has shown to be a promising route to sensitize the material to visible light. Localized surface plasmon resonances (LSPR) excited in the NPs can in fact decay via the injection of electrons in the surrounding oxide leading to transient modifications that can enhance the material activity.

We performed a time-resolved photoemission spectroscopy (tr-PES) experiment on a system made of Ag NPs embedded in CeO_2, using the high-harmonic generator source available at the NFFA-SPRINT facility at ELETTRA, Trieste [1]. We showed that the intensity variation of valence band tr-PES features, generated by the space charge, can be modelled to provide information on the dynamics of pump-generated surface carriers on time scales above 15 ps. The results are schematically summarized in Fig. 1. An excitation energy above the band gap (BG) of cerium oxide leads to the for-

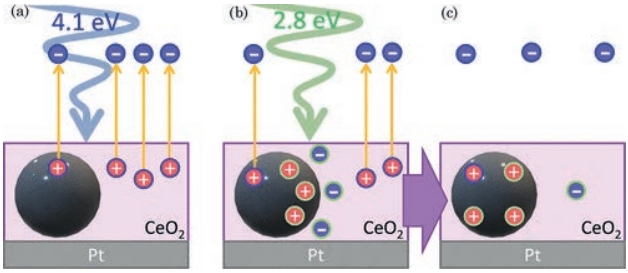

Fig. 1
Sketch of the processes that dominate after photoexcitation at different pump energies for Ag@CeO2. (a) A pump at 4.1 eV (above the CeO2 BG) forms holes in the NPs and in the oxide on defect states and by multiphoton-induced photoemission; (b) a pump at 2.8 eV (LSPR) forms a few holes in the oxide and in the NPs by multiphoton-induced photoemission (blue contour) and a relevant number of holes on the NPs via plasmon-mediated electron injection from the NP to the oxide (green contour); (c) in the oxide the electrons and holes recombine within short times (<15 ps) and leave uncompensated long-living positive charges on the NPs surface.

mation of holes with lifetimes around 100 ps, while the excitation of sub-BG LSPR in the NPs leads to the formation of uncompensated positive charges on the metal surface with much longer lifetimes, above 300 ps.

If Au NPs are used, LSPR excitations relax by transferring electrons to the surrounding semiconductor, as shown in a femtosecond transient absorbance study [2]. A few picoseconds after photoexcitation, both the BG and LSPR excitation lead to the same bulk-like polaronic state. At shorter delay times below a few picoseconds, a markedly different energetic and temporal dynamics is observed in the case of LSRP-mediated injection as compared to BG excitation (Fig. 2). The electron injection efficiency following LSPR excitation shows a maximum over 30% at a photon energy that does not correspond to the maximum of LSPR-related optical absorptance, suggesting that different injection mechanisms take place at the different photoexcitation energies.

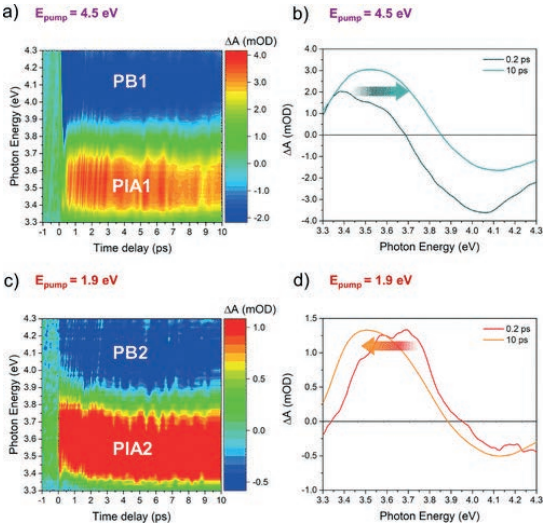

Fig. 2
False-color map of the transient absorption spectra of Au@CeO2 excited with pumps at (a) 4.5 eV (above the CeO2 BG) and (c) 1.9 eV (below BG at LSPR). (b, d) The transient absorption spectra at selected delay times of 0.2 and 10 ps show a different evolution with delay time for the two pump energies, ascribed to the different electronic properties at the interface between the metal NP and the oxide.

Contact persons
Paola Luches (paola.luches@nano.cnr.it)
Stefania Benedetti (stefania.benedetti@nano.cnr.it)

References

[1] Lifetime of Photogenerated Positive Charges in Hybrid Cerium Oxide-Based Materials from Space and Mirror Charge Effects in Time-Resolved Photoemission Spectroscopy. J. S. Pelli Cresi, E. Spurio, L. Di Mario, P. O'Keeffe, S. Turchini, S. Benedetti, G. M. Pierantozzi, A. De Vita, R. Cucini, D. Catone, and P. Luches. J. Phys. Chem. C 126, 11174 (2022).
[2] Injecting Electrons into CeO2 via Photoexcitation of Embedded Au Nanoparticles. E. Spurio, J. S. Pelli Cresi, G. Ammirati, S. Pelatti, A. Paladini, S. D'Addato, S. Turchini, P. O'Keeffe, D. Catone, and P. Luches. ACS Photonics 10, 1566 (2023).

Projects

NextGenerationEU PNRR MUR National Sustainable Mobility Center CN00000023 Spoke 11, Innovative Materials & Lightweighting.

Distinguishing different stackings in layered materials via luminescence spectroscopy

We present a combined experimental and theoretical study on ultraviolet-light emission in hexagonal and rhombohedral bulk boron nitride crystals. Emission spectra of high-quality samples are measured via cathodoluminescence spectroscopy, displaying characteristic differences between the two polytypes. These differences are explained using a fully first-principles computational technique that takes into account radiative emission resulting from the coupling of excitons (bound electron-hole pairs) and phonons. We show that with this approach the differences in peak positions, number of peaks and relative intensities can be qualitatively and quantitatively explained.

The microscopic control of Van der Waals stacking configurations is emerging as an important tool for tailoring the optoelectronic properties of layered materials. Stacking variations have been shown to induce non-trivial topological or ferroelectric properties and enhance carrier mobilities, making it crucial to understand their impact on electronic excitations.

We conduct a theoretical and experimental spectroscopic investigation of boron nitride in the hexagonal (hBN) and rhombohedral (rBN) stacking configurations. These are two prototypical polytypes of low-dimensional layered materials with indirect band gaps, and are hardly distinguishable with standard crystallographic tools.

Our focus is on cathodoluminescence (CL) spectroscopy. With an original CL setup, we are able to resolve the intrinsic rBN fine structure, enabling a clear comparison with analogous results for hBN. We demonstrate that the stacking sequence affects the emission fine structure, making CL an ideal experimental probe to distinguish the two crystals [1].

The experimental luminescence spectra are quantitatively reproduced by first-principles calculations, explicitly including exciton-phonon interactions with a new approach based on many-body perturbation theory (Fig. 1). In fact, the radiative emission spectra are affected by the coupling between electronic excitations and lattice vibrations, as different phonon modes mediate the recombination of electron-hole bound pairs (excitons). Our calculations allow for a thorough analysis of finite-momentum exciton states and their coupled phonons: the critical discriminating role is played by out-of-plane lattice vibrations, which assist excitonic radiative recombination in rBN but not in hBN, where their coupling to the excitons is forbidden by symmetry, thus causing the difference in the spectral fine structures.

Our methodology may aid in growing and characterizing indirect-gap layered materials, enabling the discrimination of various layer-stacking sequences and thus linking sample quality and properties to the expected performance of optoelectronic devices.

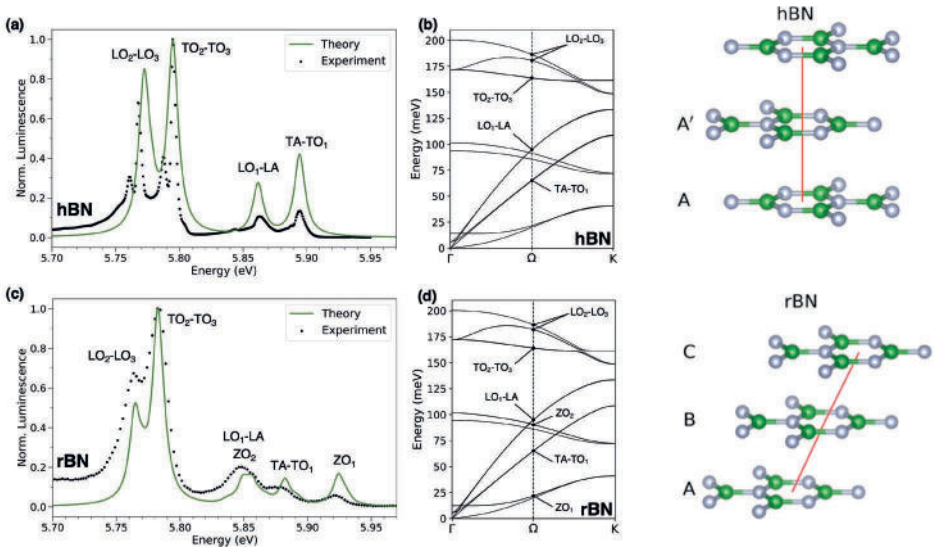

Fig. 1
Experimental (black dots) and theoretical (green lines) luminescence spectra for hBN (a) and rBN (c). The exciton-phonon satellites are labeled according to the phonon mode responsible for the exciton recombination. Phonon dispersions in hBN (b) and rBN (d) along the Γ-K direction: phonon branches contributing to the luminescence spectra are highlighted at the Ω point, in the middle of the Γ-K direction. The stacking difference between hexagonal and rhombohedral BN atomic lattices is displayed on the right (boron atoms in green, nitrogen atoms in gray).

Contact persons
Fulvio Paleari (fulvio.paleari@nano.cnr.it)
Daniele Varsano (daniele.varsano@nano.cnr.it)

References
[1] Distinguishing Different Stackings in Layered Materials via Luminescence Spectroscopy. M. Zanfrognini, A. Plaud, I. Stenger, F. Fossard, L. Sponza, L. Schué, F. Paleari, E. Molinari, D. Varsano, L. Wirtz, F. Ducastelle, A. Loiseau, and J. Barjon. Phys. Rev. Lett. 131, 206902 (2023).

Projects
HORIZON-EUROHPC-JU-2021-COE-01 MaX - MAterials design at the eXascale (GA 101093374).
NextGenerationEU - PNRR ICSC – Centro Nazionale di Ricerca in High Performance Computing, Big Data and Quantum Computing.

Tracking the conversion from graphene to hydrogenated graphene

The conversion of free-standing graphene (Gr) into graphane - where each C atom is sp_3 bound to a hydrogen atom - is investigated by combining X-ray photoelectron spectroscopy and spectro-microscopy, Raman spectroscopy, and high-resolution electron energy-loss spectroscopy (HREELS) with ab-initio based modelling. The different results are all compatible with the predicted fingerprints of H adsorption on both sides of Gr, corresponding to the graphane configuration. Valence band photoemission and HREELS spectra show the appearance of a large-gap semiconducting phase upon hydrogenation, consistent with ab-initio prediction of a large quasiparticle gap opening and huge exciton binding energy.

Maximum storage of hydrogen in carbon-based materials is ideally achieved in graphene by forming the so-called graphane, where each carbon atom in the honeycomb lattice is bound to hydrogen with alternately up and down sp_3 distorted bonds. However, the experimental observation of the graphane phase has been hindered so far, with H storage capacity far from ideal on single-layer graphene, in addition to contamination, defects, and substrate effects. Thanks to a novel approach for the controlled hydrogenation of high-quality and high-specific-area samples of nanoporous graphene (NPG) and to the combination of complementary experimental techniques with ab initio simulations, we have been able to identify well-defined hallmarks of the conversion from graphene to free-standing graphane. The effects of local rehybridization from sp_2 to sp_3 chemical bonding are investigated by combining X-ray photoelectron spectroscopy and spectro-microscopy, high-resolution electron energy-loss spectroscopy (HREELS) with ab-initio based modelling. By exploiting the D isotope, the characteristic stretching frequency of adatoms on the C sites is studied with vibrational HREELS and density-functional theory (DFT) simulations, allowing us to unequivocally identify the predicted fingerprints of adsorption on both sides of Gr corresponding to the graphane configuration [1]. Moreover, the photoemission spectral density shows the presence of a valence band maximum (VBM) at about 3.50 eV below the Fermi level, which is paired to the appearance of a transition onset at about 3.25 eV resulting from electron energy loss, clearly confirming the transition from semimetallic suspended graphene to a semiconducting phase with a large optical band gap (Fig. 1), in conformity with theoretical predictions [2]. All these signatures prefigure a semiconducting phase, key for both fundamental knowledge of 2D materials and for emerging applications of graphene in electronic and opto-electronic devices.

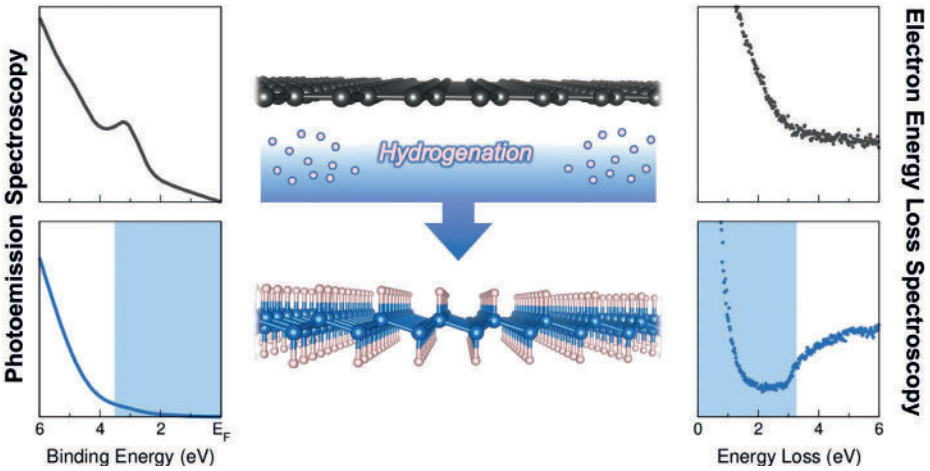

Fig. 1
Photoemission and electron energy loss spectroscopies evidence the graphene to graphane (double-sided hydrogenated graphene) transition thanks to the corresponding gap opening.

Contact persons
Deborah Prezzi (deborah.prezzi@nano.cnr.it)
Valentina De Renzi (vderenzi@unimore.it)

References
[1] Dielectric response and excitations of hydrogenated free-standing graphene. M. G. Betti, D. Marchiani, A. Tonelli, M. Sbroscia, E. Blundo, M. De Luca, A. Polimeni, R. Frisenda, C. Mariani, S. Jeong, Y. Ito, N. Cavani, R. Biagi, P. N. O. Gillespie, M. A. Hernandez Bertran, M. Bonacci, E. Molinari, V. De Renzi, and D. Prezzi. Carbon Trends 12, 100274 (2023).
[2] Gap Opening in Double-Sided Highly Hydrogenated Free-Standing Graphene. M. G. Betti, E. Placidi, C. Izzo, E. Blundo, A. Polimeni, M. Sbroscia, J. Avila, P. Dudin, K. Hu, Y. Ito, D. Prezzi, M. Bonacci, E. Molinari, and C. Mariani. Nano Lett. 22, 2971 (2022).

Projects
H2020-INFRAEDI-2018-1 MaX – Materials design at the eXascale (GA 824143). HORIZON-EUROHPC-JU-2021-COE-1 MaX – Materials design at the eXascale (GA 101093374).
POR FESR 2014-2020 Regione Emilia-Romagna SUPER (Supercomputing Unified Platform-Emilia-Romagna).

Epitaxial graphene growth on porous 4H-SiC(0001): a versatile platform for gas storage and sensing

The outstanding properties of graphene rely on its perfect 2D hexagonal crystal structure. However, several applications, such as sensing, energy applications, catalysis, drug delivery, and many others, require a high surface-to-volume ratio and a three-dimensional structure. The growth of epitaxial graphene in a 3D arrangement on the contours of a porous backbone of 4H-SiC(0001) allows the realization of high-quality graphene with a three-dimensional structure (3DG). Indeed, the synergy between the outstanding properties of graphene and a 3D porous structure, circumventing the limits of the 2D nature of graphene, constitutes a breakthrough for many fields.

The porous 4H-SiC material is obtained via a sequence of metal-assisted photochemical and photoelectrochemical etching in hydrofluoric acid-based electrolytes [1]. The fabrication allows the control of the local definition of the pores as well as the degree of porosity with depth. Moreover, the porosification technique allows obtaining stacked layers of different porosity, increasing the versatility of this material. Epitaxial graphene is successively grown on this porous substrate via thermal annealing in an ultra–high vacuum environment. Fig. 1a shows the scanning electron microscopy (SEM) image of a 3DG sample top surface, Fig. 1b the transmission electron microscopy (TEM) image of the cross-section. The role of chemisorption and physisorption, in the hydrogen uptake of 3DG, is investigated by exposing samples to atomic and molecular hydrogen at room temperature and at low temperature (100 K) [2]. We demonstrate, for the first time, the adsorption of molecular hydrogen in 3DG samples (Fig. 1c). Indeed, while the ability of epitaxial graphene to bind atomic hydrogen is well documented, the binding of molec-

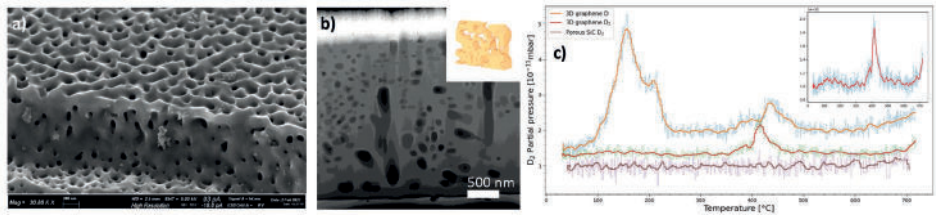

Fig. 1
a) SEM image of the top surface and edge of a 3DG sample after epitaxial growth of graphene at 1370 °C under ultra-high vacuum conditions. b) TEM cross section of a 3DG sample. The inset shows the electron tomographic reconstruction of the porous structure. c) Thermal desorption spectra after hydrogenation of 3DG with atomic and molecular hydrogen. Orange and red curves show the hydrogen desorption peaks after the exposure to atomic (orange) and molecular (red) hydrogen, demonstrating the hydrogen uptake. The lower flat curve is the hydrogenation of the porous SiC before the graphene growth, showing a negligible hydrogen uptake.

ular hydrogen at room temperature has never been reported before. This feature highlights the peculiar characteristics of 3DG in the molecular hydrogen uptake, suggesting that catalytic sites able to split hydrogen molecules are active in 3DG. In view to enhance hydrogen storage efficiency, 3DG samples have been functionalized with metal nanoparticles (Fig. 2a), in particular Au and Pd nanoparticles. Besides, we have utilized a 3DG sample as sensor of the Volatile Organic Compounds related to the degradation of hazelnuts, demonstrating the ability to discriminate between healthy and damaged hazelnuts (Fig. 2b) [3]. Our results open the perspective of sensor development utilizing specific functionalization for the target molecules.

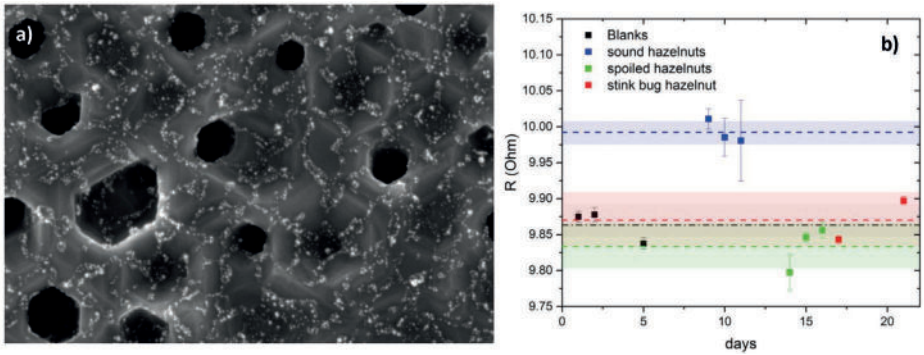

Fig. 2
a) SEM image of the top surface of a 3DG sample after functionalization with Pd nanoparticles. b) Sensor resistance in a series of measurements covering several days. The sensor ability to discriminate between healthy and damaged hazelnut is evident.

Contact persons
Stefan Heun (stefan.heun@nano.cnr.it)
Stefano Veronesi (stefano.veronesi@nano.cnr.it)

References
[1] 3D arrangement of epitaxial graphene conformally grown on porousified crystalline SiC. S. Veronesi, G. Pfusterschmied, F. Fabbri, M. Leitgeb, O. Arif, D. A. Esteban, S. Bals, U. Schmid, and S. Heun. Carbon 189, 210 (2022).
[2] Study of hydrogen absorption in a novel three-dimensional graphene structure: Towards hydrogen storage applications. A. Macili, Y. Vlamidis, G. Pfusterschmied, M. Leitgeb, U. Schmid, S. Heun, and S. Veronesi. Applied Surface Science 615, 156375 (2023).
[3] Three-dimensional graphene on a nano-porous 4H-SiC backbone: a novel material for food sensing applications. S. Veronesi, Y. Vlamidis, L. Ferbel, C. Marinelli, C. Sanmartin, I. Taglieri, G. Pfusterschmied, M. Leitgeb, U. Schmid, F. Mencarelli, and S. Heun. J. Sci. Food Agric. http://doi org/10.1002/jsfa.13118 (2023).

Superlattice nanowires for phonon engineering and thermoelectric energy conversion

The growth and characterization of two kinds of nanowire superstructures are presented: GaAs/GaP superlattice embedded in GaP nanowires and InAsSb twin superlattice nanowires. In the first case, we show the appearance of new phonon modes and their tunability by changing the superlattice periodicity. In the second case, we demonstrate a drastic reduction of the thermal conductivity in InAsSb nanowires, as a result of the introduction of periodic twin planes along the growth axis. Our results prove the possibility to obtain nanomaterials with designed tunable thermal, acoustic, and optoelectronic properties by controlling their structure and composition during the growth process.

Semiconductor nanowires (NWs) offer a myriad of possibilities to engineer systems at the nanoscale by controlling the size, the growth orientation, the chemical composition, and by combining different materials or crystal phases in heterostructures which cannot be realized in conventional geometries. This provides a great opportunity to explore new optical, electrical, and vibrational properties resulting from the superstructure.
In this context, we investigated the growth of GaAs/GaP superlattices embedded in GaP NWs by means of Au-assisted chemical beam epitaxy. By optimizing the growth conditions, we could obtain a great control of nanowire diameter, growth rate, interface sharpness, and superlattice periodicity (Fig. 1a), offering a high degree of freedom for engineering phononic and photonic properties at the nanoscale [1]. In fact, we observed clear modifications in the dispersion relation for both acoustic and optical phonons (Fig. 1b), as well as a strong room temperature photoluminescence (Fig. 1c) in the superlattice NWs. Moreover, we found that we can tune the phonon frequencies by controlling the superlattice periodicity (Fig. 1d) [2].

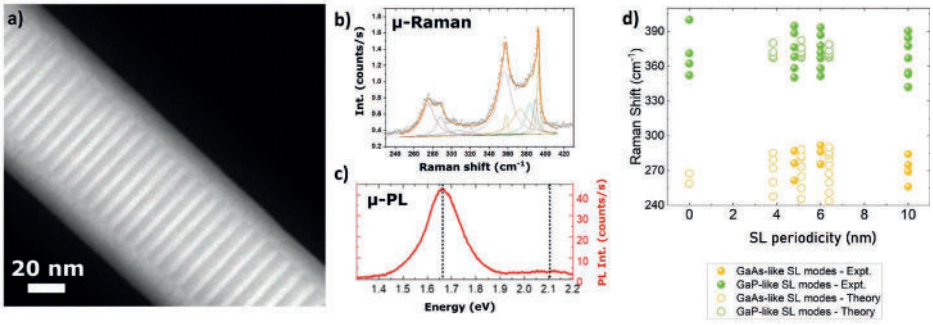

Fig. 1
GaAs/GaP superlattice NWs. (a) STEM image of a portion of a superlattice NW: GaAs segments appear brighter than GaP segments. (b) μ-Raman and (c) μ-photoluminescence spectra acquired in the superlattice portion of a single NW. (d) Raman peak positions extracted from experimental measurements (filled circles) and calculated (open circles) for superlattice NWs with different periodicity.

NWs with functional interfaces are extremely promising also for thermoelectric applications since they may display suppressed phonon transport, while preserving good electrical transport properties. In fact, we could demonstrate a drastic reduction of the thermal conductivity of InAsSb NWs as a result of the introduction of periodic crystal-lattice twin planes during growth. Importantly, the amount of Sb incorporated in the NWs can be tuned by the precursor fluxes and determines the twin periodicity (Fig. 2a,b). The electrical and thermal transport of these nanostructures, known as twinning superlattice NWs, were probed and compared with their twin-free counterparts (Fig. 2c,d), showing up to ten-fold enhancement of the thermoelectric figure of merit, ZT [3]. Our studies shed fresh insights into how material engineering at the nanoscale can tailor the phonon dispersion and open new pathways for thermal engineering.

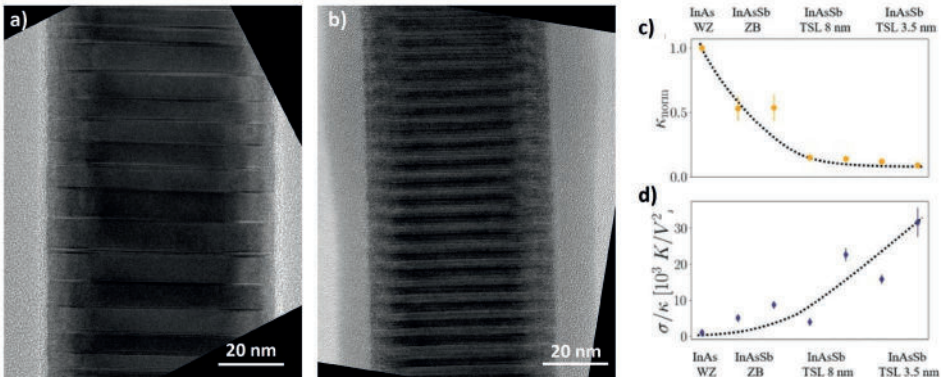

Fig. 2
InAsSb twin superlattice NWs. HRTEM images of a portion of the superlattice NWs with: (a) 2% Sb and 8 nm twin periodicity and (b) 5% Sb and 3.5 nm twin periodicity. (c) Measured thermal conductivity normalized for the NW diameter for different NWs (wurtzite InAs, pure zincblende InAsSb, and twinned InAsSb with different periodicity). (c) Ratio of electrical and thermal conductivity for the different NWs, indicating a strong increase of the thermoelectric figure of merit ZT as the number of twin planes increases.

Contact persons
Valentina Zannier (valentina.zannier@nano.cnr.it)
Lucia Sorba (lucia.sorba@nano.cnr.it)

References
[1] GaAs/GaP superlattice nanowires: growth, vibrational and optical properties. O. Arif, V. Zannier, F. Rossi, D. De Matteis, K. Kress, M. De Luca, I. Zardo, and L. Sorba. Nanoscale 15, 1145 (2023).
[2] GaAs/GaP Superlattice Nanowires for Tailoring Phononic Properties at the Nanoscale: Implications for Thermal Engineering. A. Kanjampurath Sivan, B. Abad, T. Albrigi, O. Arif, J. Trautvetter, A. Ruiz-Caridad, C. Arya, V. Zannier, L. Sorba, R. Rurali, and I. Zardo. ACS Applied Nano Materials 6, 18602 (2023).
[3] Giant reduction of thermal conductivity in twinning superlattice InAsSb nanowires. L. Peri, D. Prete, V. Demontis, V. Zannier, F. Rossi, L. Sorba, F. Beltram, and F. Rossella. Nano Energy 103, 107700 (2022).

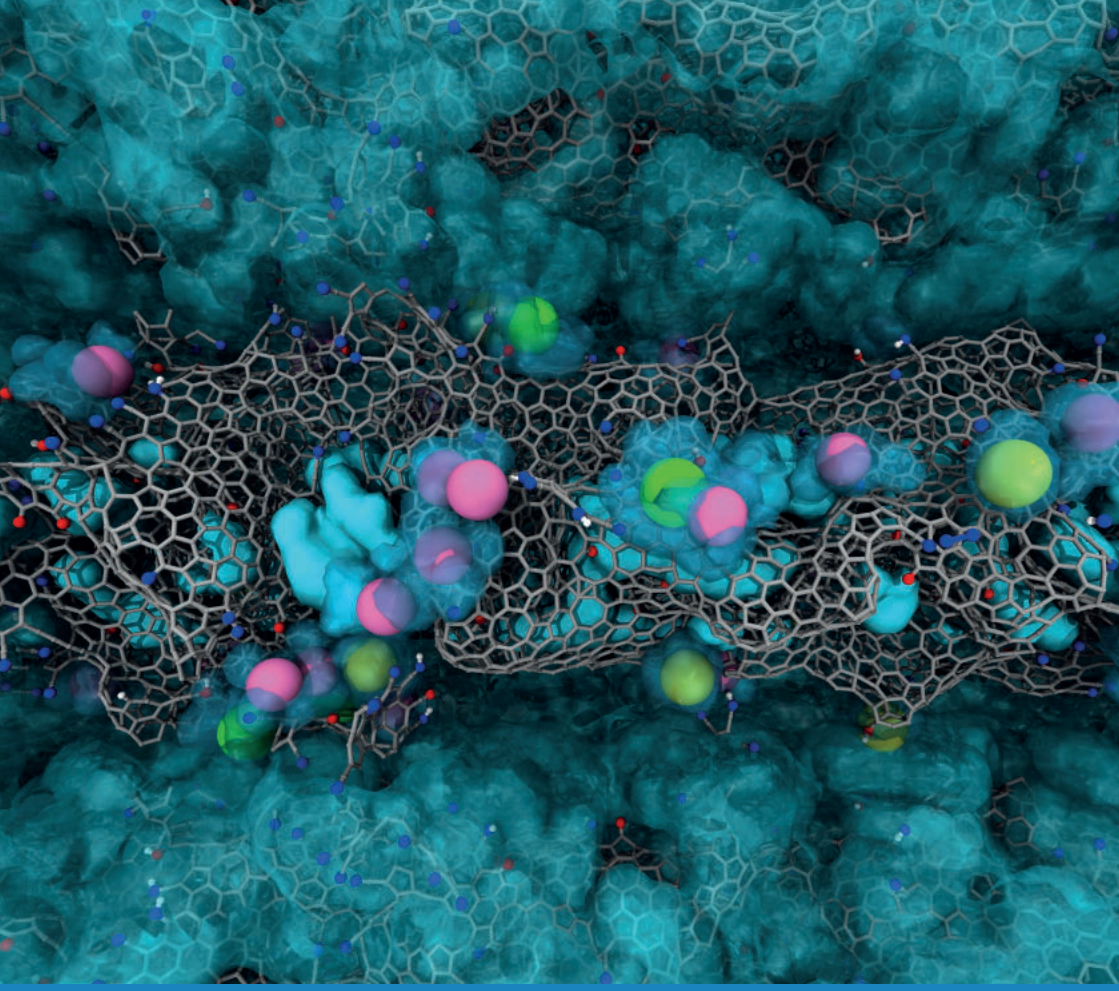

Highlights
-
Nanoscale theory modelling and computation

Driven by continuous progress in theory and algorithms and taking advantage of the rapid evolution of hardware capabilities, **theory modelling and computation** have reached an extraordinary level of predictive accuracy in characterising materials properties and exploring novel states of matter. This progress is coupled with computational efficiency, enabling the intricate complexities of realistic systems to be captured at an atomistic level.

The continuously expanding toolkit encompasses classical and quantum molecular dynamics simulations, to ab-initio approaches targeting both the ground state and excited states, and time dependent methods that access ultrafast timescales. These approaches allowed the investigation of **light-driven carrier excitations in Germanium via attosecond transient reflection spectroscopy**. Or the studies **on how III-V nanowires doping affects their optical absorption spectra.** But there are also examples of multi-scale hybrid quantum/classical computational approaches, and a variety of modelling procedures.

Cnr Nano research plays a pivotal role in expanding this toolkit by contributing to the development of models that describe emerging physical phenomena and by pioneering new theoretical frameworks. One example is the development of **Ensemble DFT that solves excited-state problems by interpolating solutions from the high-and low-electron density cases**. The institute further contributes to the computational landscape with the development of new algorithms and workflows designed to expedite and enhance the accuracy of large scale many body perturbation theory calculations, such as **an efficient frequency description of the screened Coulomb interaction**. These contributions are disseminated both through in-house written codes and legacy codes shared within the wider scientific community, fostering collaborative advancements in the field.

This field of research also leverages on existing state of the art methods to access a diverse array of physical phe-

nomena. This encompasses investigations of light matter interaction and ultrafast electron dynamics, magnetism and magnetic anisotropy, spin-orbit interactions, doping, charge transfer and excitations in many-body systems. One of the highlight presented here contributes to **enhance the spin lifetimes of single-atom magnets on oxide substrates**. A second one investigates the **thermodynamics and kinetics of charge transfer events in complex biomolecular systems.**

The materials under study are as diverse as the methods, ranging from model systems to complex organic molecules, with a special interest in low dimensional materials. In the selected highlights one can find fermion lattices, single crystals, carbon nanotubes, and also 3D graphene architectures, 2D monolayers, nanowires, single atom magnets on oxide substrates, photoenzymes and functionalized peptides. In the next pages, we present studies exploring **3D graphene architectures for water filters and neutrino detectors, as well as also Feringa molecular motors.**

These materials are put to use in applications as diverse as photocatalysis, light harvesting and nanophotonic sources, and nanomedicine. They serve to the development of nanoscale devices, quantum computing gates. Some are useful also as laboratories for the study of fundamental physical phenomena such as **permanent Bose-Einstein condensate of excitons**.

Nanoscale theory modelling and computation is an ever expanding part of Cnr Nano research activities. Simulations can reveal physical processes that are not accessible by experiments alone, can accelerate the design and understanding of new materials and devices, as well as give insight to fundamental physics problems. Either incorporating established methodologies or creating new ones, researchers can comprehensively probe and understand a wide spectrum of intricate phenomena in materials science and computational physics.

Field-driven Attosecond Charge Dynamics in Germanium

The major route towards the possibility to manipulate the electro-optical properties of a solid is based on the employment of short light pulses to excite and control charges in matter on ultrafast timescales. We investigated the light-driven carrier excitation in monocrystalline Germanium via attosecond transient reflection spectroscopy. We show that the complex regime established during light–matter interaction eludes the scope of commonly used simplified models but requires a detailed analysis in time and reciprocal space to address diverse phenomena such as tunneling, band dressing, intra-band motion, and multiphoton injection.

Pump-probe spectroscopy is one of the most advanced, and yet intuitive ways, to experimentally study ultrafast electron dynamics. The development of experimental methods to generate attosecond light pulses was awarded with the Nobel Prize in Physics in 2023. In this technique, an ultrashort pulse is split in two time-delayed portions; the intense part of the beam (pump) is used to excite the material, generating a non-equilibrium state; the weak part of the beam (probe) is used to measure the pump-induced changes in optical constants such as reflectivity or absorbance. The time-dependent features of the resulting transmission, reflection or absorption spectrum yield information about the excitation and relaxation dynamics of charge carriers in the material. Many mechanisms are involved in such processes, such as direct tunneling, one-photon and multi-photon transitions, virtual transitions, intraband motion of charge, etc. Understanding their roles and interplay is a crucial step in designing efficient photo-electronic devices.
In this work [1], the ultrafast charge dynamics in bulk germanium is investigated by means, of experimental and simulated transient reflectance spectra. We have calculated the time-dependent occupations of states in the conduction band, and identified several excitation channels with distinct charge dynamics patterns, such as:
I) Below-resonance direct tunneling (blue line in Fig. 1b) oscillating with 90-degree phase shift with respect to the square of the vector field (top panel in black line);
II) One-photon resonances coherent to square of the vector field (orange/purple lines);
III) Two-photon transitions oscillating with full period of vector field (green/red lines);
IV) Transient charge excitations (grey circles in Fig. 1c), coherent to square of the vector field and completely disappear after the pump pulse is gone.
Overall, this work unveils the complexity of light field-driven electron dynamics in germanium and lays the foundation for studies of other materials and design of experimental setups that allow to zoom on specific electronic features at ultrafast timescales. It significantly extends the scope of previous studies of GaAs [Nat. Phys. 14, 560 (2018)], where the excited charge dynamics was governed by the one-photon transitions.

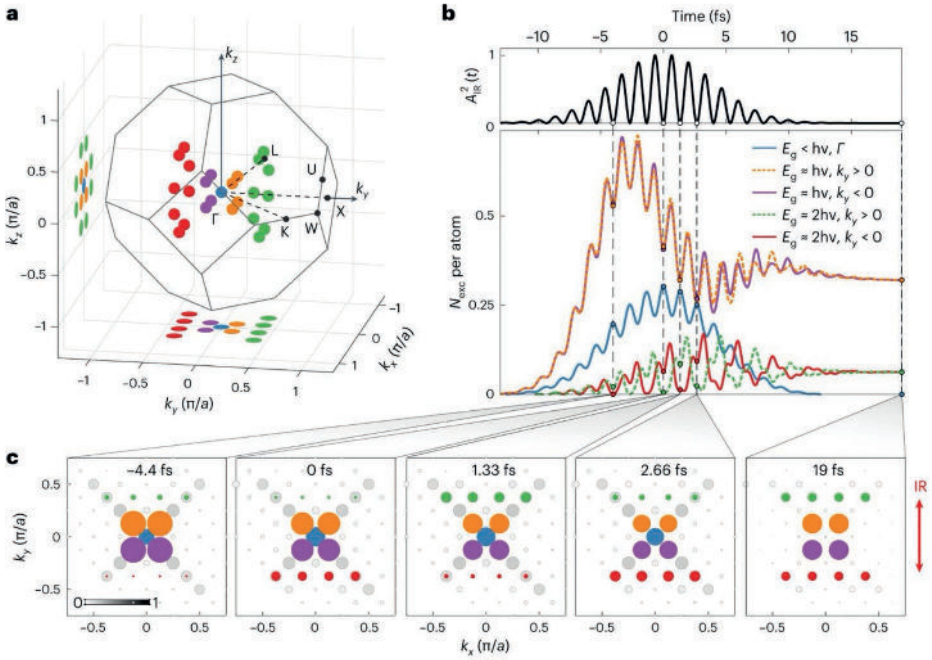

Fig. 1
Time-dependent excited electron population in reciprocal space. a. Three-dimensional positions of the selected k-points participating in carrier injection. The blue dot is located at the Γ point. Orange and violet dots represent the points at which the energy gap between the valence and conduction bands is resonant with the IR photon energy. Red and green points are associated with a two-photon absorption mechanism. a is the Ge lattice constant equal to 5.658 Å. b. Time-dependent excited electron population computed by TDDFT at the selected k-points and normalized by the number of k-points of the same family. The colour coding is the same as in a. c. Projection of the excited electron population along the kz direction at selected time instants marked by the dots in b. The size (and greyness) of each dot (same colour coding as in a.) is proportional to the normalized excited electron population. The figure is reproduced from [1].

Contact persons
Carlo Andrea Rozzi (carloandrea.rozzi@nano.cnr.it)

References
[1] Field-driven attosecond charge dynamics in germanium. G. Inzani, L. Adamska, A. Eskandari-asl, N. di Palo, G. L. Dolso, B. Moio, L. J. D'Onofrio, A. Lamperti, A. Molle, R. Borrego-Varillas, M. Nisoli, S. Pittalis, C. A. Rozzi, A. Avella, and M. Lucchini. Nat. Photon. 17, 1059 (2023).

Projects
MIUR PRIN aSTAR (No. 2017RKWTMY).

Rare-earth Single-Atom Magnets (SAMs) on Oxide Substrates

The study of the interaction between a magnetic impurity and a nonmagnetic host, and the role of the hybridization between the two in determining the magnetic anisotropy of the system, led to the discovery of single atom magnets (SAMs) in the case of rare-earth (RE) adatoms on oxides or graphene.
We present case studies of RE single atoms (Dy, Ho) deposited on the surface of different oxides - i.e., $SrTiO_3$, BaO and MgO - using a combined theoretical (DFT) and experimental approach, focusing on the interplay between the atom-substrate interaction (adsorption sites, structural relaxations, charge transfer) and the observed magnetic properties.

Recent investigations on the magnetic properties of rare earth (Ho, Dy) individual atoms on MgO thin films on Ag(100) [Science 352, 318 (2016)] or graphene/Ir(111) [Nano Lett. 16, 7610 (2016)] demonstrated that long magnetic relaxation times could be reached with strongly axial chemical bonds leading to uniaxial magnetic anisotropy (see Fig. 1 for a schematic representation of these systems).
Along this line, we have investigated the magnetic properties of Dy and Ho atoms adsorbed on the (001) surface of $SrTiO_3$ [1]. X-ray magnetic circular dichroism (XMCD) reveals slow relaxation of the Dy magnetization on a time scale of about 800 s at 2.5 K, unusually associated with an easy-plane magnetic anisotropy. We attribute these properties to Dy atoms occupying hollow adsorption sites on the TiO_2-terminated surface. Conversely, Ho atoms adsorbed on the same surface show paramagnetic behavior down to 2.5 K. Density-functional theory (DFT) suggests that Dy also populates the top-O and bridge sites on the coexisting SrO-terminated surface. Most interestingly, the adsorption of Dy on the insulating $SrTiO_3$ crystal leads, regardless of the surface termination, to the formation of a spin-polarized two-dimensional electron gas of Ti $3d_{xy}$ character, together with an antiferromagnetic Dy–Ti coupling (see Fig. 2).

The magnetic properties of Dy and Ho have also been studied for adatoms adsorbed on BaO(100) thin films on Pt(100) [2]. Dy shows hysteresis in magnetic fields up to ≈3.5 T and long spin lifetime, exceeding 300 s at 2.5 K and 0.5 T. It displays superior magnetic stability on the bridge site than on the top-O site. Surprisingly, Ho shows paramagnetism, as opposed to its long spin lifetime on MgO. DFT characterization helps to trace back these differences to the local surface distortions induced by the adatoms. On MgO, minimal distortions involve only the closest O atoms, while, on BaO, they affect both the closest anions and cations.
Our works help to identify the criteria for the optimum combination of rare-earth, oxide substrate and adsorption site maximizing the spin lifetimes of lanthanide single-atom magnets.

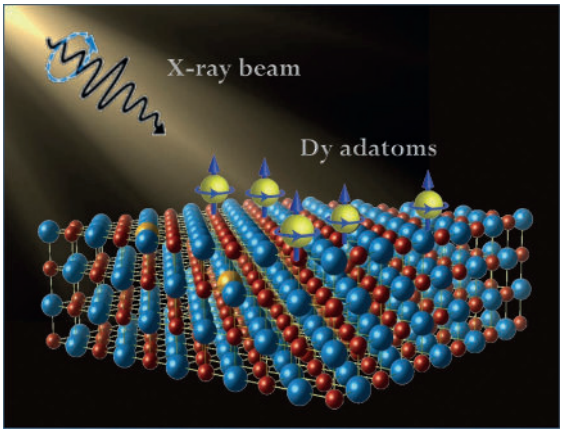

Fig. 1
Geometry of the XMCD experiment and schematic representation of isolated RE adatoms on oxide films.

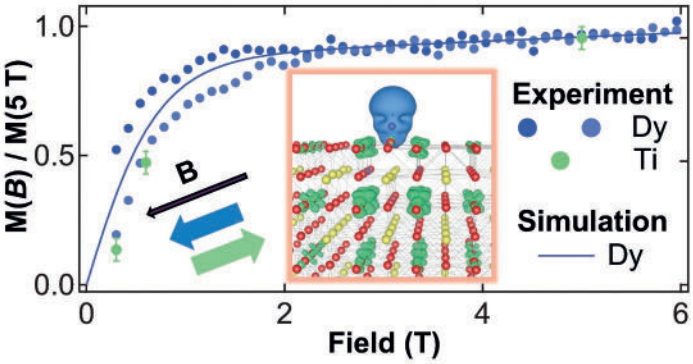

Fig. 2
Magnetic field dependence of the Ti 3d orbital magnetic moment (green dots) and the Dy total 4f moment (blue dots and line), extracted by XMCD; in the inset of the DFT spin-polarized charge density (isovalue of 10^{-3} e^{-}/A^{-3}) is shown.

Contact persons
Valerio Bellini (valerio.bellini@nano.cnr.it)

References
[1] Slow Magnetic Relaxation of Dy Adatoms with In-Plane Magnetic Anisotropy on a Two-Dimensional Electron Gas. V. Bellini, S. Rusponi, J. Kolorenč, S. K. Mahatha, M. A. Valbuena, L. Persichetti, M. Pivetta, B. V. Sorokin, D. Merk, S. Reynaud, D. Sblendorio, S. Stepanow, C. Nistor, P. Gargiani, D. Betto, A. Mugarza, P. Gambardella, H. Brune, C. Carbone, and A. Barla. ACS Nano 16, 11182 (2022).
[2] The Impact of Lattice Distortions on the Magnetic Stability of Single Atoms: Dy and Ho on BaO(100). B. V. Sorokin, M. Pivetta, V. Bellini, D. Merk, S. Reynaud, A. Barla, H. Brune, and S. Rusponi. Adv. Funct. Mater. 2213951 (2023).

Projects
CNR-CAS Italy-Czech Republic. PRIN2022 MAGNETISE (No. 2022KXN79M).

Molecular motors touch down

Molecular motors have chemical properties that enable unidirectional motion, thus breaking microscopic reversibility. They are well studied in solution, but much less is known regarding their behavior on solid surfaces, key in view of their potential applications. In combination with scanning tunneling microscopy (STM) experiments, first-principles calculations show how the molecule conformations are modified by surface adsorption on Cu(111), which is demonstrated to alter significantly the molecule energetics. Calculations also unveil the origin of unidirectional rotation that is observed when the molecules are excited by voltages pulses from an STM tip.

Molecular motors (MMs) have attracted much attention in the last two decades, due to their ability to transform energy from an external source into useful motion, for instance, a translation or rotation in one direction. Usually active in biological matter, these processes are mimicked in artificial MM in solution with great success. Deposition on a surface is however essential to realize one of the potential applications of MMs, i.e., their usage in molecular machines for the transport of

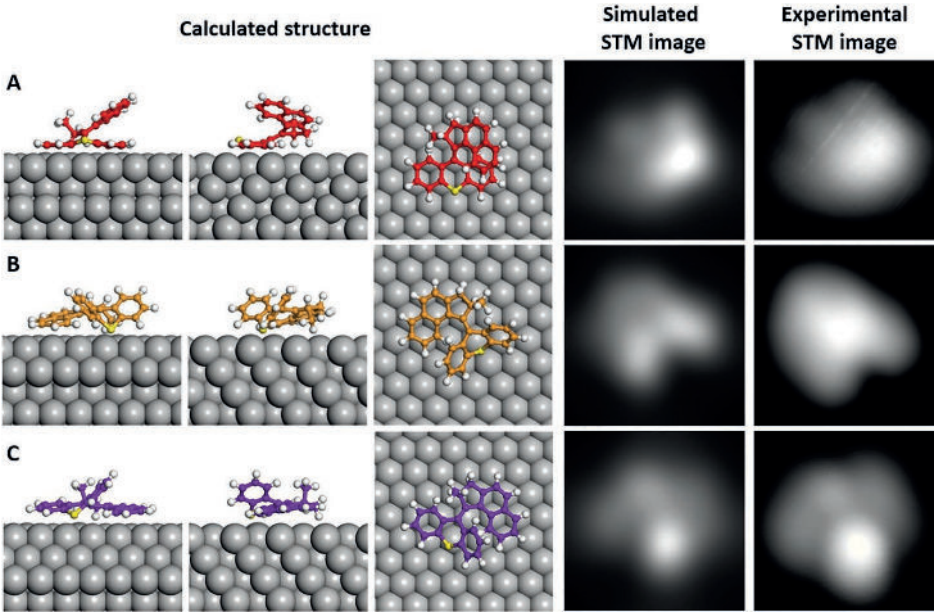

Fig. 1
Comparison of the calculated MM structures on the Cu(111) surface (left: two side views and one top view) with simulated and experimental STM images (right).

material along a given path. While the presence of a substrate offers the advantage to constrain the motion in 2 dimensions, it also brings in additional issues, since the molecule-surface interaction could inhibit molecular motion either via strong adsorption, or by quenching electronic states which are required for the chemical process.

We have investigated the adsorption and stability of a unidirectional Feringa motor by first-principles simulations, demonstrating how the molecule potential energy surface is altered by the presence of the substrate and its effect on the preferred intramolecular conformations of the molecule (Fig. 1). Those are known to play a crucial role in the motor rotary cycle that characterizes the MM motion in solution (Fig. 2). Simulated STM images are compared to low-temperature STM experiments, confirming our theoretical predictions. Moreover, when the MMs are excited by voltages pulses from an STM tip, unidirectional, enantiomer-specific rotation around a fixed pivot point is observed. Calculations support the identification of the rotation mechanism, which does not rely on the activation of the motor molecule, the latter having higher energy barrier than the simple rotation of the molecule as a rigid object, which is therefore preferred. These results represent important though still preliminary steps towards the long-term goal of fully taking advantage of the surface itself to steer and, ultimately, control the molecular motion.

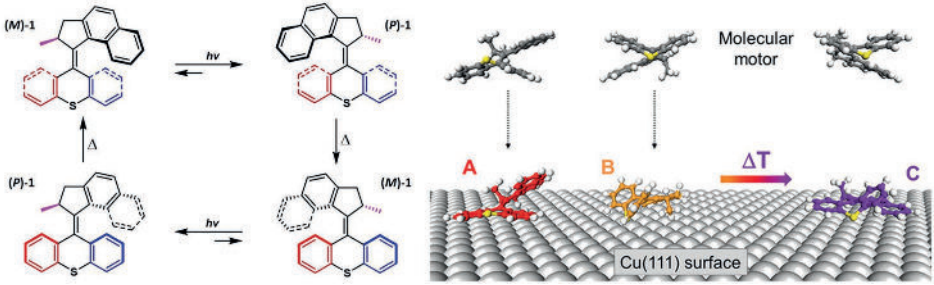

Fig. 2
Full 360° rotary cycle of the molecular motor in solution (left). Scheme of the molecular adsorption on the surface from the gas phase and the origin of the on-surface conformations A, B, and C identified. Notably, the most stable adsorbed conformation (C) corresponds to an excited state conformation in solution, (P)-1.

Contact persons
Deborah Prezzi (deborah.prezzi@nano.cnr.it)
Stefano Corni (stefano.corni@unipd.it)

References
[1] Chirality-Specific Unidirectional Rotation of Molecular Motors on Cu(111). M. Schied, D. Prezzi, D. Liu, S. Kowarik, P. A. Jacobson, S. Corni, J. M. Tour, and L. Grill. ACS Nano 17, 3958 (2023).
[2] Inverted Conformation Stability of a Motor Molecule on a Metal Surface. M. Schied, D. Prezzi, D. Liu, P. A. Jacobson, S. Corni, J. M. Tour, and L. Grill. J. Phys. Chem. C 126, 9034 (2022).

Exploring charge transfer thermodynamics and kinetics for engineering novel systems

The investigation of the thermodynamics and kinetics of charge transfer (CT) events in complex (bio)molecular systems is of pivotal importance, not only for a deeper understanding of these ubiquitous reactions that are at the basis of several fundamental processes, but also for engineering bioresponsive materials or non-natural biomolecular systems with specific and tunable properties. We employed a multiscale hybrid quantum/classical computational methodology to investigate CT reactions from either a thermodynamic or a kinetic perspective, in two systems with relevant application potentialities, such as nanomedicine and photocatalysis.

We investigated two CT reactions in complex systems using a multiscale procedure based on classical molecular dynamics simulations, quantum mechanical calculations, and the Perturbed Matrix Method. This method has the merit of being able to incorporate large-scale environmental effects on CT reactions.
Using this approach, we investigated gold nanoclusters (AuNC) functionalized with peptide ligands, a promising class of bioresponsive material. Experiments on a series of peptide-functionalized AuNC revealed pH-sensitive photoluminescence (PL), but the underlying mechanism remained unclear. Through systematic calculation of local environment-dependent deprotonation free energies, we provide insight into

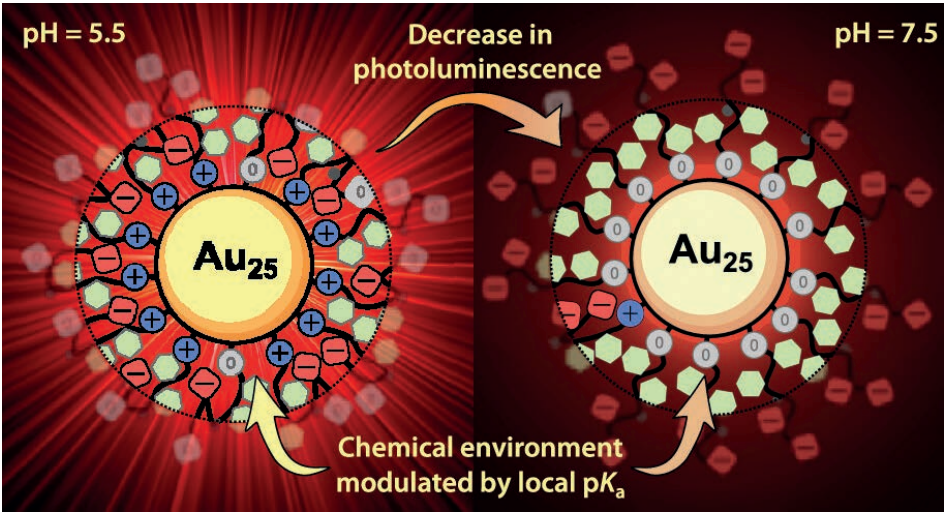

Fig. 1
Schematics showing the effect of pH on AuNC PL: PL variation is determined by the concurrent change in the number of protonated N-terminals (boosting PL), deprotonated sidechain groups (quenching PL), and interactions between protonated N-terminals and deprotonated sidechain groups (quenching PL).

how the PL emission intensity is related to solution pH [1]. Specifically, we find that the pH-sensitive nature of AuNC PL emission can be explained through pH-tunable electrostatic interactions between titratable groups in the peptides. These findings contribute to the rational design of programmable peptide-functionalized AuNC for use in biomedical applications requiring deliberate modulation of their PL properties, e.g., biosensing and diagnostic technologies.

We also investigated lactate monooxygenase (LMO), a flavin-based enzyme that, besides its native function, has been shown to respond to light acting as a photoenzyme. Given the rarity of natural photoenzymes, this reaction holds potential value, motivating an in-depth investigation into its mechanism. In combination with femtosecond spectroscopy and site-directed mutagenesis, we studied the primary step of the photoreaction-the photoinduced electron transfer (ET)- reconstructing its kinetics and obtaining ET rates that align well with the experimental rates [2]. We also show that the environment affects the ET reactions in multiple entangled ways, both affecting the active site geometry and through fast environmental conformational arrangements. The molecular mechanism we propose opens avenues for future engineering of LMO as a photoenzyme as well as of new photocatalytic enzymes from the abundance of natural flavoenzymes.

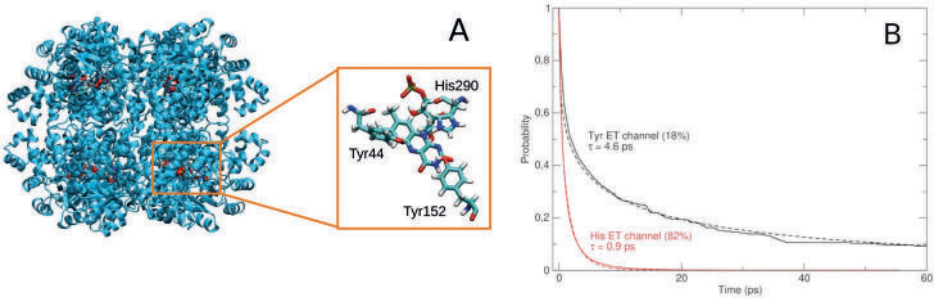

Fig. 2

A: Structure of LMO and zoom of the active site cleft encompassing flavin mononucleotide (FMN) and the sidechains of three aromatic residues, tyrosine 44, tyrosine 152, and histidine 290. B: kinetic profiles - and corresponding mean lifetimes - for the two ET channels in LMO: FMN^{*+}His290→FMN^{-}+$His290^{+}$ (red) and FMN*+His290→FMN^{-}+His290+ (black).

Contact persons

Laura Zanetti-Polzi (laura.zanettipolzi@nano.cnr.it)

References

[1] Origins of the pH-Responsive Photoluminescence of Peptide-Functionalized Au Nanoclusters. L. Zanetti-Polzi, P. Charchar, I. Yarovsky, and S. Corni. ACS Nano 16, 20129 (2022).

[2] Mechanism and Dynamics of Photodecarboxylation Catalyzed by Lactate Monooxygenase. X. Li, C. G. Page, L. Zanetti-Polzi, A. P. Kalra, D. G. Oblinsky, I. Daidone, T. K. Hyster, and G. D. Scholes. J. Am. Chem. Soc. 145, 13232 (2023).

Tuning graphene interactions for advanced applications

In addition to the distinctive band structure of graphene, which gives rise to unique electronic properties, equally noteworthy are its remarkable robustness coupled with extraordinary flexibility and its extensive exposed surface, which are used in several advanced applications.
However, the enhancement of particular properties, such as the capability of interacting with large amounts of a specific substance, often requires graphene engineering, involving processes like functionalization or nano-structuring. This report illustrates our latest multi-methodological studies aimed at designing graphene-based materials for two different kinds of devices: water filters from food waste, and neutrinos detectors to explore the early universe.

The seemingly disparate applications are connected through the utilisation of extensive exposed surfaces for trapping particles and the need of specific 3D architectures. The first study regards transformation of amyloid aggregates into nano-porous materials for water purification. By using atomistic molecular dynamics with reactive (Reax) Force Fields previously tested on graphene materials [1], we elucidated the structure of nanoporous graphene produced by freezing-drying and pyrolysis of albumen [2]. Simulations reveal a fibrous structure (Fig. 1) rich in defects and edges (for which we proposed a general classification scheme [3]) capable of trapping particles of different sizes. Besides, due to the biological origin, the residual N and O introduce charged defects, which are optimal traps for ions. Therefore, these materials have proven remarkably effective in water desalinisation and anti-pollution filters, and completely biocompatible, since obtainable from egg white or meat processing waste.
On a completely different side, we investigate the possible use of graphene-based materials in a detector for “relic” neutrinos. Neutrinos decoupled from the other matter

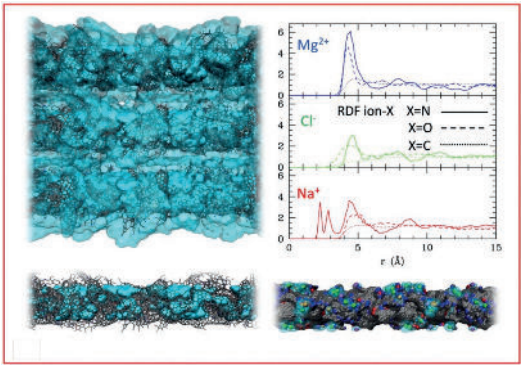

Fig. 1
Illustration of the structure deriving from the pyrolysis of egg albumen and of its action as ions filter. The nanoporous fibers of graphene are in gray, while water is represented as light blue isosurfaces of the 3D density map in the interstitial areas (upper left) and within the fiber (lower left). On the right, the plots of the radial distribution functions of the main ions with respect to the fiber components are reported, illustrating their accumulation in proximity of N or O sites of the fiber. On the bottom right panel, the structure of a single fiber with the ions and their hydration shell is reported.

~1 sec after the Big Bang and therefore bear crucial information on the early universe. They are normally detected by the analysis of the spectrum of the β electron resulting from their interaction with tritium (^{3}H=T), but "relic" neutrinos are rare and have very small energies (< meV). Therefore, their detection requires a high concentration of T to enhance sensitivity without hindering the resolution. While liquid T_2 would have sufficient concentration, the optimal condition for resolution would be T in free atomic form, because the tight bonding potential implies localization and uncertainty in momentum. We recently explored the possibility of storing T in graphene-based materials [4]. We investigated by means of DFT the potential experienced by T under different conditions (Fig. 2) and showed that T encapsulated in nanotubes may be a good compromise between high concentration and flat potential for T.

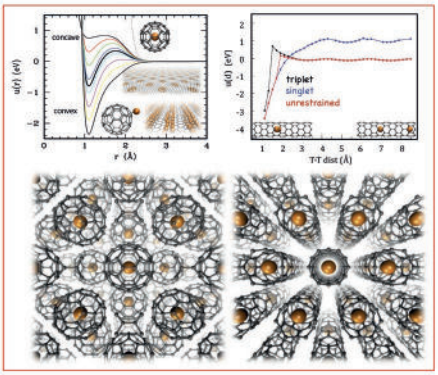

Fig. 2
Designing a material for relic neutrinos detectors. Upper left plot: The potential felt by ^{3}H (orange spheres) interacting with graphene (grey bonds) depends on the amount and organization of tritium on the sheet (stripes, islands, see insets) and its local curvature. Upper right plot: the potential felt ^{3}H along the axis of a small nanotube is basically flat (upper right plot), and, depending on the spin state, a barrier to the dimerization can be present, favouring the atomic state. Lower right panel: arranging nanotubes into bundles facilitates the attainment of a substantial sufficient tritium concentration. Bottom left panel: tritium encapsulated within fullerenes packed in fullerite might be a useful alternative.

Contact persons
Valentina Tozzini (valentina.tozzini@nano.cnr.it)

References
[1] Evaluating the performance of ReaxFF potentials for sp2 carbon systems (graphene, carbon nanotubes, fullerenes) and a new ReaxFF potential. Z. G. Fthenakis, I. D. Petsalakis, V. Tozzini, and N. N. Lathiotakis. Front Chem 10, 951261 (2022).
[2] Egg protein derived ultralightweight hybrid monolithic aerogel for water purification. S. Ozden, S. Monti, V. Tozzini, N. S. Dutta, S. Gili, N. Caggiano, A. J. Link, N. M. Pugno, J. Higgins, R. D. Priestley, and C. B. Arnold. Mat Today 59, 46 (2022).
[3] A proposed nomenclature for graphene pores: a systematic study of their geometrical features and an algorithm for their generation and enumeration. Z. G. Fthenakis. Carbon 199, 508 (2022)
[4] Heisenberg's uncertainty principle in the PTOLEMY project: A theory update. A. Apponi, [...], V. Tozzini, et al (PTOLEMY collaboration). Phys Rev D 106, 053002 (2022).

Projects
H2020-EIC-FETPROACT LESGO (GA 952068). MIUR PRIN2017 MONSTRE-2D (No. KFMJ8E). ISCRA-B SETE HPC@CINECA. PTOLEMY international collaboration for relic neutrinos detection.

Assessing spin-orbit effects on carrier states in III-V nanowires

We study electronic states of III-V (single-material and core-shell) nanowires, where carriers can be either strongly localized in the wire core or form a curved 2D electron gas. Our modeling is based on an 8-band k.p model and a local density-functional simulation code, specifically developed in-house. We map the ensuing multiband envelope function and Poisson equations to optimize, nonuniform real-space grids and solve the self-consistent problem by the finite element method, including arbitrary material modulation, doping profile, and external fields. We show that signatures of the evolution of the band structure can be singled out in the anisotropy of polarized optical absorption.

Semiconductor nanowires based on III-V materials are demonstrating a wealth of physical properties stemming from the tailoring of their electronic states by material modulation, doping and external electrostatic and magnetic fields. Their proposed applications go from light harvesting devices and nanophotonic sources, to quantum computing gates and nanoscale FETs with novel geometries. Since many applications, in particular spintronic devices, are largely driven by spin-orbit interaction (SOI), it is crucial to assess different SOI regimes and how to control them. For example, one critical issue bridging material science and device nanofabrication is the control of doping in modulation-doped heterostructures and radial p–n junctions, and its rule in enhancing SOI.

We developed a high-performance simulation software that solves self-consistently the 8-band Burt-Foreman k.p Hamiltonian and the electrostatic Poisson equation in real space, including arbitrary material modulation, doping, and external fields. The numerical burden arising from the self-consistent approach is reduced by adopting the finite element method with nonuniform real-space grids (Fig. 1).

We have computed the evolution of spin-orbit coupled valence-band states with doping of either n or p type nanowires. This is an important piece of information for the characterization of such materials where doping is still an issue [Jadczak et al., Nano Lett.14, 2807 (2014)]. We show that high-doping brings about a strong carrier localization towards the core-shell interface (Fig. 2), as well as mass inversions and non-trivial changes in the spinorial character of the low-energy valence states [1]. We show by explicit calculations that indications of the band structure's evolution with doping can be exposed in the anisotropy patterns of linearly polarized optical absorption spectra.

Furthermore, we found that for a magnetic field directed along the wire axis, the orbital effects are strongly reduced by the confinement [arXiv:2307.04265 (2023)] and the effective Landé g factor depends on the axial component of spin polarization.

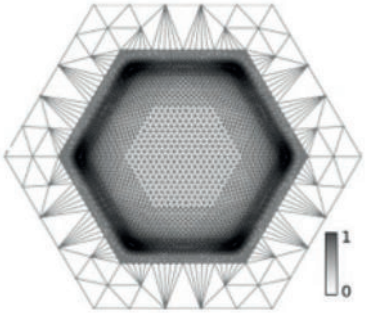

Fig. 1
Example of an optimized Finite-Element grid used to solve the k.p Hamiltonian on the hexagonal section of a GaAs/AlGaAs core-shell nanowire.

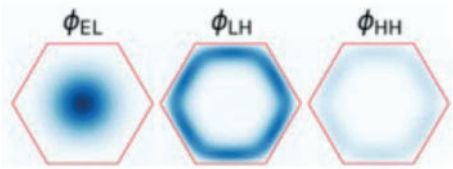

Fig. 2
Probability distribution of electrons, heavy and light holes, in the corresponding first subbands, at k=0, at the doping concentration nA= 1.8x10^{18} cm^{-3}.

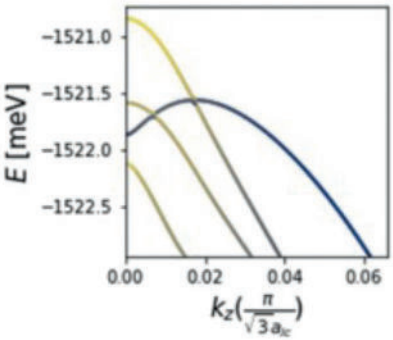

Fig. 3
Self-consistent valence bands for a doping of nD= 1.9x10^{18} cm^{-3}.

Contact persons
Andrea Bertoni (andrea.bertoni@nano.cnr.it)

References
[1] Band structure of n- and p-doped core-shell nanowires. A. Vezzosi, A. Bertoni, and G. Goldoni. Phys. Rev. B 105, 245303 (2022).

Efficient many-body perturbation theory calculations in 2D materials

Electronic-structure simulations, and in particular many-body perturbation theory calculations, give a substantial contribution to the design and understanding of new materials with both theory and algorithms progressing swiftly. We have developed the multipole approximation (MPA) and the W-av methods, that accelerate the convergence with respect to the frequency sampling of the screened Coulomb interaction and the Brillouin zone sampling for 2D systems. These approaches were used to obtain accurate results for graphene quasiparticle band structure and electron energy loss spectra at finite momentum transfer. We have also introduced a set of new algorithms and workflows that automate the convergences for GW and BSE calculations, accompanied by GW band interpolation based on maximally localized Wannier.

Low dimensional systems, like 2D materials, pose specific challenges to many-body perturbation theory calculations (MBPT). On the one hand, the dielectric function changes rapidly for small momentum transfers, requiring a dense and computationally expensive sampling over the Brillouin zone (BZ). On the other hand, an accurate description of the frequency dependence of the screening may require methods beyond the plasmon-pole approximation (PPA), such as the often-prohibitive full frequency approaches.

We have recently introduced two new developments, the multipole approximation (MPA) [1] and the W-av methods [2], that address respectively the frequency sampling of the screened Coulomb interaction and the convergence with respect to the BZ sampling. The combined approach was used to obtain accurate results for graphene quasiparticle (QP) band structure. The latter is finally used to calculate electron energy loss spectra (EELS) of graphene at finite momentum transfer via the Bethe-Salpeter equation (BSE), showing excellent agreement with recent high-resolution experimental data, provided that the electron-hole interaction is properly considered. The MPA and W-av methods were implemented in the YAMBO code (https://www.yambo-code.eu).

Another important aspect is automation, essential in view of performing high-throughput computational screenings, that can greatly accelerate the identification, characterisation and optimisation of new materials. We have introduced a set of new algorithms

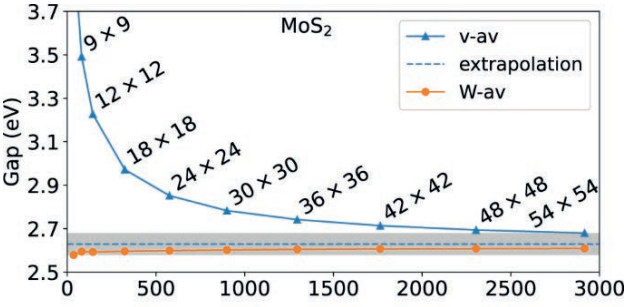

Fig. 1
Convergence of the quasiparticle band gap of MoS2 with respect to the number of sampling points of the BZ when using the standard v-av and the new W-av methods [2].

and workflows that perform efficient and robust convergences for many-body perturbation theory calculations, including GW and BSE, accompanied by an automatic GW band interpolation scheme based on maximally localised Wannier [3]. The algorithms were implemented in the AiiDA framework and guarantee a seamless interoperability of different software codes involved in MBPT simulations, i.e., the DFT starting point (here using Quantum ESPRESSO), the GW-BSE calculations (Yambo), and the required post-processing (Wannier90).

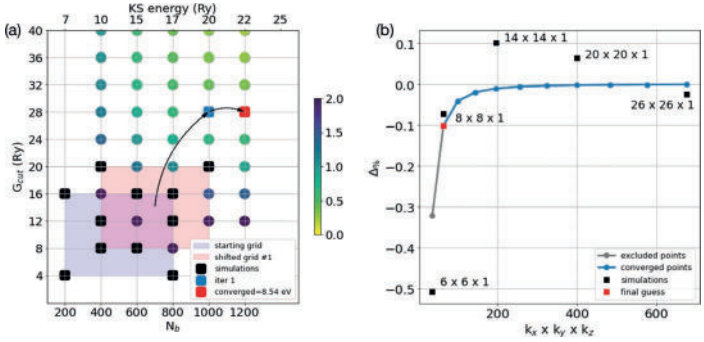

Fig. 2
a) Convergence of the direct quasiparticle band gap at the Γ point with respect to the coupled parameters Nb and Gcut. Black squares represent the actual performed calculations; the blue square is the first guess for the converged parameters; the red square indicates the final, converged point. b) Convergence of the direct quasiparticle band gap at the Γ point with respect to the k-mesh. The black points represent the actual calculations performed by the workflow, whereas the blue points are the ones obtained within the fitting procedure and used to predict the convergence. The final converged mesh (red square) is achieved with five calculations [3].

Contact persons
Claudia Cardoso (claudia.cardoso@nano.cnr.it)

References
[1] Efficient full frequency GW for metals using a multipole approach for the dielectric screening.
D. A. Leon, A. Ferretti, D. Varsano, E. Molinari, and C. Cardoso. Phys. Rev. B 107, 155130 (2023).
[2] Efficient GW calculations in two dimensional materials through a stochastic integration of the screened potential. A. Guandalini, P. D'Amico, A. Ferretti, and D. Varsano. npj Computational Materials 9, 44 (2023).
[3] Towards high-throughput many-body perturbation theory: efficient algorithms and automated workflows. M. Bonacci, J. Qiao, N. Spallanzani, A. Marrazzo, G. Pizzi, E. Molinari, D. Varsano, A. Ferretti, and D. Prezzi. npj Computational Materials 9, 74 (2023).

Projects
HORIZON-EUROHPC-JU-2021-COE-01 MaX - MAterials design at the eXascale (GA 101093374).
NextGenerationEU - PNRR ICSC – Centro Nazionale di Ricerca in High Performance Computing, Big Data and Quantum Computing (Missione 4 Componente 2 Investimento 1.4).

Electronic structure of excitations via auxiliary ensemble states

Modeling and predicting excitations in many-body systems is of utmost importance. For instance, excitations underpin new state of matters, define the properties of advanced quantum materials, intervene in biological processes such as vision, and can be used to engineer functionalities of devices such as photovoltaics. Here, we summarize recent methodological developments done within the domain of density functional theory (suitable for calculations on classical computers) and within the domain of wave-function theories (suitable for calculations on quantum computers) – both resting on the formal and computational exploitation of mixed quantum states.

Quantum excitations play an ever-increasing role in multiple and interconnected fields of fundamental and applied research. There is therefore a high demand for methodologies that can model and compute excited-state properties realistically and yet efficiently. Refs. [1,2] show that working from ensembles instead of pure states can help to solve long-standing problems involving excitations in many-electron systems.
Ref. [1] demonstrates that Ensemble DFT (EDFT) – a statistical extension of DFT – can solve excited-state problems by interpolating solutions from the extreme, yet

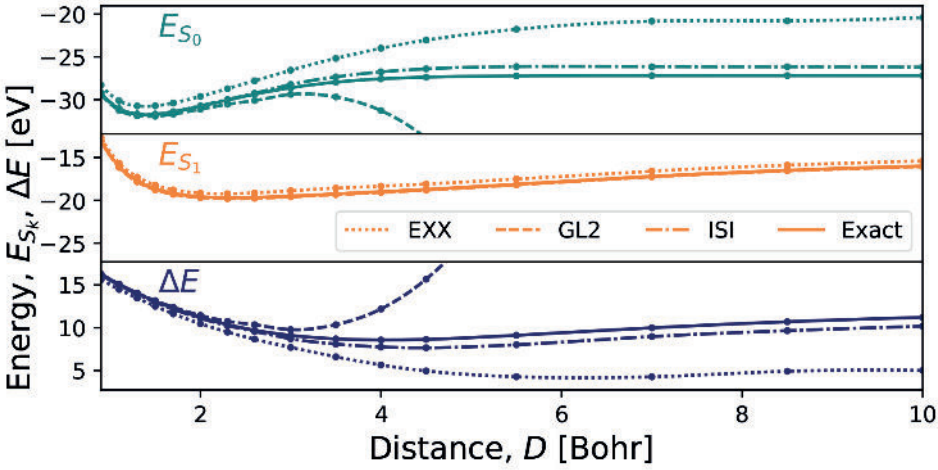

Fig. 1
Energies for dissociating H2: (top, teal) ground state energies; (middle, orange) first excited singlet state energies; (bottom, navy) excitation energies. *EXX* and *GL2* are approximations which accounts only for the high-density limit correctly; *ISI* is the functional approximation that accounts for both the extreme limits correctly; *Exact* denotes the exact solutions. All the approximations must be intended as the "ensembled" versions as described in [1].

exact, cases of high-electron density (where the electrons distribution is squeezed) and at low-electron density (where the electrons distribution is stretched). As a result, problems which were too difficult may instead soon become computable via EDFT, routinely. To illustrate the power of the findings, the approach was used to compute the excitation energies in two test cases: hydrogen molecule at all bond lengths, and a model system of disordered quantum wells (Fig. 1). The work is of direct importance for traditional analytic-driven models of materials. It also provides constraints for modern data-driven methodologies based on machine learning.

Ref. [2] shows how the advantages of state-average and state-specific calculations can be merged in one approach. The new method exploits the purification of mixed states via a duplication of the Hilbert space and the unitary coupled-cluster approach in such a way to determine an ensemble of excited states as if they were just "one" state. To illustrate the effectiveness of the method, the approach was used to compute the excitation energies in a lattice model of fermions ranging from weakly to strongly correlated regimes (Fig. 2). The approach is suitable for an efficient implementation on quantum computers and may, thus, enable unprecedented calculations.

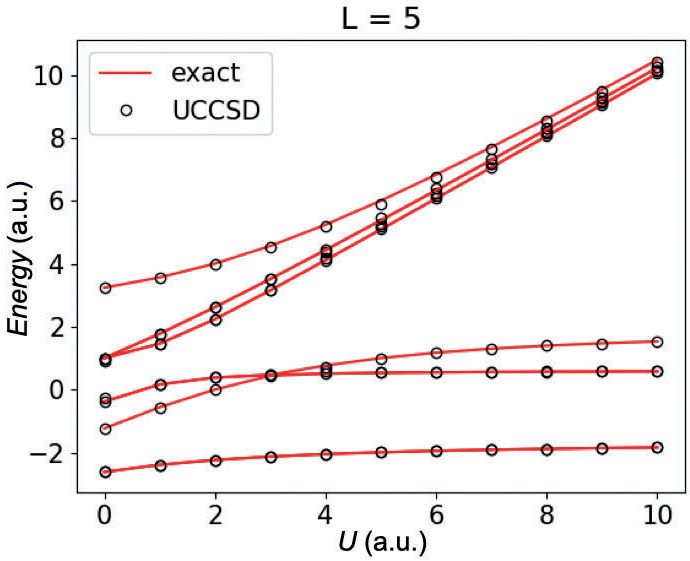

Fig. 2
The spectrum for two spinless fermions on a one-dimensional lattice with 5 sites. Electrons can hop at nearest sites and there is penalty in energy, U, to occupy the same sites. Red lines correspond to the exact energies; black circles correspond to the results obtained by means of the new methods as described in [2].

Contact persons
Stefano Pittalis (stefano.pittalis@nano.cnr.it)

References

[1] Electronic Excited States in Extreme Limits via Ensemble Density Functionals. T. Gould, D. P. Kooi, P. Gori-Giorgi, and S. Pittalis. Phys. Rev. Lett. 130, 106401 (2023).
[2] Excitations of Quantum Many-Body Systems via Purified Ensembles: A Unitary-Coupled-Cluster-Based Approach. C. L. Benavides-Riveros, L. Chen, C. Schilling, S. Mantilla, and S. Pittalis. Phys. Rev. Lett. 129, 066401 (2022).

The hunt for the excitonic insulator

We report our search for the excitonic insulator (EI) in bulk low-dimensional materials. This phase is a permanent Bose-Einstein condensate of excitons -electron-hole pairs bound by Coulomb attraction- that spontaneously form at thermodynamic equilibrium. This state of matter may exhibit novel forms of superfluidity different from superconductivity, since excitons are neutral particles. Here we investigate two candidate materials that may be excitonic insulators and exhibit macroscopic quantum coherent properties, i.e., monolayer WTe_2 and narrow-gap carbon nanotubes.

The EI has been elusive so far, partly because good candidate materials are rare, and partly because it is difficult to pinpoint the phase experimentally. The main goal of our activity is to establish the EI as a novel phase of matter with unique properties. In a first work, together with the experimental group of David Cobden (Univ. Washington, Seattle, WA, US), we have demonstrated that the two-dimensional bulk of monolayer WTe_2 contains excitons that spontaneously form in thermal equilibrium [1]. The natural paradigm to interpret the ground state turns out to be the EI, which breaks the pristine symmetry of the crystal though the Bose-Einstein condensation of excitons. Since lowest-energy excitons have finite momentum, one expects the EI to break the periodicity of the crystal, but no charge order has been observed at low temperature [1]. We predict that the EI is a spin density wave, on the basis of a full microscopic theory that builds on the ab-initio treatment of excitons. Key to our claim is the strong spin-orbit interaction of WTe_2, which largely enhances the splitting between spin singlet and triplet excitons, and thus stabilizes the spin order. In a second work, we have reconsidered narrow-gap carbon nanotubes, after our seminal prediction that armchair (zero-gap) tubes are EIs [D. Varsano et al., Nature Commun 8, 1461 (2017)]. We have now investigated in depth [2] the screening of Coulomb interaction, which controls many-body physics in carbon nanotubes, as it tunes the range and strength of the force that acts on charge carriers and binds electron-hole pairs into excitons. Critically, the effective Coulomb interaction dictates the Mott or excitonic nature of the correlated insulator observed at low temperature. Here, by computing the dielectric function of selected narrow- and zero-gap tubes from first principles, we have shown that the standard effective-mass model of screening systematically underestimates the interaction strength at long wavelength, hence missing the binding of low-energy excitons. The reason is that the model critically lacks the full three-dimensional topology of the tube, being adapted from graphene theory. A striking result is that the screened interaction remains long-ranged even in gapless tubes, as an effect of the microscopic local fields generated by the electrons moving on the curved tube surface. Our findings confirm the EI scenario, since the anomalous long range of Coulomb interaction stabilizes the excitonic against the Mott insulator.

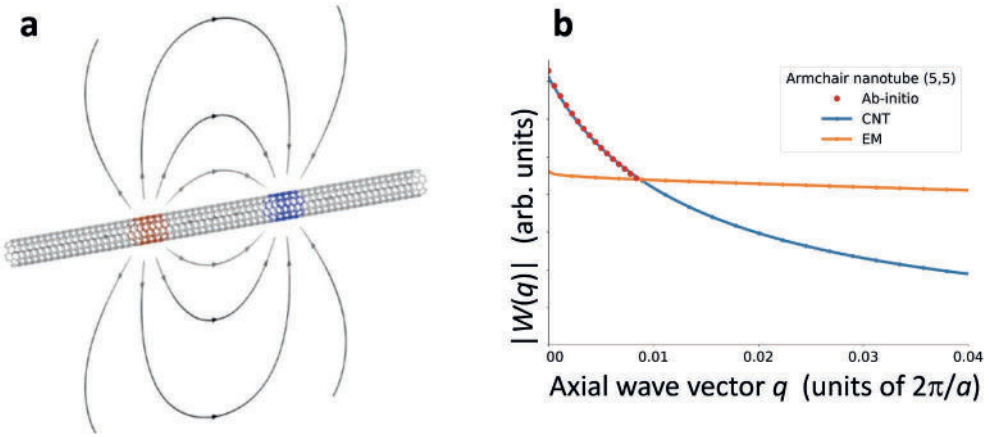

Fig. 1
Ultrastrong Coulomb interaction in a gapless (armchair) carbon nanotube. a. Sketch of the field lines of electron-hole attraction. After [Varsano et al., Nature Commun 8, 1461 (2017)]. b. Screened electron-hole attraction in reciprocal space, |W(q)|, vs q, for the (5,5) tube. The orange curve is the effective-mass (EM) prediction, which is almost featureless as it complies with Thomas-Fermi model of metallic screening, corresponding to a contact interaction in real space. The dots are the results from first principles and follow a logarithmic-like singularity (here regularized due to numerical discretization), corresponding to a long-range interaction in real space. This long range is the effect of local fields generated by the motion of charges on the curved tube surface. Adapted by [2].

Contact persons
Massimo Rontani (massimo.rontani@nano.cnr.it)
Daniele Varsano (daniele.varsano@nano.cnr.it)

References
[1] Evidence for equilibrium exciton condensation in monolayer WTe2. B. Sun, W. Zhao, T. Palomaki, Z. Fei, E. Runburg, P. Malinowski, X. Huang, J. Cenker, Y. T. Cui, J. H. Chu, X. Xu, S. S. Ataei, D. Varsano, M. Palummo, E. Molinari, M. Rontani, and D. H. Cobden. Nature Physics 18, 94 (2022).
[2] Anomalous screening in narrow-gap carbon nanotubes. G. Sesti, D. Varsano, E. Molinari, and M. Rontani. Physical Review B 105, 195404 (2022).

Projects
PRIN2017 EXC-INS Excitonic insulator in two-dimensional long-range interacting system (No. 2017BZPKSZ_002).

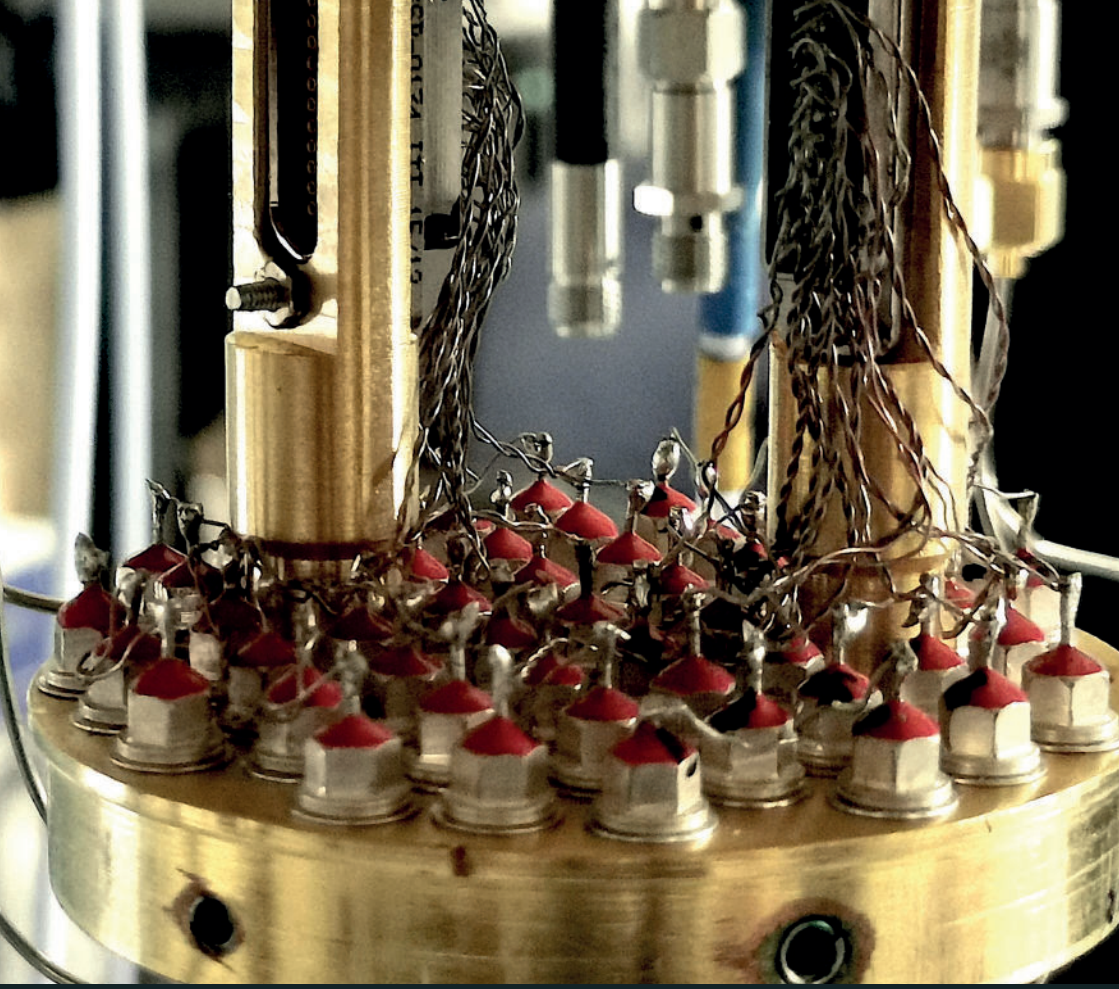

Projects and grants

Cnr Nano research activity is mainly supported by funding obtained through competitive calls at different levels, from international to local. Projects running in 2022-2023 are listed below with the following details: acronym, project name, call details, project ID, coordinator, Cnr Nano principal investigator (if different from coordinator), dates, website (if available). A short abstract is given for European-funded projects.
For further information, please contact the project's Cnr Nano principal investigator.

European projects

AndQC. Andreev qubits for scalable quantum computation. H2020-FETOPEN-2018-2020-01; GA 828948. Chalmers Tekniska Hoegshkola AB, SE (A. Geresdi); Cnr Nano Pisa (L. Sorba). 2019-2024.
www.andqc.eu

Abstract. The goal is to establish the foundations of a radically new solid-state platform for scalable quantum computation, based on Andreev qubits. This platform is implemented by utilizing the discrete superconducting quasiparticle levels (Andreev levels) that appear in weak links between superconductors. Each Andreev level can be occupied by zero, one, or two electrons. The even occupation manifold gives rise to the first type of Andreev qubit. We will characterize and mitigate the factors limiting the coherence of this qubit to promote these proofs of concept experiments towards a practical technology. The odd occupation state gives rise to a second type of qubit, the Andreev spin qubit, with an unprecedented functionality: a direct coupling between a single localized spin and the supercurrent across the weak link. Further harnessing the odd occupation state, we will investigate the so far unexplored scheme of fermionic quantum computation, with the potential of efficiently simulating electron systems in complex molecules and novel materials. The recent scientific breakthrough by the Copenhagen node of depositing of superconductors with clean interfaces on semiconductor nanostructures opened a realistic path to implement the Andreev qubit technology. In these devices, we can tune the qubit frequency by electrostatic gating. We will demonstrate single- and two-qubit control of Andreev qubits, and benchmark the results against established scalable solid-state quantum technologies, in particular semiconductor spin qubits and superconducting quantum circuits.

Attract Phase II - H-CUBE. Micromechanical Bolometers arrays for Terahertz hyperspectral imaging. H2020-INFRAINNOV-2019-2020; GA 10100442. Cnr Nano Pisa (A. Pitanti). 2021-2025.
www.attract-eu.com/attract-phase-2

Abstract. The h-cube project addresses the emerging need for low-cost, portable solutions for hyperspectral imaging in the terahertz (THz) region of the electromagnetic spectrum. THz waves sensing has important applications across a diverse range of fields such as health, security, construction, agriculture, drug development, monitoring of transport and civil infrastructure, inspection and quality control in production lines, and astronomy. Building on the synergies and results of three ATTRACT Phase 1 projects (GRANT, ROTOR and TACTICS) h-cube will demonstrate a THz sensor for hyperspectral imaging with unprecedented sensitivity, broad THz response and a design optimized for low-cost production. H-cube will therefore extend the use THz imaging from costly, extremely low-volume applications such as large body scanners in airports,

expensive inline machines for production quality control and sophisticated research tools, to larger-volume, every-day applications such as crop monitoring, building control and weapon identification in crowded environments.

BIG MAP. Battery interface Genome – Materials Acceleration Platform. H2020-LC-BAT-2020-3; GA 957189. Technical University of Denmark – DTU, DK (T. Wegge); Cnr Nano Modena (E. Molinari). 2020-2024.
www.big-map.eu

Abstract. Energy production and transport are evolving rapidly to meet today's growing demand and environmental goals. However, low-cost and high-performance solutions are lacking when it comes to energy storage. To address the absence of innovative battery technologies, the EU-funded BIG-MAP project aims to develop a modular, closed-loop infrastructure and methodology to bridge physical insights and data-driven approaches. To this end, it will cohesively integrate machine learning, computer simulations and AI-orchestrated experiments and synthesis to accelerate the discovery and optimisation of sustainable battery materials. The project will play a role in the creation of a versatile and chemistry-neutral European Materials Acceleration Platform that can significantly increase the rate of discovery of new battery materials and interfaces.

BIOIMD. Bioresorbable self-powered implantable device. H2020-MSCA-IF-2019; GA 896811. Cnr Nano Pisa (L. Persano). 2021-2023.
www.nano.cnr.it/bioimd

Abstract. Novel implantable medical devices (IMDs) allow the monitoring or detection of diseases inside the human body, yet the challenge is that these devices need to be supplied with continuous power. The implantable batteries suffer from limited lifetime and maintenance problems, and they require periodic replacement through surgery. Scavenging energy from biomechanical sources using piezoelectric devices presents a smart strategy since they can harvest electric supply from the inexhaustible motions of organs such as the heart, lungs, and diaphragm. The focus of the EU-funded BIOIMD project is to develop high-performance piezoelectric polymer-based biodegradable IMDs which can be accommodated by the body and finally resorbed without any toxicity.

EXTREME-IR. Extreme Optical Nonlinearities in 2D materials for Far-Infrared Photonics. H2020-FETOPEN-2018-2020; GA 896811. CNRS, FR (S. Dhillon); Cnr Nano Pisa (M. S. Vitiello). 2021-2025.
www.extreme-ir.eu

Abstract. Generating light across the mid-infrared and terahertz regions of the spectrum has opened up a plethora of sensing applications and enabled the study of fundamental light-matter interactions. Quantum cascade lasers, which have recently moved from laboratory curiosity to industrial mainstay, have largely increased the range of

practical applications. Despite their potential, they are limited in their ability to fill the far-infrared gap, namely the frequency region between 5 and 12 THz. The EXTREME-IR project aims to overcome this barrier by pioneering a radically new platform that exploits nonlinear optics in 2D materials to realise compact and coherent far-infrared sources.

GENESIS. GatE-coNtrollEd Superconducting TransIStors. H2020-FETOPEN-2018-2019-2020-4; GA 101034849. Cnr Nano Pisa (F. Giazotto). 2021-2022.

Abstract. As global internet traffic continues to increase, existing telecommunications (TLC) infrastructures face technological restrictions due to their speed and the enormous amount of data processed at network nodes. Although improved transmission bitrate (Tb/s) will be achieved using microwave (GHz) or terahertz (THz), data sorting-related radio frequency signals will become more difficult. The EU-funded GENESIS project will propose a new paradigm for electronics in which the basic building blocks rely on gate-controlled superconducting transistors solving the TCL infrastructure problem. The project will assess the expected superior performances for superconducting devices. It will perform a stakeholder analysis to confirm the system's functionalities as well as crucial requirements for the technology's integration into selected application scenarios, and also carry out a Freedom to Operate analysis.

Graphene Flagship Core Project 3. H2020-SGA-FET-GRAPHENE-2019; GA 881603. Chalmers Tekniska Högskola AB, SE (J. Kinaret); Cnr Nano Pisa (M. S. Vitiello). 2020-2023.
www.graphene-flagship.eu

Abstract. The EU-funded GrapheneCore3 project aims to secure a major role for Europe in the ongoing technological revolution, helping to bring graphene innovation out of the lab and into commercial applications by 2023. In its third core project, the Graphene Flagship gathers over 160 academic and industrial partners from 23 countries, all exploring different aspects of graphene and related materials. Bringing diverse competencies together, the Graphene Flagship facilitates cooperation between its partners, accelerating the timeline for industry acceptance of graphene technologies.

IMPRESS. Interoperable electron Microscopy Platform for advanced RESearch and Services. HORIZON-INFRA-2022-TECH-01; GA 101094299. Cnr IOM, IT (R. Ciancio); Cnr Nano Modena (V. Grillo). 2023-2027.
www.e-impress.eu

Abstract. For fast, precise and high-resolution imaging, transmission electron microscopy (TEM) is capable of unparalleled results. Taking it a step further, the EU-funded IMPRESS project will develop advanced methods and tools to revolutionise how TEM is used by scientific communities. The project's main aim is to develop a standardised cartridge-based interoperable platform for TEM that is grounded on common interfaces and

data formats. It will be flexible and adaptable; moreover, it will allow users to perform advanced correlative experiments using different instruments and co-develop methodological options that are not yet satisfied by commercially available electron microscopes. An open-knowledge and innovation hub for TEM will also be created.

INTERSECT. Interoperable Material-to-Device simulation box for disruptive electronics. H2020-NMBP-TO-IND-2018; GA 814487. Cnr Nano Modena (A. Calzolari). 2019-2022.
www.intersect-project.eu

Abstract. INTERSECT wants to leverage European leadership in materials' modelling software and infrastructure to provide industry-ready integrated solutions that are fully compliant with a vision of semantic interoperability driven by standardized ontologies. The resulting IM2D framework - an interoperable material-to-device simulation platform - will integrate some of the most used open-source materials modelling codes (Quantum ESPRESSO and SIESTA) with models and modelling software for emerging devices via the SimPhony infrastructure for semantic interoperability and ontologies, powered by the AiiDA workflow engine, and its data-on-demand capabilities and apps interface. API-compliance with established standards will allow pipelines to and from public repositories, and embedding into the front-end of materials hubs, such as MarketPlace, while testing, validation, and standardization will take place together with the industrial partners. INTERSECT will drive the uptake of materials modelling software in industry, bridging the gap between academic innovation and industrial novel production, with a goal of accelerating by one order of magnitude the process of materials' selection and device design and deployment.

IQubits. Integrated Qubits Towards Future High-Temperature Silicon Quantum Computing Hardware Technologies. H2020-FETOPEN-2018-2019-2020-01; GA 829005. Akademia Gorniczo-Hutnicza Im. Stanislawa Staszica W Krakowie, PL (D. Zito); Cnr Nano Modena (E. Molinari and F. Troiani). 2019-2024.
www.iqubits.eu

Abstract. The objectives of the interdisciplinary project IQubits are to (i) develop and demonstrate experimentally high-temperature (high-T) Si and SiGe electron/hole-spin qubits and qubit integrated circuits (ICs) in commercial 22nm Fully-Depleted Silicon-on-Insulator (FDSOI) CMOS foundry technology as the enabling fundamental building blocks of quantum computing technologies, (ii) verify the scalability of these qubits to 10nm dimensions through fabrication experiments and (iii) prove through atomistic simulations that, at 2nm dimensions, they are suitable for 300K operation. The proposed 22nm FDSOI qubit ICs consist of coupled quantum-dot electron and hole spin qubits, placed in the atomic-scale channel of multi-gate n- and p-MOSFETs, and of 60-240GHz spin control/readout circuits integrated on the same die in state-of-the-art FDSOI CMOS foundry technology. To assess the impact of future CMOS scaling, more aggressively scaled Si-channel SOI and nitride-channel qubit structures will also be designed and fabricated in two experimental processes with 10nm gate half pitch. The

latter will be developed in this project. The plan is for the III-nitrides (III-N) qubits to be ultimately grown on a SOI wafer, to be compatible with CMOS.

LESGO. Light to Store chemical Energy in reduced Graphene Oxide for electricity generation. FETPROACT-EIC-05-2019; GA 952068. ICFO, ES (J. Martorell); Cnr Nano Pisa (V. Tozzini). 2020-2023.
www.lesgo-project.eu

Abstract. Electricity generation based on renewables is unpredictable, but hydrogen (H2) could be a promising energy storage route. Since over 95% of H2 comes from breaking the carbon-hydrogen bond in hydrocarbons, storing hydrogen bound to carbon may provide a long-term solution. However, extracting hydrogen from liquid hydrocarbons includes CO2 emissions. To address this problem, the EU-funded LESGO project aims to store energy in the C-H bond of reduced graphene oxide (rGO-H). The advantages of rGO-H include safe storage, easy transportation, an energy density over 100 times larger than that of H2 gas and no CO2 emissions in the electricity generation process. The project will promote an affordable and eco-friendly means of supplying electrical power on demand where required.

MaX. Materials design at the exascale. Materials design at the exascale. European Centre of Excellence in materials modelling, simulations, and design. H2020-INFRAEDI-2018-1; GA 824143. Cnr Nano Modena (E. Molinari). 2018-2022. HORIZON-EUROHPC-JU-2021-COE-01; GA 101093374. Cnr Nano Modena (E. Molinari). 2023-2026.
www.max-centre.eu

Abstract. MaX aims at allowing the pre-exascale and exascale computers expected in Europe in the 2020's to meet the demands from a large and growing base of researchers committed to materials discovery and design. This goal will be achieved by: i) an innovative software development model, based on the concept of separation of concerns, that will enable performance of the community codes on heterogeneous hardware architectures, without disrupting their internal structure, the richness of their simulation capabilities, and their distributed and open development model. In this way, the most important community codes for quantum mechanical materials modelling will be ready for pre-exascale machines by the completion of MaX programme, and prepared to be ported to new architectures as they will become available; ii) an integrated ecosystem enabling the convergence of HPC and HTPC, that will allow steering the millions to hundreds of millions of simulations that are needed to optimise the properties and performances of a material or a device, with robust and reproducible workflows, all contributing to an ever growing repository of curated data; iii) a new approach to scientific computing in which hardware and software are co-designed and co-developed taking into mutual account the constraints and goals; iv) innovative measures for easy access to materials science applications, for engaging academic and industrial communities and fostering a broader and diverse pool of well-trained users and developers.

MINEON. MINiaturized Electron Optics for Nano-controlled beams. H2020-FETOPEN-2018-2020 Launchpad; GA 101035013. Cnr Nano Modena (V. Grillo). 2021-2022.
www.mineon.eu

Abstract. Novel electron beam shaping enhances functionality in compact electron microscopy system. The evolution of technologies in virtually all fields follows a similar route, packing ever greater functionality into increasingly compact designs that simultaneously expand access due to portability and space requirements. Much as computers have evolved from mainframes to minicomputers, personal computers and now laptops, the same evolution is happening with technologies that enable us to visualise and control materials' properties down to atomic resolution. The EU-funded MINEON project is perfecting the next evolutionary leap for electron microscopy. The team is laying the foundations for commercialisation of its revolutionary electron microscopy plug-in components harnessing electron beam shaping based on miniaturised micro-electromechanical systems technology.

MUQUABIS. Multiscale quantum bio-imaging and spectroscopy. HORIZON-CL4-2021-DIGITAL-EMERGING-01; GA 101070546. Cnr Ino, IT (N. Fabbri); Cnr Nano Pisa (M. S. Vitiello). 2022-2026.
www.sites.google.com/lens.unifi.it/muquabis-project

Abstract. MUQUABIS aims at developing synergetic tools of quantum bio-sensing and bio-imaging. Such sensors will offer biology a distinctive host of powerful features – non-invasiveness, sensitivity, spatial and temporal resolutions, likely to conquer new frontiers in imaging and spectroscopy, out-of-reach of their classical counterparts. A focus is a global structural and functional understanding of cardiac cell layers from molecules to cells to tissues. Their study in healthy and diseased conditions will shed light on cardiac arrhythmias, largely responsible for morbidity and sudden cardiac death. Advancing beyond modern tools of photonics and quantum measurements, new concepts for quantum frequency combs and infrared lasers will be explored. Low-light-level spectro-imaging will detect cell-membrane proteins and gaseous metabolites nearby cell tissues, below the quantum noise limit. Concurrently, a quantum magneto-microscope based on diamond nitrogen-vacancy centers will be combined to optical imaging for electrophysiology. Such a hybrid sensor will simultaneously and locally reveal the magnetic and electric fields in cardiac-cell activity. MUQUABIS will pave the way to ground-breaking quantum-based tools and protocols for medical diagnostics and treatments, a strategic objective for the European Quantum Technology flagship.

OPENMODEL. Integrated Open Access Materials Modelling Innovation Platform for Europe. H2020-NMBP-TO-IND-2018-2020; GA 953167. Fraunhofer IFAM, DE (W. Leite Cavalcanti); Cnr Nano Modena (A. Calzolari). 2021-2025.
www.open-model.eu

Abstract. OpenModel aims to design, create, provide, and maintain a sustainable integrated open platform for innovation which delivers predictable, validated, and traceable simulation workflows integrating seamlessly third-party physics-based models, solvers, post-processors and databases. OpenModel thus bridges the gap from industry challenge via translation to actionable results that enable well informed business decisions. Six use cases (Success Stories) show the applicability to a wide range of materials and their related processing technologies and demonstrate how OpenModel facilitates setting up experiments, reducing error and enhancing development efficiency.

PERSEUS. 2D Material-Based Multiple Oncotherapy Against Metastatic Disease Using a Radically New Computed Tomography Approach. HORIZON-EIC-2022-PATHFINDEROPEN-01; GA 101099423. Cnr Imem, IT (G. Salvati); Cnr Nano Pisa (F. Fabbri). 2023-2027.

Abstract. Computed tomography (CT) is a diagnostic imaging modality that combines X-rays to produce images of any part of the body. Funded by the European Innovation Council, the PERSEUS project comes to extend the usability of CT to treat tumours that are inaccessible by other methods, such as metastatic triple negative breast cancer and pancreatic cancer. PERSEUS plans to implement a new nanotechnology-based therapy using a nano-system that is activated by the CT beam and causes cancer cell death through heat and reactive oxygen species. Moreover, the release of cancer antigens has the potential to activate the immune system and generate anti-cancer immunity.

QATACOMB. Quantum correlations in Terahertz qcl COMBs. H2020-ERA-NET-QuantERA II Call 2021; GA 731473 and GA 101017733. Cnr Ino, IT (L. Consolino); Cnr Nano Pisa (M. S. Vitiello and L. Sorba). 2022-2025.
www.quantera.eu/qatacomb

Abstract. Quantum technology (QT) migration to the terahertz (THz) frequency range is technologically challenging, although of huge technological potential. In fact, continuous-variable entangled THz states preparation can become the founding blocks for future implementation of quantum computation protocols, quantum teleportation or to increase capacity, robustness and security of selected free-space quantum communication channels. For example, the peculiar features of THz radiation, transmissivity through otherwise opaque materials, or robustness with respect to Rayleigh scattering, can potentially allow a plethora of frontier applications, such as quantum-secured fast digital data transfer in opaque or harsh environments (dust, smog, particulate) or quantum-enhanced sensitivity in spectroscopic and metrological THz setups.

QC4QT. Advancing Quantum Computers for (and with) Quantum Thermodynamics. HORIZON-MSCA-2021-PF-01; GA 101063316. Cnr Nano Pisa (M. Campisi). 2022-2024.

Abstract. Inspired by synergy between quantum computers (QCs) and quantum ther-

modynamics (QT), this proposal includes two thrusts to advance progress along these two fronts. For the first thrust, the aim is to develop new algorithms packaged into well-documented, open-source software for simulating thermal properties and behaviors of quantum systems on QCs. This work will culminate in attempting the first-ever experimental validation fluctuation relations (theoretical pillars of QT) for open quantum systems on a QC. For the second thrust, to use the principles of QT to implement an algorithmic cooling scheme that can improve the overall performance of qubits for any desired application on a QC. This work will culminate in attempting the first-ever experimental demonstration of algorithmic cooling on a QC. The proposed research requires an interdisciplinary approach encompassing quantum information and computation; thermodynamics and statistical mechanics; and computational science (CS). The complementary expertise and experience of the experienced researcher (in QC and CS) and the supervising host (in QT) will foster a productive two-way transfer of knowledge and facilitate the success of the research goals.

SMART-electron. Ultrafast all-optical spatio-temporal electron modulators: opening frontiers in electron microscopy. H2020 FETOPEN 2018-2020; GA 964591. University of Milan – Bicocca, IT (G. Vanacore); Cnr Nano Modena (V. Grillo). 2021-2025.
www.smartelectron.eu

Abstract. SMART-electron aims at developing an innovative technological platform for designing, realizing and operating all-optical rapidly programmable phase masks for electrons. SMART-electron will introduce a new paradigm where properly synthesized ultrafast electromagnetic fields will be used for engineering the phase space of a free-electron wave function. This will allow us to achieve unprecedented space/time/energy/momentum shaping of electron matter waves, thus surpassing conventional passive monolithic schemes, and revolutionizing the way materials are investigated in electron microscopy.

SPECTRUM
THE QUANTUM SWITCH

SPECTRUM. SuPErConducTing Radio-frequency switch for qUantuM technologies. HORIZON-EIC-2021-TRANSITIONOPEN-01; GA 101057977. Cnr Nano Pisa (C. Puglia and F. Giazotto). 2022-2025.
www.spectrum-project.eu

Abstract. Spectrum introduces QueSt, the first switch developed specifically for QCs, which provides ultrashort down to near-zero downtimes between switching events and negligible heat injection. Poor scalability and high cost are among the main limiting factors for the development and deployment of quantum computers. Both problems are related to the bulkiness and multiplicity of the signal lines that run through the quantum computer. The large number of wires limits scalability and decreases the thermal stability of the quantum processing units (QPUs).
Through the innovative radiofrequency (RF) switch QueSt, Spectrum aims to increase the scalability and minimize problems related to heating, thus expediting the development of QCs. Thanks to a new technological approach, the Quantum sUpErconducting

SwiTch (QueSt) allows: low power dissipation; control of multiple qubit configurations; voltage control and compatibility with cmos systems; high switching speed.

SPRINT. Ultra-short pulse laser resonators in the Terahertz. ERC-2015-CoG; GA 681379. Cnr Nano Pisa (M. S. Vitiello). 2016-2023.

Abstract. Ultra-short light pulses with large instantaneous intensities can probe light-matter interaction phenomena, capture snapshots of molecular dynamics and drive high-speed communications. In a semiconductor laser, mode-locking is the primary way to generate ultrafast signals. Despite the intriguing perspectives, operation at Terahertz (THz) frequencies is facing fundamental limitations: engineering "ultrafast" THz semiconductor lasers from scratch or finding an integrated technology to shorten THz light pulses are currently two demanding routes. SPRINT aims to innovatively combine the groundbreaking quantum cascade laser (QCL) technology with graphene, to develop a new generation of passive mode-locked THz photonic laser resonators, combined with unexplored electronic nanodetectors for ultrafast THz sensing and imaging.

STAR. HyperSpectral Terahertz near-field nanoscope exploiting miniaturized frequency-combs. ERC-2022-POC2; GA 101081567. Cnr Nano Pisa (M. S. Vitiello). 2022-2024.

Abstract. Ever-finer lasers can open new ways to gaze on the smallest objects, such as the structures of proteins. The EU-funded STAR project will further develop such nanoscale imaging with the creation of a new graphene-integrated, quantum cascade laser that operates at terahertz frequencies. The project aims to provide a compact and low-cost solution to create amplitude- and phase-resolved images without making use of an external detector. The resulting nanoscope will be able to image objects between 40 100 nm. The project will develop a prototype and demonstrate the technology at trade shows with commercial end users and could see uses in biology, medicine, and materials science.

SUPERCONTACTS. Solid state diffusion for atomically sharp interfaces in semiconductor-superconductor hybrid structures. H2020-MSCA-IF-2020; GA 101022473. Cnr Nano Pisa (E. Strambini). 2021-2023.

Abstract. A matchmaker's delight strengthens the field of superconducting optoelectronics. Semiconductors, materials that literally 'semi-conduct' electricity, have revolutionised our lives with applications in everything from consumer electronics and solar cells to lasers. Integrating semiconductors with superconductors opens the door to limitless possibilities of device functionality and new applications including quantum processing, communication, and encryption. However, fine-tuning and optimising the actual physical interface between the two types of materials has been challenging due to lack of control. With the support of the Marie Skłodowska-Curie Actions programme, the SuperCONtacts project intends to overcome these limitations with a new fabrication technique that will lead to the

realisation of atomically sharp superconductor–semiconductor interfaces.

SUPERGALAX. Highly sensitive detection of single microwave photons with coherent quantum network of superconducting qubits for searching galactic axions. H2020-FETOPEN-2018-2019-2020-0; GA 863313. Cnr Spin, IT (M. Lisitskiy); Cnr Nano Modena (M. Affronte). 2020-2023.
www.supergalax.eu

Abstract. Breakthrough method of detecting low-energy microwave photons. Detecting single photons at the microwave frequency range is important in the search for axion dark matter, quantum computing and metrology applications. The EU-funded SUPERGALAX project proposes a novel approach for the acquisition of extremely low-energy microwave signals. Researchers will fabricate and explore the dynamics of coherent quantum networks comprising a large amount of strongly interacting superconducting qubits – transmons and flux qubits. The team expect that the measurement sensitivity of their superconducting network detector will reach the Heisenberg limit – the standard limit on the precision with which a quantum measurement can be carried out. Manipulating and measuring individual photons at particularly low microwave frequencies will aid in the detection of hypothetical dark-matter axions, making information processing more efficient.

SUPERGATE. Gate Tunable Superconducting Quantum Electronics. H2020-FETOPEN-2018-2020; GA 964398. University of Kostanz, DE (E. Scheer); Cnr Nano Pisa (F. Giazotto). 2021-2024.
www.supergate.uni-konstanz.de

Abstract. A new approach to superconducting logic gates could usher in a new age of supercomputing. Calculators were a major improvement over pencil and paper, but computers truly revolutionised our ability to do calculations, exponentially increasing the number and complexity of computations possible in a fraction of the time. Supercomputers relying on superconducting quantum logic gates have extended those possibilities. They are increasingly invaluable to numerous fields but are facing challenges in terms of enhancing performance while reducing energy consumption. The EU-funded SuperGate project will develop a new approach to superconducting logics that will enable the same or better performance while minimising current problems, ushering in the next evolution of supercomputers.

SUPERTED. Thermoelectric detector based on superconductor-ferromagnet heterostructures. H2020-FETOPEN-1-2016-2017; GA 800923. Jyvaskylan Yliopisto, FI (T. Heikkilä); Cnr Nano Pisa (F. Giazotto). 2018-2023.
www.superted-project.eu

Abstract. Superted proposes to study a new type of sensor based on the thermoelectric conversion of the radiation signal to electrically measurable one. This approach is based on the newly found giant thermoelectric effect taking place in superconductor/ferromagnet heterostructures. Utilizing this effect, the sensor pixels can be self-powered by the measured radiation, and therefore extra bias lines are not needed (patent pending for the detector concept). Within the project, we aim to establish a proof of concept of this device by (i) fabricating such detector elements, and (ii) characterizing single pixels of thermoelectric detectors for X-ray and THz imaging via approaches that are scalable to large arrays.

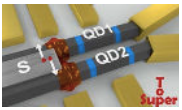

SUPERTOP. Topologically protected states in double nanowire semiconductor hybrids. H2020 QuantERA ERA-NET Cofund in Quantum Technologies 2017. Budapest University of Technology and Economics, HU (S. Csonka); Cnr Nano Pisa (L. Sorba). 2018-2022.
www.dept.physics.bme.hu/Supertop

Abstract. To realize fully topologically protected universal quantum computation, more exotic anyons, such as parafermions are required. Thus, the unambiguous demonstration of parafermion states will have a great impact on the development of universal quantum computation. The experimental realization of parafermions is challenging, since they are based on the combination of various ingredients, such as crossed Andreev reflection, electron-electron or spin-orbit interaction, and high-quality quantum conductors. Thus, the investigation of all these ingredients is essential and timely to achieve further experimental progress. The main objectives of SuperTop are: a) development of different DNW (double nanowire-based hybrid devices geometries), which consist of two parallel 1D spin-orbit nanowires coupled by a thin superconductor stripe and b) investigation of the emerging exotic bound states at the superconductor/semiconductor interface of the DNW.

TeraApps. TeraApps. Doctoral Training Network in Terahertz Technologies for Imaging, Radar and Communication Applications. H2020-MSCA-ITN-2017; GA 765426. University of Glasgow, UK (E. Wasige); Cnr Nano Pisa (M. S. Vitiello). 2018-2022.
www.gla.ac.uk/research/az/teraapps

Abstract. This network addresses the future societal need in Teraherz technologies, by addressing the training gap, and crystallizing world leading groups in a concentrated research effort. Emerging research areas in this field link, e.g., semiconductor materials synthesis, high-speed electronic device physics and engineering, antenna design, THz optics, and a raft of diverse applications and a new generation of academic and industry leaders in developing these devices and systems in the terahertz spectral band is now required. In particular, the project focuses on tunneling devices that have been shown to be the leading candidate in realizing compact, low-cost, high-performance THz transmitters and receivers once coupled to suitable antennas. Also, new two-dimensional (2D) materials such as graphene or 1D nanowires are emerging as suitable platforms for realizing highly sensitive detectors of THz radiation.

TERASEC. THz imaging technology for public security. ERC-2019-PoC; GA 899315. Cnr Nano Pisa (F. Giazotto). 2020-2022.

Abstract. The objectives of TERASEC project entail the activities aimed at pre-commercial validation of the technological performances and market potential of a novel device for the detection of security threats, such as weapons, explosives, drugs, etc. The functionality of TERASEC is enabled through combination of superconducting and ferromagnetic materials that delivers frequency selective THz sensors showing unprecedented sensitivity (single-photon resolution), fast response time, high dynamic range, and low noise-equivalent-power. Specifically, starting from the outstanding outcomes reached so far, the capacity of the TERASEC system to detect the above threats with given level of accuracy, range and selectivity will be verified in accordance with the requirements of prospect users (to be collected during the project implementation). Moreover, a detailed market, IPR and regulatory compliance study will be carried out, to enable smooth implementation of TERASEC in the complicated context of the public security market. To enhance this, an advisory board gathering Key Opinion Leaders of the sector will be secured and involved into project activity throughout all the project duration. In parallel, comprehensive communication strategy addressing all the stakeholders of the relevant value chain will be rolled out, with strong focus on prospect consumers and users, so to ensuring market traction. Overall, the goal of TERASEC is to deliver an unrivalled novel security scanner device leveraging harmless THz waves, that widely overpasses the accuracy performances of all the conventional systems, thus contributing to the safety of European citizens and the security of sensitive infrastructures.

TOPOCIRCUS. Simulations of Topological Phases in Superconducting Circuits. H2020-MSCA-IF-2018; GA 841894. Cnr Nano Pisa (F. Giazotto). 2019-2022.

Abstract. The discovery of topological order characterising novel exotic phases of matter has generated a breakthrough in the comprehension of complex condensed matter phases. Topological invariants entirely determine the behaviour of certain observables and confer to the systems a strong robustness to perturbations. Going beyond condensed matter states, topological order can be engineered in different setups that can benefit from it and represent alternative platform for the simulation of exotic topological phases. Among the most promising candidates for such a plan are the superconducting circuits based on the Josephson effect. This project aims at studying the interconnections between the topological notion and the Josephson effect and to propose superconducting circuits as a platform for the simulation and manipulation of novel topological phases of matter.

National projects

AI-TEM. Artificial intelligence enhanced transmission electron microscopy for advanced imaging. MUR Prin 2022; project nr. 2022249HSF. Cnr Nano Modena (V. Grillo). 2023-2025.

AMONIX. Amorphous conductors as a new route for plasmonics. MUR Prin 2022; project nr. 2022BTMXZT. Cnr Nano Modena (S. Benedetti). 2023-2025.

ARTES4.0. Advanced Robotics and enabling digital Technology and Systems. MISE D.D. del 29.01.2018. Cnr Nano Pisa (L. Persano). 2019-2022.

aSTAR. Attosecond transient absorption and reflectivity for the study of exotic materials. MIUR Prin 2017; project nr. 2017RKWTMY. Politecnico di Milano (C. Vozzi); Cnr Nano Modena (S. Pittalis). 2019-2022.

ASTRO SECRET. Molecular mechanisms of astrocyte maturation and secretome in neurodevelopmental disorders associated with prenatal inflammation. MIUR Prin 2022; project nr. 2022Y544HH. Cnr Nano Modena (G. Losi). 2022-2025.

CHERISH-C. Chemical and electrochemical energy storage materials from organic wastes: the treasure hidden in C based materials. MUR Prin 2022; project nr. 202278NHAM. Cnr Nano Pisa (L. Bellucci). 2023-2025.

Early dysfunctions of intercellular signalling in brain disorders. MIUR Prin 2017; project nr. 20175C22WM. Cnr Ibcn (F. Mammano); Cnr Nano Pisa (G. M. Ratto). 2019-2022.

ENGInerve. Development of nano/micro-engineered devices for applications in peripheral nervous system pathological models. MUR Prin 2022; project nr. 2022ZH5M72. Cnr Nano Pisa (I. Tonazzini). 2023-2025.

EnvELOP. Environmental tuning of microbial rhodopsins Electronic Landscape for new Optogenetic Potentialities. MUR Prin 2022; project nr. 2022WS44W4. Cnr Nano Modena (L. Zanetti Polzi). 2023-2025.

EQUATE. Defect engineered for electro-thermal quantum technology. MUR Prin 2022; project nr. 2022Z7RHRS. Cnr Nano Pisa (F. Bianco). 2023-2025.

ERACLITO. Earth abundant and non-toxic doped metal oxide-based electro optic photonic structures for smart windows and radiative cooling. MUR Prin 2022; project nr. 2022ZMA4X3. Cnr Nano Modena (A. di Bona). 2023-2025.

EXC-INS. Excitonic insulator in two-dimensional long-range interacting system. MIUR Prin 2017; project nr. 2017BZPKSZ. Università di Modena e Reggio Emilia (E. Molinari); Cnr Nano Modena (M. Rontani). 2019-2022.

GAMESQUAD. Gate-induced microscopic effects on superconducting quantum devices. MUR Prin 2022; project nr. 2022A8CJP3. Cnr Nano Pisa (A. Crippa). 2023-2025.

GROUNDS. Growth and optical studies of tunable quantum dots and superlattices in semiconductor nanowires. MUR Prin 2022; project nr. 20223WZ245. Cnr Nano Pisa (V. Zannier). 2023-2025.

HARVEST. Learning from natural pigment-protein complexes how to design artificial light-harvesting systems. MIUR Prin 2017; project nr. 201795SBA3. Politecnico di Milano (G. Cerullo); Cnr Nano Modena (D. Prezzi). 2019-2022.

TRIPARTITE AD. Interaction between cholinergic and glumatergic synaptic trasmission at tripartite synapse in the pathophysiology of Alzehimer's disease. MIUR Prin 2020; project nr. 2020AMLXHH. Cnr Nano Modena (G. Losi). 2022-2025.

LOVE. Lab-on-chip for sustainable olive value chain: development of a lab-on-chip for detecting polyphenolic compounds in olives and its derivates. MUR Prin 2022; project nr. 2022M4WB3M. Cnr Nano Pisa (A. Battisti). 2023-2025.

MAGNETISE. Rare-earth single atom magnets anchored at oxide surfaces as a platform for new low-consumption magnetic devices. MUR Prin 2022; project nr. 2022KXN79M. Cnr Nano Modena (V. Bellini). 2023-2025.

MONTRE2D. Monolithic strain engineering platform for two-dimensional materials. MIUR Prin 2017; project nr. 2017KFMJ8E. Università di Pisa (A. Tredicucci); Cnr Nano Pisa (V. Tozzini). 2019-2022.

NEMO. Next generation of molecular and supramolecular machines: towards functional nanostructured devices, interfaces, surfaces and materials. MIUR Prin 2017; project nr. 20173L7W8K. Università di Bologna (A. Credi); Cnr Nano Pisa (L. Persano). 2019-2022.

NEThEQS. Non-equilibrium coherent thermal effects in quantum systems. MUR Prin 2022; project nr. 2022B9P8LN. Cnr Nano Pisa (F. Taddei). 2023-2025.

PACECOR. Early phase preclinical development of PACECOR, a mutation-independent Anti-SARS-Co2 therapeutic strategy. MIUR Prin 2021; project nr. 2020LW7XWH. Cnr Nano Modena (G. Brancolini). 2022-2025.

QCC. Quantum computing for computational chemistry and materials science. MUR Prin 2022; project nr. 2022W9W423. Cnr Nano Modena (R. Di Felice). 2023-2025.

q-LIMA. Light-matter interactions and the collective behavior of quantum 2D materials. MIUR Prin 2020; project nr. 2020JLZ52N. Cnr Nano Pisa (F. Bianco). 2022-2025.

TOAC. Touch on a chip. MUR Prin 2020; project nr. 20208TPFLN. Cnr Nano Pisa (I. Tonazzini). 2022-2025.

TOPOFLAG. Non-reciprocal supercurrent and topological transitions in hybrid Nb-InSb nanoflags. MUR Prin 2022; project nr. 2022PH852L. Cnr Nano Pisa (S. Heun). 2023-2025.

TRUST. Trampolines as ultra-sensitive thermomechanical bolometers. MUR Prin 2022; project nr. 2022M5RSK5. Cnr Nano Pisa (A. Pitanti). 2023-2025.

TUNES. Tuning the electronic structure of graphene from low to high electron doping. MUR Prin 2022; project nr. 2022NXLTYN. Cnr Nano Modena (A. Ferretti). 2023-2025.

UTFROM. Understanding and tuning friction through nanostructure manipulation. MIUR Prin 2017; project nr. 20178PZCB5. Università di Genova (R. Ferrando); Cnr Nano Modena (G. Paolicelli). 2019-2022.

VIBETWO. Understanding and optimizing coherent vibronic coupling in 2D hybrid light-harvesting heterostructures for photovoltaic performance. MUR Prin 2022; project nr. 202284JP34. Cnr Nano Modena (C. A. Rozzi). 2023-2025.

VIOLoC. Analisi vino e olio 4.0: sviluppo di un laboratorio on-chip (LoC) a connettività remota (clouding). MIUR FISR 2018-2019; project nr. FISR2019_03020. Cnr Nano Pisa (M. Cecchini). 2021-2023.

2D-FRONTIERS. 2D van der Waals heterostructures for novel concepts in energy storage. MUR Prin 2022; project nr. 20228879FT. Cnr Nano Modena (D. Prezzi). 2023-2025.

MUR Prin 2022 PNRR

(Mission 4, Component 2, Investment 1.1)

A molecular platform for intracellular nitric oxide sensing. PE4; Code: P2022F4WR8; CUP: B53D23025310001. Cnr Nano Pisa (R. Nifosì). 2023-2025.

ResET. Resonant energy transfer from plasmonic nanoparticles to semiconductors: a route to improve solar photocatalytic efficiency. Code: P2022ZHCT3; CUP: B53D23028720001. Cnr Nano Modena (P. Luches). 2023-2025.

THERmIR. Continuous thermal monitoring with wearable mid-infrared sensors. PE7; Code: P2022AHXE5; CUP: B53D23023880001. Cnr Nano Pisa (L. Viti). 2023-2025.

Next Generation EU - PNRR (2022-2025)

(M indicates Mission, C Component, I Investment)

EcosistER. Ecosystem for Sustainable Transition in Emilia-Romagna. M 4, C 2, I 1.5; Code: ECS_00000033.
Spoke 1 "Materials for sustainability and ecological transition". Cnr Nano Modena (S. Benedetti).
Spoke 3 "Green manufacturing for a sustainable economy". Cnr Nano Modena (G. Paolicelli).
www.ecosister.it

THE. Tuscany Health Ecosystem. M 4, C 2, I 1.5; Code: ECS_00000017.
Spoke 1 "Advanced radiotherapies and diagnostics in oncology". Cnr Nano Pisa (V. Tozzini).
Spoke 4 "Nanotechnologies for diagnosis and therapy". Cnr Nano Pisa (A. Camposeo and M. Cecchini).
www.tuscanyhealthecosystem.it

CN1 HPC. National Centre for HPC, Big Data and Quantum Computing. M 4, C 2, I 1.4; Code: CN0000013.
Spoke 7 "Materials and Molecular Sciences". Cnr Nano Modena (A. Ferretti).
Spoke 10 "Quantum Computing". Cnr Nano Modena (R. Di Felice).
www.supercomputing-icsc.it/en/icsc-home

CN3 RNA Drug development. National Centre for Gene Therapy and Drugs based on RNA Technology. M 4, C 2, I 1.4; Code: CN00000041.
Spoke 6 "RNA Drug Development". Cnr Nano Pisa (B. Storti).

CN4 MOST. Centro Nazionale Mobilità Sostenibile. M 4, C2, I 1.5; Code: CN00000023.
Spoke 11 "Innovative Materials and Lightweighting Description of the Spoke Activities". Cnr Nano Modena (P. Luches).
www.centronazionalemost.it

PE2 NEST. Enlarged partnership "Network 4 Energy Sustainable Development". M 4, C2, I 1.3; Code: PE00000021.
Spoke 2 "Energy harvesting and off-shore renewables". Cnr Nano Pisa (L. Persano).

PE4 NQSTI. Enlarged partnership "National Quantum Science and Technology Institute". M 4, C 2, I 1.3; Code: PE0000023.
Spoke 2 "Simulation, sensing and metrology". Cnr Nano Modena (F. Troiani).
Spoke 4 "Photonic platform for quantum technologies". Cnr Nano Pisa (M. S. Vitiello).

Spoke 5 "Electron-based platform for quantum technologies". Cnr Nano Pisa (L. Sorba); Cnr Nano Modena (V. Grillo).
www.nqsti.it

PE11 3A-ITALY. Enlarged partnership "Made-in-Italy circolare e sostenibile". M 4, C 2, I 1.3; Code: PE0000004.
Spoke 6 "Additive manufacturing as disruptive enabler of the twin transition". Cnr Nano Pisa (A. Camposeo).

PE13 INF-ACT. Enlarged partnership "One Health Basic and Translational Research Actions addressing Unmet Needs on Emerging Infectious Diseases". M 4, C 2, I 1.3; Code: PE00000007.
Spoke 5 "New therapeutic strategies". Cnr Nano Pisa (A. Sgarbossa); Cnr Nano Modena (G. Brancolini).

PE14 RESTART. Enlarged partnership "Research and innovation on future Telecommunication systems and networks, to make Italy more smart". M 4, C 2, I 1.3; Code: PE00000001.
Spoke 3 "Wireless Networks and Technologies". Cnr Nano Pisa (M. S. Vitiello).
www.fondazione-restart.it/2022/11/10/restart-foundation-the-telecommunications-of-the-future

iENTRANCE@ENL. Infrastructure for Energy Transition and Circular Economy @ EuroNanoLab. M 4, C 2, I 1.3; Code: IR0000027. Cnr Nano Modena (V. Grillo).
www.ientrance.eu/home/index.php

D3 4 Health. Digital Driven Diagnostics, prognostics and therapeutics for sustainable Health care. Piano nazionale per gli investimenti complementari al PNRR - Next Generation EU; Codice: PNC 0000001 D3 4 Health.
Spoke 3 "Wearable technologies, sensors and biomarkers for care through Digital Twin approaches". Cnr Nano Pisa (I. Tonazzini).
www.sites.google.com/uniroma1.it/d3forhealth/home

Cnr projects

Heat conduction experiments on topological superconductors. Joint Bilateral Agreement CNR/NSFC National Natural Science Foundation of China. Cnr Nano Pisa (F. Paolucci). 2021-2022.

Research tools for measuring and manipulating chloride in the brain. Joint Bilateral Agreement CNR/Royal Society (UK). Cnr Nano Pisa (G. M. Ratto). 2022.

TEROCODE. Terahertz optoelectronics for communication in difficult environments. Progetti di Ricerca@CNR. Cnr Nano Pisa (L. Viti). 2021-2023.

Regional projects

ADAPTA. Sinonasal cancer: In depth genetic analysis of patients for personalized treatment and disease monitoring. Regione Toscana; Bando Ricerca Salute 2018 - DD15397/2018. Università di Pisa, IT (A. Franchi); Cnr Nano Pisa (L. Persano). 2020-2024. *www.unipi.it/index.php/risultati-e-prodotti/item/18731-adapta*

DECODE-EE. Developmental and epileptic encephalopathies: epidemiology, comorbidities, molecular diagnosis, personalized management, and costs analysis. Regione Toscana; Bando Ricerca Salute 2018 - DD15397/2018. Scuola Superiore S. Anna, IT (P. Castoldi); Cnr Nano Pisa (G. M. Ratto and M. Satti). 2020-2024.

DEM-AGING. Neurodegenerative disorders throughout the lifespan. Autophagy-dependent biomarkers for trial readiness from infantile neuronal ceroid-lipofuscinoses to senile dementias. Regione Toscana; Bando Ricerca Salute 2018 - DD15397/2018. IRCCS Stella Maris, IT (F. Santorelli); Cnr Nano Pisa (G. M. Ratto and M. Satti). 2020-2024.

RIMMEL. RIvestimenti Multi-funzionali e multi-scala, per componenti MEccanici in acciaio e Leghe di alluminio fabbricati con additive manufacturing. Regione Emilia-Romagna POR FESR 2014-2021 - Azione 1.2.2. Cnr Nano Modena (S. Valeri). 2019-2022. *www.rimmel.nano.cnr.it*

TOSCANO. The Omics SCiences AgaiNst Osteosarcoma. Regione Toscana - Bando Ricerca Salute 2018; DD15397/2018. Cnr Nano Pisa (M. Cecchini). 2020-2024.

Other funding agencies

END. Isolation and molecular characterization of neuronal exosomes in models of neu-

rodevelopmental disorders. Regione Toscana – Fondazione Pisana Scienza 2021; project nr. DSB.AD008.729. Cnr Nano Pisa (I. Tonazzini). 2022-2024.

Growth of nanowire based heterostructures. University of Basel. Cnr Nano Pisa (L. Sorba). 2021-2022.

InnovAS. Innovative brain-targeting nano-tools and imaging methods for therapeutic development in Angelman Syndrome. Angelman Syndrome Alliance. Cnr Nano Pisa (I. Tonazzini). 2022-2025.

Intracellular. Chloride dynamics in autistic brain: a better understanding is needed for tailored cures. Telethon GP12701. Cnr Nano Pisa (G. M. Ratto). 2019-2023.
www.telethon.it/cosa-facciamo/ricerca/progetti-finanziati/la-regolazione-del-cloro-intracellulare-nel-cervello-autistico-dalla-ricerca-di-base-alla-identificazione-di-nuovi-bersagli-farmacologici

NanoERT. Nanoparticle based Enzyme Replacement Therapy for the Treatment of Krabbe disease: a pre-clinical study in the Twitcher Mouse. European Leukodystrophy Association (ELA); Grant n. 2019-008I2. Cnr Nano Pisa (M. Cecchini). 2020-2022.

Optoelectronics and nano-photonics in two-dimensional nanomaterial heterostructures. Fondazione Internazionale Premio Balzan. Cnr Nano Pisa (M. S. Vitiello). 2018-2025.
www.thz-photonics.nano.cnr.it/balzan-research-project

q-Land. Investigation of Quantum Landauer Principle on a Quantum Annealer. ISCRA-CINECA. Cnr Nano Pisa (M. Campisi). 2021-2022.

SAWINE. Laboratorio on-chip basato su onde acustiche di superficie. Bando CARILUCCA 2019 – 2021 "Ricerca". Cnr Nano Pisa (M. Cecchini). 2020-2022.

THESEUs. Miniaturized Terahertz sources for Humans and Environmental SEcUrity. NATO Science for Peace and Security Programme. project nr. MYPG57. Cnr Nano Pisa (F. Bianco). 2020-2023.
http://web.nano.cnr.it/theseus

2022 - 2023 external fundings (in €)

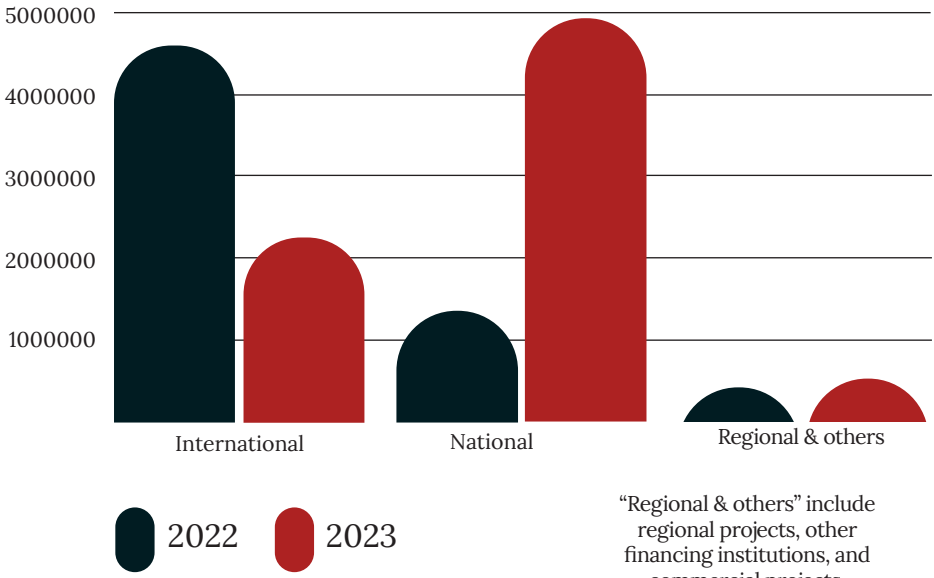

"Regional & others" include regional projects, other financing institutions, and commercial projects.

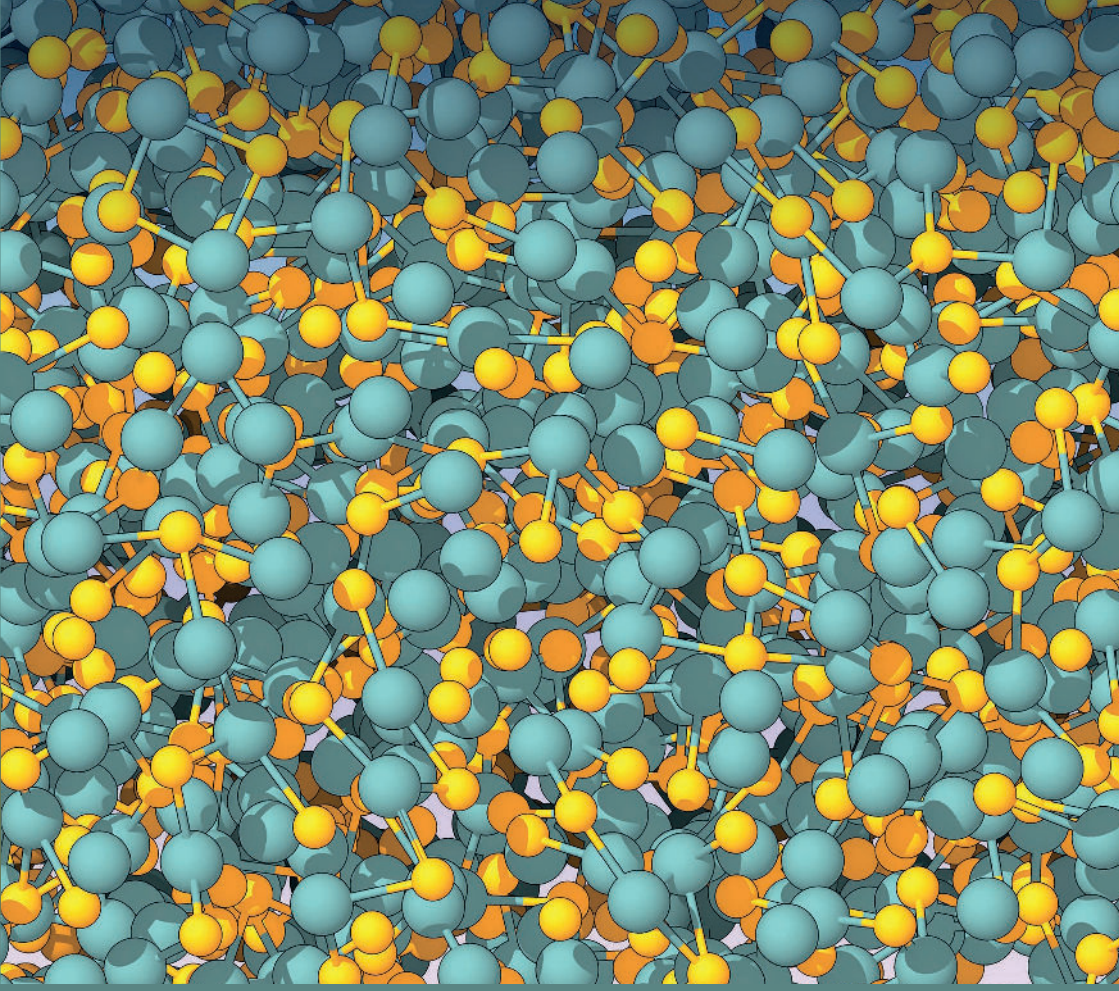

Publications

A list of publications from journals with IF ≥ 8.6 (i.e., Physical Review Letter's IF in 2023) ordered by their JCR 2023 IF is given. A full and updated list of publications is available on the Institute website at the page "Publications" (http://www.nano.cnr.it/publications). Publications marked with © earned a cover in the corresponding journal. Covers are displayed at the end of this section.

2022

Spin cross-correlation experiments in an electron entangler.
A. Bordoloi, V. Zannier, L. Sorba, C. Schönenberger, and A. Baumgartner. Nature 612, 454-458 (2022).

Machine learning in scanning transmission electron microscopy.
S. V. Kalinin, C. Ophus, P. M. Voyles, R. Erni, D. Kepaptsoglou, V. Grillo, A. R. Lupini, M. P. Oxley, E. Schwenker, M. K. Y. Chan, J. Etheridge, X. Li, G. G. D. Han, M. Ziatdinov, N. Shibata, and S. J. Pennycook. Nature Reviews Methods Primers 2, 11 (2022).

Quenching the bandgap of two-dimensional semiconductors with a perpendicular electric field.
D. Domaretskiy, M. Philippi, M. Gibertini, N. Ubrig, I. Gutiérrez-Lezama, and A. F. Morpurgo. Nature Nanotechnology 17, 1078-1083 (2022).

Bipolar thermoelectric Josephson engine.
G. Germanese, F. Paolucci, G. Marchegiani, A. Braggio, and F. Giazotto. Nature Nanotechnology 17, 1084-1090 (2022).

Quasi-1D Electronic Transport in a 2D Magnetic Semiconductor.
F. Wu, I. Gutiérrez-Lezama, S. A. López-Paz, M. Gibertini, K. Watanabe, T. Taniguchi, F. O. von Rohr, N. Ubrig, and A. F. Morpurgo. Advanced Materials 34, 2109759 (2022).

Astrocytes mediate long-lasting synaptic regulation of ventral tegmental area dopamine neurons.
L. M. Requie, M. Gómez-Gonzalo, M. Speggiorin, F. Managò, M. Melone, M. Congiu, A. Chiavegato, A. Lia, M. Zonta, G. Losi, V. J. Henriques, A. Pugliese, G. Pacinelli, G. Marsicano, F. Papaleo, A. L. Muntoni, F. Conti, and G. Carmignoto.
Nature Neuroscience 25, 1639-1650 (2022).

Egg protein derived ultralightweight hybrid monolithic aerogel for water purification.
S. Ozden, S. Monti, V. Tozzini, N. S. Dutta, S. Gili, N. Caggiano, A. J. Link, N. M. Pugno, J. Higgins, R. D. Priestley, and C. B. Arnold. Materials Today 59, 46-55 (2022).

Magnetic behavior in metal-free radical thin films.
T. Junghoefer, A. Calzolari, I. Baev, M. Glaser, F. Ciccullo, E. Giangrisostomi, R. Ovsyannikov, F. Kielgast, M. Nissen, J. Schwarz, N. M. Gallagher, A. Rajca, M. Martins, and M. B. Casu. Chem 8, 801-814 (2022).

Hydrogen Spillover and Storage on Graphene with Single-Site Ti Catalysts.
J. W. Chen, S. H. Hsieh, S. S. Wong, Y. C. Chiu, H. W. Shiu, C. H. Wang, Y. W. Yang, Y. J. Hsu, D. Convertino, C. Coletti, S. Heun, C. H. Chen, and C. L. Wu. ACS Energy Letters 7, 2297-2303 (2022).

To measure a magnon population.
M. Carrega and S. Heun. Nature Physics 18, 3-4 (2022).

Evidence for equilibrium exciton condensation in monolayer WTe2.
B. Sun, W. Zhao, T. Palomaki, Z. Fei, E. Runburg, P. Malinowski, X. Huang, J. Cenker, Y. T. Cui, J. H. Chu, X. Xu, S. S. Ataei, D. Varsano, M. Palummo, E. Molinari, M. Rontani, and D. H. Cobden. Nature Physics 18, 94-99 (2022).

Thermal superconducting quantum interference proximity transistor.
N. Ligato, F. Paolucci, E. Strambini, and F. Giazotto. Nature Physics 18, 627-632 (2022).

© Surface-Acoustic-Wave (SAW) Induced Mixing Enhances the Detection of Viruses: Application to Measles Sensing in Whole Human Saliva with a SAW Lab-On-a-Chip.
M. Agostini, F. Lunardelli, M. Gagliardi, A. Miranda, L. Lamanna, A. G. Luminare, F. Gambineri, M. Lai, M. Pistello, and M. Cecchini. Advanced Functional Materials 32, 2201958 (2022).

Highly-Packed Proximity-Coupled DC-Josephson Junction Arrays by a Direct-Write Approach.
F. Porrati, F. Jungwirth, S. Barth, G. C. Gazzadi, S. Frabboni, O. V. Dobrovolskiy, and M. Huth. Advanced Functional Materials 32, 2203889 (2022).

Giant reduction of thermal conductivity and enhancement of thermoelectric performance in twinning superlattice InAsSb nanowires.
L. Peri, D. Prete, V. Demontis, V. Zannier, F. Rossi, L. Sorba, F. Beltram, and F. Rossella. Nano Energy 103, 107700 (2022).

Dynamical evolution of Ge quantum dots on Si(111): From island formation to high temperature decay.
N. Preetha Genesh, F. De Marchi, S. Heun, S. Fontana, R. Belkhou, R. Purandare, N. Motta, A. Sgarlata, M. Fanfoni, J. MacLeod, O. MacLean, and F. Rosei. Aggregate 3, e201 (2022).

Insight on Chirality Encoding from Small Thiolated Molecule to Plasmonic Au@Ag and Au@Au Nanoparticles.
A. Carone, P. Mariani, A. Désert, M. Romanelli, J. Marcheselli, M. Garavelli, S. Corni, I. Rivalta, and S. Parola. ACS Nano 16, 1089-1101 (2022).

Unexpected Electron Transport Suppression in a Heterostructured Graphene-MoS2Multiple Field-Effect Transistor Architecture.
G. Ciampalini, F. Fabbri, G. Menichetti, L. Buoni, S. Pace, V. Mišeikis, A. Pitanti, D. Pisignano, C. Coletti, A. Tredicucci, and S. Roddaro. ACS Nano 16, 1291-1300 (2022).

Evidence of Josephson Coupling in a Few-Layer Black Phosphorus Planar Josephson Junction.
F. Telesio, M. Carrega, G. Cappelli, A. Iorio, A. Crippa, E. Strambini, F. Giazotto, M. Serrano-Ruiz, M. Peruzzini, and S. Heun. ACS Nano 16, 3538-3545 (2022).

Electrically Tunable Nonequilibrium Optical Response of Graphene.
E. A. A. Pogna, A. Tomadin, O. Balci, G. Soavi, I. Paradisanos, M. Guizzardi, P. Pedrinazzi, S. Mignuzzi, K. J. Tielrooij, M. Polini, A. C. Ferrari, and G. Cerullo. ACS Nano 16, 3613-3624 (2022).

Van der Waals Heteroepitaxy of Air-Stable Quasi-Free-Standing Silicene Layers on CVD Epitaxial Graphene/6H-SiC.
Z. Ben Jabra, M. Abel, F. Fabbri, J. N. Aqua, M. Koudia, A. Michon, P. Castrucci, A. Ronda, H. Vach, M. De Crescenzi, and I. Berbezier. ACS Nano 16, 5920-5931 (2022).

Slow Magnetic Relaxation of Dy Adatoms with In-Plane Magnetic Anisotropy on a Two-Dimensional Electron Gas.
V. Bellini, S. Rusponi, J. Kolorenč, S. K. Mahatha, M. A. Valbuena, L. Persichetti, M. Pivetta, B. V. Sorokin, D. Merk, S. Reynaud, D. Sblendorio, S. Stepanow, C. Nistor, P. Gargiani, D. Betto, A. Mugarza, P. Gambardella, H. Brune, C. Carbone, and A. Barla. ACS Nano 16, 11182-11193 (2022).

Origins of the pH-Responsive Photoluminescence of Peptide-Functionalized Au Nanoclusters.
L. Zanetti-Polzi, P. Charchar, I. Yarovsky, and S. Corni. ACS Nano 16, 20129-20140 (2022).

Superconducting spintronic tunnel diode.
E. Strambini, M. Spies, N. Ligato, S. Ilić, M. Rouco, C. González-Orellana, M. Ilyn, C. Rogero, F. S. Bergeret, J. S. Moodera, P. Virtanen, T. T. Heikkilä, and F. Giazotto. Nature Communications 13, 2431 (2022).

Anomalous non-equilibrium response in black phosphorus to sub-gap mid-infrared excitation.
A. Montanaro, F. Giusti, M. Zanfrognini, P. Di Pietro, F. Glerean, G. Jarc, E. M. Rigoni, S. Y. Mathengattil, D. Varsano, M. Rontani, A. Perucchi, E. Molinari, and D. Fausti. Nature Communications 13, 2667 (2022).

Metamaterial-enabled asymmetric negative refraction of GHz mechanical waves.
S. Zanotto, G. Biasiol, P. V. Santos, and A. Pitanti. Nature Communications 13, 5939 (2022).

Plasmonic high-entropy carbides.
A. Calzolari, C. Oses, C. Toher, M. Esters, X. Campilongo, S. P. Stepanoff, D. E. Wolfe, and S. Curtarolo. Nature Communications 13, 5993 (2022).

Sensitivity and spectral control of network lasers.
D. Saxena, A. Arnaudon, O. Cipolato, M. Gaio, A. Quentel, S. Yaliraki, D. Pisignano, A. Camposeo, M. Barahona, and R. Sapienza. Nature Communications 13, 6493 (2022).

Current treatment options and novel nanotechnology-driven enzyme replacement strategies for lysosomal storage disorders.
A. Del Grosso, G. Parlanti, R. Mezzena, and M. Cecchini. Advanced Drug Delivery Reviews 188, 114464 (2022).

Self-Induced Phase Locking of Terahertz Frequency Combs in a Phase-Sensitive Hyperspectral Near-Field Nanoscope.
V. Pistore, E. A. A. Pogna, L. Viti, L. Li, A. G. Davies, E. H. Linfield, and M. S. Vitiello. Advanced Science 9, 2200410 (2022).

Unveiling the Cation Exchange Reaction between the NASICON Li1.5Al0.5Ge1.5(PO4)3 Solid Electrolyte and the pyr13TFSI Ionic Liquid.
A. Paolella, G. Bertoni, W. Zhu, D. Campanella, A. La Monaca, G. Girard, H. Demers, A. C. G. Nita, Z. M. Feng, A. Vijh, A. Guerfi, M. Trudeau, M. Armand, and S. A. Krachkovskiy. Journal of the American Chemical Society 144, 3442-3448 (2022).

High-Spin (S = 1) Blatter-Based Diradical with Robust Stability and Electrical Conductivity.
S. Zhang, M. Pink, T. Junghoefer, W. Zhao, S. N. Hsu, S. Rajca, A. Calzolari, B. W. Boudouris, M. B. Casu, and A. Rajca. Journal of the American Chemical Society 144, 6059-6070 (2022).

Enhancement and Function of the Piezoelectric Effect in Polymer Nanofibers.
L. Persano, S. K. Ghosh, and D. Pisignano. Accounts of Materials Research 3, 900-912 (2022).

3d Metal Doping of Core@Shell Wüstite@ferrite Nanoparticles as a Promising Route toward Room Temperature Exchange Bias Magnets.
B. Muzzi, M. Albino, M. Petrecca, C. Innocenti, C. D. J. Fernández, G. Bertoni, C. Marquina, M. R. Ibarra, and C. Sangregorio. Small 18, 2107426 (2022).

Enhancing Tungsten Oxide Gasochromism with Noble Metal Nanoparticles: The Importance of the Interface.
A. Longato, M. Vanzan, E. Colusso, S. Corni, and A. Martucci. Small 19, 2205522 (2022).

Controlling Atom-Photon Bound States in an Array of Josephson-Junction Resonators.
M. Scigliuzzo, G. Calajò, F. Ciccarello, D. Perez Lozano, A. Bengtsson, P. Scarlino, A. Wallraff, D. Chang, P. Delsing, and S. Gasparinetti. Physical Review X 12, 031036 (2022).

Impact of size effects on photopolymerization and its optical monitoring in-situ.
A. Camposeo, A. Arkadii, L. Romano, F. D'Elia, F. Fabbri, E. Zussman, and D. Pisignano. Additive Manufacturing 58, 103020 (2022).

3D arrangement of epitaxial graphene conformally grown on porousified crystalline SiC.
S. Veronesi, G. Pfusterschmied, F. Fabbri, M. Leitgeb, O. Arif, D. A. Esteban, S. Bals, U. Schmid, and S. Heun. Carbon 189, 210-218 (2022).

A proposed nomenclature for graphene pores: a systematic study of their geometrical features and an algorithm for their generation and enumeration.
Z. G. Fthenakis. Carbon 199, 508-519 (2022).

Multifunctional Switch Based on Spin-Labeled Gold Nanoparticles.
V. Lloveras, P. Elías-Rodríguez, L. Bursi, E. Shirdel, A. R. Goñi, A. Calzolari, and J. Vidal-Gancedo. Nano Letters 22, 768-774 (2022).

Gap Opening in Double-Sided Highly Hydrogenated Free-Standing Graphene.
M. G. Betti, E. Placidi, C. Izzo, E. Blundo, A. Polimeni, M. Sbroscia, J. Avila, P. Dudin, K. Hu, Y. Ito, D. Prezzi, M. Bonacci, E. Molinari, and C. Mariani. Nano Letters 22, 2971-2977 (2022).

Moiré-Induced Transport in CVD-Based Small-Angle Twisted Bilayer Graphene.
G. Piccinini, V. Mišeikis, P. Novelli, K. Watanabe, T. Taniguchi, M. Polini, C. Coletti, and S. Pezzini. Nano Letters 22, 5252-5259 (2022).

Josephson Diode Effect in High-Mobility InSb Nanoflags.
B. Turini, S. Salimian, M. Carrega, A. Iorio, E. Strambini, F. Giazotto, V. Zannier, L. Sorba, and S. Heun. Nano Letters 22, 8502-8508 (2022).

Tuning the Electronic Response of Metallic Graphene by Potassium Doping.
D. Marchiani, A. Tonelli, C. Mariani, R. Frisenda, J. Avila, P. Dudin, S. Jeong, Y. Ito, F. S. Magnani, R. Biagi, V. De Renzi, and M. G. Betti. Nano Letters 23, 170-176 (2022).

Intrinsic Control of Interlayer Exciton Generation in Van der Waals Materials via Janus Layers.
E. Torun, F. Paleari, M. V. Milošević, L. Wirtz, and C. Sevik. Nano Letters 23, 3159- 3166 (2022).

Exotic interactions mediated by a non-Hermitian photonic bath.
F. Roccati, S. Lorenzo, G. Calajò, G. M. Palma, A. Carollo, and F. Ciccarello. Optica 9, 565-571 (2022).

Antenna-enhanced mid-infrared detection of extracellular vesicles derived from human cancer cell cultures.
M. E. Temperini, F. Di Giacinto, S. Romanò, R. Di Santo, A. Augello, R. Polito, L. Baldassarre, V. Giliberti, M. Papi, U. Basile, B. Niccolini, E. K. Krasnowska, A. Serafino, M. De Spirito, A. Di Gaspare, M. Ortolani, and G. Ciasca. Journal of Nanobiotechnology 20, 530 (2022).

Engineering Dynamical Couplings for Quantum Thermodynamic Tasks.
M. Carrega, L. M. Cangemi, G. De Filippis, V. Cataudella, G. Benenti, and M. Sassetti. PRX Quantum 3, 010323 (2022).

Ultrafast hot carrier transfer in WS2/graphene large area heterostructures.
C. Trovatello, G. Piccinini, S. Forti, F. Fabbri, A. Rossi, S. De Silvestri, C. Coletti, G. Cerullo, and S. Dal Conte. npj 2D Materials and Applications 6, 24 (2022).

Autonomous Dissipative Maxwell's Demon in a Diamond Spin Qutrit.
S. Hernández-Gómez, S. Gherardini, N. Staudenmaier, F. Poggiali, M. Campisi, A. Trombettoni, F. S. Cataliotti, P. Cappellaro, and N. Fabbri. PRX Quantum 3, 020329 (2022).

Twist-resilient and robust ferroelectric quantum spin Hall insulators driven by van der Waals interactions.
A. Marrazzo and M. Gibertini. npj 2D Materials and Applications 6, 30 (2022).

In-Operando Optical Spectroscopy of Field-Effect-Gated Al-Doped ZnO.
M. Sygletou, S. Benedetti, A. di Bona, M. Canepa, F. Bisio, and E. Bellingeri. ACS Applied Materials and Interfaces 15, 3112 (2022).

Quantum computing algorithms: getting closer to critical problems in computational biology.
L. Marchetti, R. Nifosì, P. L. Martelli, E. Da Pozzo, V. Cappello, F. Banterle, M. L. Trincavelli, C. Martini, and M. D'Elia. Briefings in Bioinformatics 23, 1-15 (2022).

Unusual Red Light Emission from Nonmetallic Cu2Te Microdisk for Laser and SERS Applications.
Q. Li, H. Rao, X. Ma, H. Mei, Z. Zhao, W. Gong, A. Camposeo, D. Pisignano, and X. Yang. Advanced Optical Materials 10, 2101976 (2022).

All in One-Chip, Electrolyte-Gated Graphene Amplitude Modulator, Saturable Absorber Mirror and Metrological Frequency-Tuner in the 2–5 THz Range.
A. Di Gaspare, E. A. A. Pogna, E. Riccardi, S. M. A. Sarfraz, G. Scamarcio, and M. S. Vitiello. Advanced Optical Materials 10, 2200819 (2022).

A Superfolder Green Fluorescent Protein-Based Biosensor Allows Monitoring of Chloride in the Endoplasmic Reticulum.
K. Shariati, Y. Zhang, S. Giubbolini, R. Parra, S. Liang, A. Edwards, J. F. Hejtmancik, G. M. Ratto, D. Arosio, and G. Ku. ACS Sensors 7, 2218-2224 (2022).

Dynamics of Hole Singlet-Triplet Qubits with Large g -Factor Differences.
D. Jirovec, P. M. Mutter, A. Hofmann, A. Crippa, M. Rychetsky, D. L. Craig, J. Kukucka, F. Martins, A. Ballabio, N. Ares, D. Chrastina, G. Isella, G. Burkard, and G. Katsaros. Physical Review Letters 128, 126803 (2022).

Classical Physics and Blackbody Radiation.
J. Wang, G. Casati, and G. Benenti. Physical Review Letters 128, 134101 (2022).

Colossal Orbital Edelstein Effect in Noncentrosymmetric Superconductors.
L. Chirolli, M. T. Mercaldo, C. Guarcello, F. Giazotto, and M. Cuoco. Physical Review Letters 128, 217703 (2022).

Excitations of Quantum Many-Body Systems via Purified Ensembles: A Unitary-Coupled-Cluster-Based Approach.
C. L. Benavides-Riveros, L. Chen, C. Schilling, S. Mantilla, and S. Pittalis. Physical Review Letters 129, 066401 (2022).

SWAP Gate between a Majorana Qubit and a Parity-Protected Superconducting Qubit.
L. Chirolli, N. Y. Yao, and J. E. Moore. Physical Review Letters 129,177701 (2022).

2023

Short pulse generation from a graphene-coupled passively mode-locked terahertz laser.
E. Riccardi, V. Pistore, S. Kang, L. Seitner, A. De Vetter, C. Jirauschek, J. Mangeney, L. Li, A. G. Davies, E. H. Linfield, A. C. Ferrari, S. S. Dhillon, and M. S. Vitiello. Nature Photonics 17, 607-614 (2023).

Field-driven attosecond charge dynamics in germanium.
G. Inzani, L. Adamska, A. Eskandari-asl, N. Di Palo, G. L. Dolso, B. Moio, L. J. D'Onofrio, A. Lamperti, A. Molle, R. Borrego-Varillas, M. Nisoli, S. Pittalis, C. A. Rozzi, A. Avella, and M. Lucchini. Nature Photonics 17, 1059-1065 (2023).

Gate-Controlled Magnetotransport and Electrostatic Modulation of Magnetism in 2D Magnetic Semiconductor CrPS4.
F. Wu, M. Gibertini, K. Watanabe, T. Taniguchi, I. Gutiérrez-Lezama, N. Ubrig, and A. F. Morpurgo. Advanced Materials 35, 2211653 (2023).

The Impact of Lattice Distortions on the Magnetic Stability of Single Atoms: Dy and Ho on BaO(100).
B. V. Sorokin, M. Pivetta, V. Bellini, D. Merk, S. Reynaud, A. Barla, H. Brune, and S. Rusponi. Advanced Functional Materials 33, 2213951 (2023).

Chirality-Specific Unidirectional Rotation of Molecular Motors on Cu(111).
M. Schied, D. Prezzi, D. Liu, S. Kowarik, P. A. Jacobson, S. Corni, J. M. Tour, and L. Grill. ACS Nano 17, 3958–3965 (2023).

Site-Selective Chemical Vapor Deposition on Direct-Write 3D Nanoarchitectures.
F. Porrati, S. Barth, G. C. Gazzadi, S. Frabboni, O. M. Volkov, D. Makarov, and M. Huth. ACS Nano 17, 4704–4715 (2023).

Real-Time Measure of the Lattice Temperature of a Semiconductor Heterostructure Laser via an On-Chip Integrated Graphene Thermometer.
L. Viti, E. Riccardi, H. E. Beere, D. A. Ritchie, and M. S. Vitiello. ACS Nano 17, 6103–6112 (2023).

Expansion of the Materials Cloud 2D Database.
D. Campi, N. Mounet, M. Gibertini, G. Pizzi, and N. Marzari. ACS Nano 17, 11268-11278 (2023).

Phonon-mediated room-temperature quantum Hall transport in graphene.
D. Vaquero, V. Clericò, M. Schmitz, J. A. Delgado-Notario, A. Martín-Ramos, J. Salvador-Sánchez, C. S. A. Müller, K. Rubi, K. Watanabe, T. Taniguchi, B. Beschoten, C. Stampfer, E. Diez, M. I. Katsnelson, U. Zeitler, S. Wiedmann, and S. Pezzini. Nature Communications 14, 318 (2023).

Sub-picosecond collapse of molecular polaritons to pure molecular transition in plasmonic photoswitch-nanoantennas.
J. Kuttruff, M. Romanelli, E. Pedrueza-Villalmanzo, J. Allerbeck, J. Fregoni, V. Saavedra-Becerril, J. Andréasson, D. Brida, A. Dmitriev, S. Corni, and N. Maccaferri. Nature Communications 14, 3875 (2023).

Multiple antiferromagnetic phases and magnetic anisotropy in exfoliated CrBr3 multilayers.
F. Yao, V. Multian, Z. Wang, N. Ubrig, J. Teyssier, F. Wu, E. Giannini, M. Gibertini, I. Gutiérrez-Lezama, and A. F. Morpurgo. Nature Communications 14, 4969 (2023).

Sub-THz wireless transmission based on graphene-integrated optoelectronic mixer.
A. Montanaro, G. Piccinini, V. Mišeikis, V. Sorianello, M. A. Giambra, S. Soresi, L. Giorgi, A. D'Errico, K. Watanabe, T. Taniguchi, S. Pezzini, C. Coletti, and M. Romagnoli. Nature Communications 14, 6471 (2023).

Daily rhythm in cortical chloride homeostasis underpins functional changes in visual cortex excitability.
E. Pracucci, R. T. Graham, L. Alberio, G. Nardi, O. Cozzolino, V. Pillai, G. Pasquini, L. Saieva, D. Walsh, S. Landi, J. Zhang, A. J. Trevelyan, and G. M. Ratto. Nature Communications 14, 7108 (2023).

Heat-Driven Iontronic Nanotransistors.
D. Prete, A. Colosimo, V. Demontis, L. Medda, V. Zannier, L. Bellucci, V. Tozzini, L. Sorba, F. Beltram, D. Pisignano, and F. Rossella. Advanced Science 10, 2204120 (2023).

Self-Induced Mode-Locking in Electrically Pumped Far-Infrared Random Lasers.
A. Di Gaspare, V. Pistore, E. Riccardi, E. A. A. Pogna, H. E. Beere, D. A. Ritchie, L. Li, A. G. Davies, E. H. Linfield, A. C. Ferrari, and M. S. Vitiello. Advanced Science 10, 2206824 (2023).

Advances in ultrafast plasmonics.
A. N. Koya, M. Romanelli, J. Kuttruff, N. Henriksson, A. Stefancu, G. Grinblat, A. De Andres, F. Schnur, M. Vanzan, M. Marsili, M. Rahaman, A. Viejo Rodríguez, T. Tapani, H. Lin, B. D. Dana, J. Lin, G. Barbillon, R. Proietti Zaccaria, D. Brida, D. Jariwala, L. Veisz, E. Cortés, S. Corni, D. Garoli, and N. Maccaferri. Applied Physics Reviews 10, 021318 (2023).

Mechanism and Dynamics of Photodecarboxylation Catalyzed by Lactate Monooxygenase.
X. Li, C. G. Page, L. Zanetti-Polzi, A. P. Kalra, D. G. Oblinsky, I. Daidone, T. K. Hyster, and G. D. Scholes. Journal of the American Chemical Society 145, 13232-13240 (2023).

Human Small Heat Shock Protein B8 Inhibits Protein Aggregation without Affecting the Native Folding Process.
D. Choudhary, L. Mediani, M. J. Avellaneda, S. Bjarnason, S. Alberti, E. E. Boczek, P. O. Heidarsson, A. Mossa, S. Carra, S. J. Tans, and C. Cecconi. Journal of the American Chemical Society 145, 15188-15196 (2023).

Accelerated epithelial layer healing induced by tactile anisotropy in surface topography.
F. M. Pramotton, L. Cousin, T. Roy, C. Giampietro, M. Cecchini, C. Masciullo, A. Ferrari, and D. Poulikakos. Science Advances 9, eadd1581 (2023).

Xeno-free cultured mesenchymal stromal cells release extracellular vesicles with a "therapeutic" miRNA cargo ameliorating cartilage inflammation in vitro.
M. E. F. Palamà, S. Coco, G. M. Shaw, D. Reverberi, M. Ghelardoni, P. Ostano, G. Chiorino, L. Sercia, L. Persano, M. C. Gagliani, K. Cortese, D. Pisignano, J. M. Murphy, and C. Gentili. Theranostics 13, 1470-1489 (2023).

Nuclear ERK1/2 signaling potentiation enhances neuroprotection and cognition via Importinα1/KPNA2.
M. Indrigo, I. Morella, D. Orellana, R. d'Isa, A. Papale, R. Parra, A. Gurgone, D. Lecca, A. Cavaccini, C. M. Tigaret, A. Cagnotto, K. Jones, S. Brooks, G. M. Ratto, N. D. Allen, M. J. Lelos, S. Middei, M. Giustetto, A. R. Carta, R. Tonini, M. Salmona, J. Hall, K. Thomas, R. Brambilla, and S. Fasano. EMBO Molecular Medicine 15, e15984 (2023).

Terahertz Sources Based on Metrological-Grade Frequency Combs.
E. Riccardi, V. Pistore, L. Consolino, A. Sorgi, F. Cappelli, R. Eramo, P. De Natale, L. Li, A. G. Davies, E. H. Linfield, and M. S. Vitiello. Laser and Photonics Reviews 17, 2200412 (2023).

Tuning the Electronic Response of Metallic Graphene by Potassium Doping.
D. Marchiani, A. Tonelli, C. Mariani, R. Frisenda, J. Avila, P. Dudin, S. Jeong, Y. Ito, F. S. Magnani, R. Biagi, V. De Renzi, and M. G. Betti. Nano Letters 23, 170-176 (2023).

Energy Transfer to Molecular Adsorbates by Transient Hot Electron Spillover.
M. Vanzan, G. Gil, D. Castaldo, P. Nordlander, and S. Corni. Nano Letters 23, 2719-2725 (2023).

Photoactive p-Type Spinel CuGa2O4 Nanocrystals.
O. Kendall, L. V. Melendez, J. Ren, S. P. Ratnayake, B. J. Murdoch, E. L. H. Mayes, J. van Embden, D. E. Gómez, A. Calzolari, and E. Della Gaspera. Nano Letters 23, 2974-2980 (2023).

Intrinsic Control of Interlayer Exciton Generation in Van der Waals Materials via Janus Layers.
E. Torun, F. Paleari, M. V. Milošević, L. Wirtz, and C. Sevik. Nano Letters 23, 3159-3166 (2023).

Effective Single-Mode Methodology for Strongly Coupled Multimode Molecular-Plasmon Nanosystems. M. Romanelli, R. R. Riso, T. S. Haugland, E. Ronca, S. Corni, and H. Koch. Nano Letters 23, 4938-4946 (2023).

Magnetism-Induced Band-Edge Shift as the Mechanism for Magnetoconductance in CrPS4 Transistors.
F. Wu, M. Gibertini, K. Watanabe, T. Taniguchi, I. Gutiérrez-Lezama, N. Ubrig, and A. F. Morpurgo. Nano Letters 23, 8140-8145 (2023).

Excitonic Effects in Energy-Loss Spectra of Freestanding Graphene.
A. Guandalini, R. Senga, Y. C. Lin, K. Suenaga, A. Ferretti, D. Varsano, A. Recchia, P. Barone, F. Mauri, T. Pichler, and C. Kramberger. Nano Letters 23, 11835–11841 (2023).

Light-Emitting Microfibers from Lotus Root for Eco-Friendly Optical Waveguides and Biosensing.
X. Yang, L. Xu, S. Xiong, H. Rao, F. Tan, J. Yan, Y. Bao, A. Albanese, A. Camposeo, D. Pisignano, and B. Li. Nano Letters 24, 566-575 (2023).

Stretch-activated ion channel TMEM63B associates with developmental and epileptic encephalopathies and progressive neurodegeneration.
A. Vetro, C. Pelorosso, S. Balestrini, A. Masi, S. Hambleton, E. Argilli, V. Conti, S. Giubbolini, R. Barrick, G. Bergant, K. Writzl, E. K. Bijlsma, T. Brunet, P. Cacheiro, D. Mei, A. Devlin, M. J. V. Hoffer, K. Machol, G. Mannaioni, M. Sakamoto, M. P. Menezes, T. Courtin, E. Sherr, R. Parra, R. Richardson, T. Roscioli, M. Scala, C. von Stülpnagel, and D. Smedley. American Journal of Human Genetics 3, 1356-1376 (2023).

Efficient GW calculations in two dimensional materials through a stochastic integration of the screened potential.
A. Guandalini, P. D'Amico, A. Ferretti, and D. Varsano. npj Computational Materials 9, 44 (2023).

Towards high-throughput many-body perturbation theory: efficient algorithms and automated workflows.
M. Bonacci, J. Qiao, N. Spallanzani, A. Marrazzo, G. Pizzi, E. Molinari, D. Varsano, A. Ferretti, and D. Prezzi. npj Computational Materials 9, 74 (2023).

The NF–Y splicing signature controls hybrid EMT and ECM-related pathways to promote aggressiveness of colon cancer.

G. Rigillo, S. Belluti, V. Campani, G. Ragazzini, M. Ronzio, G. Miserocchi, B. Bighi, L. Cuoghi, V. Mularoni, V. Zappavigna, D. Dolfini, L. Mercatali, A. Alessandrini, and C. Imbriano. Cancer Letters 567, 216262 (2023).

Shadow Tomography on General Measurement Frames.
L. Innocenti, S. Lorenzo, I. Palmisano, F. Albarelli, A. Ferraro, M. Paternostro, and G. M. Palma. PRX Quantum 4, 040328 (2023).

In-Operando Optical Spectroscopy of Field-Effect-Gated Al-Doped ZnO.
M. Sygletou, S. Benedetti, A. di Bona, M. Canepa, F. Bisio, and E. Bellingeri. ACS Applied Materials and Interfaces 15, 3112–3118 (2023).

Long-Term Degradation Mechanisms in Application-Implemented Radical Thin Films.
E. M. Nowik-Boltyk, T. Junghoefer, M. Glaser, E. Giangrisostomi, R. Ovsyannikov, S. Zhang, C. Shu, A. Rajca, A. Calzolari, and M. B. Casu. ACS Applied Materials and Interfaces 15, 30935-30943 (2023).

Scalable High-Mobility Graphene/hBN Heterostructures.
L. Martini, V. Mišeikis, D. Esteban, J. Azpeitia, S. Pezzini, P. Paletti, M. W. Ochapski, D. Convertino, M. G. Hernandez, I. Jimenez, and C. Coletti. ACS Applied Materials and Interfaces 15, 37794-37801 (2023).

Optical Gain Switching by Thermo-Responsive Light-Emitting Nanofibers through Moisture Sorption Swelling.
M. Archimi, E. Schoolaert, J. Becelaere, R. Hoogenboom, A. Camposeo, K. De Clerck, and D. Pisignano. Advanced Optical Materials 11, 2202056 (2023).

© Anharmonic Exciton-Phonon Coupling in Metal-Organic Chalcogenides Hybrid Quantum Wells.
C. Kastl, P. Bonfà, and L. Maserati. Advanced Optical Materials 11, 2202213 (2023).

Electronic Excited States in Extreme Limits via Ensemble Density Functionals.
T. Gould, D. P. Kooi, P. Gori-Giorgi, and S. Pittalis. Physical Review Letters 130, 106401 (2023).

Accurate Prediction of Hall Mobilities in Two-Dimensional Materials through Gauge-Covariant Quadrupolar Contributions.
S. Poncé, M. Royo, M. Gibertini, N. Marzari, and M. Stengel. Physical Review Letters 130, 166301 (2023).

Signatures of Dissipation Driven Quantum Phase Transition in Rabi Model.
G. De Filippis, A. De Candia, G. Di Bello, C. A. Perroni, L. M. Cangemi, A. Nocera, M. Sassetti,

R. Fazio, and V. Cataudella. Physical Review Letters 130, 210404 (2023).
Work Extraction Processes from Noisy Quantum Batteries: The Role of Nonlocal Resources.
S. Tirone, R. Salvia, S. Chessa, and V. Giovannetti. Physical Review Letters 131, 060402 (2023).

Distinguishing Different Stackings in Layered Materials via Luminescence Spectroscopy.
M. Zanfrognini, A. Plaud, I. Stenger, F. Fossard, L. Sponza, L. Schué, F. Paleari, E. Molinari, D. Varsano, L. Wirtz, F. Ducastelle, A. Loiseau, and J. Barjon. Physical Review Letters 131, 206902 (2023).

2022-2023 Publication chart

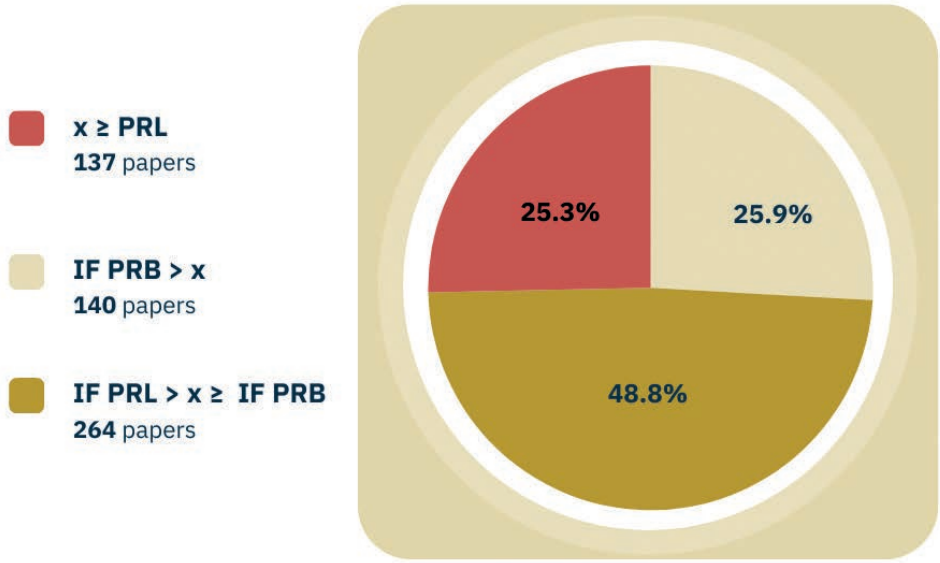

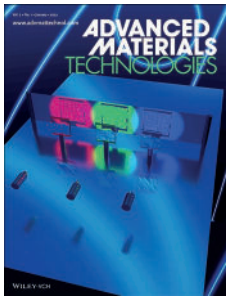

A. Tredicucci, D. Pisignano, A. Camposeo, et al., Advanced Materials Technologies 1 (7), 2022.

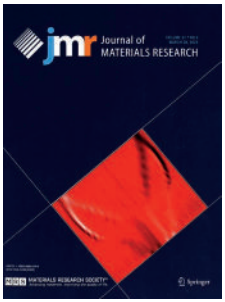

F. Moro, M. Moret, A. Ghirri, et al., Journal of Materials Research 37, 2022.

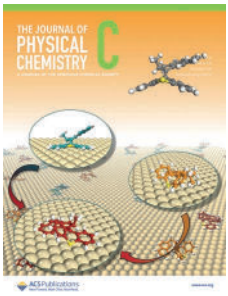

D. Prezzi, S. Corni, et al., The Journal of Physical Chemistry C 126 (21), 2022.

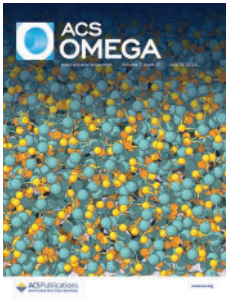

F. Tavanti, A. Calzolari, ACS Omega 2022, 7 (27), 2022.

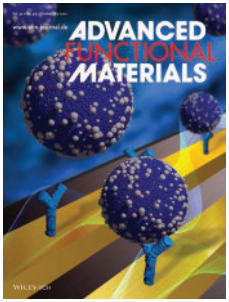

F. Lunardelli, M. Gagliardi, A. Miranda, L. Lamanna, M. Cecchini et al., Advanced Functional Materials 44 (32), 2022.

E. Passaglia, A. Sgarbossa, Pharmaceutics 15 (12), 2023.

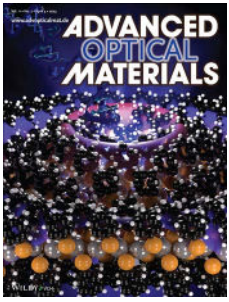

P. Bonfà, et al., Advanced Optical Materials 7, 2023.

Cnr Nano Life

Cnr Nano events in 2022

JANUARY

Women, Research, Transformations

On Jan. 21-22, Cnr Nano proudly served as the organizing partner of the Donne&Scienza Association's annual conference, "Donne, Ricerca, Trasformazioni" hosted at the Modena Main Public Library. Featuring Maria Cristina Messa, University Ministry, and Nobel Laureate Giorgio Parisi, the discussions centred on women's research roles, societal changes, and gender-specific aspects in AI, medicine, and environment. The annual event aimed at boosting the networking between science and gender-focused associations, and hosted activities for the general public, such as a play in honour of Rosalind Franklin, "Rosalind's Glasses", and a list of selected books in the Library. The participation, both on-site and online, was a resounding success.

FEBRUARY

Cnr Nano goes social!

On February 18, Cnr Nano stepped into the realm of social media, launching its Twitter profile. Cnr Nano's social presence aims to ignite curiosity and foster connections, sharing insights and innovations with a global audience.

FEBRUARY

Captivating talking

Renewing its long-standing tradition, the Nano Colloquia series once more brought together esteemed Nano scientists from Modena and Pisa, highlighting their recent work, fostering knowledge sharing and new collaborations. A pivotal platform for early-stage researchers, these virtual talks, available for download on our website, sparked insightful discussions and potential partnerships in nanoscience.

MARCH

Professione Scienziata

To mark International Day of Women and Girls in Science, Cnr Nano organized "Professione Scienziata", a dynamic event at I.I.S. Galilei-Pacinotti in Pisa on March 10. Female researchers, including Lucia Sorba, Ilaria Tonazzini, and Valentina Tozzini, shared their STEM journeys, aiming to ignite interest in scientific careers among secondary school students. With support from the Regional School Office, the interactive

session wanted to inspire student engagement both in-person and online, fostering meaningful discussions and breaking gender stereotypes.

MARCH

Starting up supercomputing revolution

Grounded on a discovery made at Cnr Nano, the new startup DSQM (Digital Superconducting Quantum Machines) will develop ultra-fast and energy-efficient electronics by exploiting superconducting materials aiming at revolutionizing telecom and supercomputing. Led by Claudio Puglia (CEO), Francesco Giazotto, Elia Strambini, and Giorgio De Simoni, it promises 100x performance gains in data rates and computing, while aligning with existing tech standards. Stemmed from research supported by European projects, DSQM bridges research and innovation, translating frontier science into transformative solutions for interconnected global networks.

APRIL

Toolbox for disruptive electronics

Introduced as part of the European project Intersect, led by Arrigo Calzolari, IM2D promotes an easy-driven semiconductor device simulation to industrial stakeholders. The platform, an interoperable simulation tool, accelerates tech development with its material-aware approach. A highly successful webinar on April 27 showcased IM2D's versatility, catering to all skill levels from beginners to experts. Project researchers highlighted its features and real-case applications, emphasizing its adaptability for diverse user backgrounds in configuring simulation parameters.

MAY

A new STAR is born

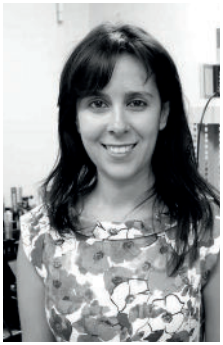

Researcher Miriam Serena Vitiello was awarded an ERC "Proof of Concept" grant for her project "Hyper-Spectral Terahertz neAR-field nanoscope" (STAR). The project aims to advance a compact THz imaging system, promising applications in electronics, pharmaceuticals, and more. Leveraging miniaturized frequency combs, Vitiello's project achieved groundbreaking spatial resolution and rapid acquisition rates, poised to transfrom the healthcare, electronics, and security realms.

MAY

Unlocking Stradivarius' charm

Exploring the allure of Stradivarius violins, researcher Carlo Andrea Rozzi led a study that compared Stradivarius violins to others, revealing their unique timbral balance, shedding light on why they stand out for their captivating sound. The findings, detailed in The Journal of the Acoustical Society of America, made headlines in major Italian newspapers and led the researcher to feature at the VideoGameLab festival (Rome, September 2022), where he led an interactive session on sound perception with the audience.

MAY

THz Photonic school

Cnr Nano hosted the Terahertz Photonics School in Pisa from May 8 to 14. Eighty-five students attended a vibrant week of lectures, that offered in-depth insights into THz science and applications focused on nanostructures and related devices. (https://terahertz-school.nano.cnr.it/)

JUNE

Revolutionizing Angelman syndrome therapy

Led by Ilaria Tonazzini (Cnr Nano) and Laura Baroncelli (Cnr IN), the new research project InnovAS has been funded by the Angelman Syndrome Alliance. With a grant of 170,000 euros, the project targets a new therapy delivery method for Angelman syndrome, overcoming current invasive approaches, and a novel non-invasive imaging methods to monitor the effectiveness of therapeutic treatments. The project's impact means to enhance patient quality of life and therapeutic outcomes.

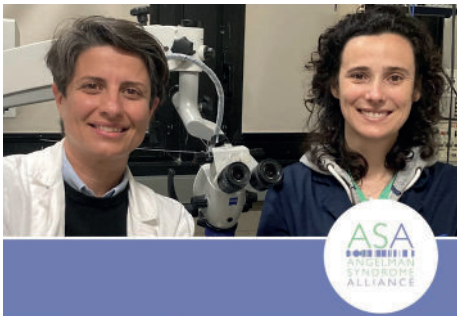

SEPTEMBER

Advancing quantum computing

The SPECTRUM project kicked off in Pisa, on September 8, gathering 20+ consortium members led by Cnr Nano researcher Francesco Giazotto, to discuss the project objectives, plans and expected actions. Engaging presentations and tours of the Cnr Nano Labs ignited stimulating scientific discussions, culminating in a team dinner fostering networking opportunities.

SEPTEMBER

Unveiling spin qubits

On 26 September, the Workshop of the EU H2020 project FET Open Iqubits was held in Modena, focusing on the simulation of spin qubits in industrial silicon MOSFETs. Filippo Troiani, Cnr Nano researcher and

organiser of the event, emphasised the potential of spin qubits for quantum computing and aimed to foster a strong scientific community through this stimulating workshop.

SEPTEMBER

Shining at Researchers' Night

Cnr Nano eagerly joined the 2022 Researchers' Night, with both Modena and Pisa units involved in a vibrant display of engaging demonstrations. Held across 25 countries on September 30, this annual event aims at maiking research and innovation accessible and entertaining for all ages. With hands-on presentations and immersive activities, the researchers showcased machine learning in game strategy, virtual exploration of proteins, and the future of electronics. The event fostered a unique interaction between researchers and the public, bringing Cnr Nano's cutting-edge research to a broader audience.

Cnr Nano events in 2023

JANUARY

Pioneering quantum electron microscopy

Vincenzo Grillo, Research Director in Modena, was awarded the Ernst Ruska Prize for pioneering advancements in quantum electron microscopy. Recognized for ground-breaking techniques and tools, Grillo's innovative approach facilitated precise electron beam modelling, revolutionizing sample analysis. His collaboration with global experts propelled the development of a revolutionary electrostatic orbital angular momentum sorter for electron microscopes.

FEBRUARY

Empowering #womenatCNR

On the International Day of Women and Girls in Science 2023, our institute proudly turned the spotlight on its remarkable female researchers, by entering the #womenatCNR social media campaign. Launched in 2022 by Cnr-Scitec, the campaign was joined in 2023 by Cnr Nano and other Cnr institutes. During the year, over 300 women shared selfies and stories on Twitter, championing women's impact in science. 27 Cnr Nano researchers took part in this empowering campaign, and presented themselves in posts labelled #womenatNANO.

FEBRUARY

Pioneering materials simulation with extreme computing

MaX, the European Centre of Excellence for Materials at the eXascale, was funded for its third phase, from 2023 to 2026. Led by Cnr Nano Modena, it is a partnership of European leaders in the materials domain, prominent European HPC centres, technology partners. With an 8.5 million euro budget, MaX propels material design into the extreme computing era. Elisa Molinari from Cnr Nano and Unimore, along with Andrea Ferretti, leads this venture aiming for breakthroughs in clean energy and cutting-edge materials for advanced technologies.

MAY

Austrian science ties

Cnr Nano received a prestigious invitation to attend the VI Italian Research Day in Austria commemorating Copernicus' 550th birth anniversary held at the Italian Embassy in Vienna. Deborah Prezzi presented Cnr Nano's collaborative initiatives with Austrian institutions, underlining its leading position as the Italian institute with the most extensive scientific ties in Austria.

MAY

Cnr's Spring of Science

La Primavera della Ricerca - The Springtime of Research was a day of discovery and engagement to celebrate the Cnr Centenary. On May 12, all Cnr institutes in Pisa invited the public to delve into sustainability, clean energy, life sciences, and more, through talks for schools, outdoor labs, and an insightful talk show. Cnr Nano was on stage with Giorgio De Simoni on the exploration of superconductors in 'The Ice Age of Computers' and Mariacristina Gagliardi with an open lab showcasing "Nanotechnologies for diagnostics and health".

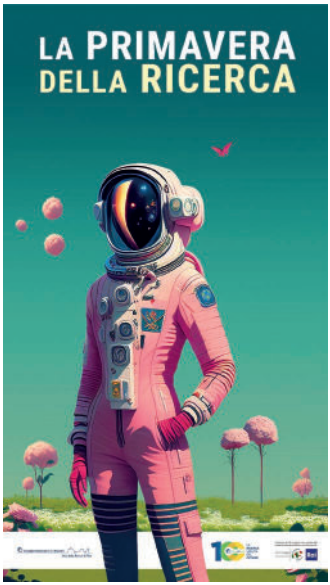

MAY

Discovering nanoscience

In May and December, Cnr Nano Pisa introduced bio-nano science to schools through a series of seminars. Ilaria Tonazzini, Valentina Tozzini, and Antonella Battisti showcased the advancements in biomaterials, quantum computing, and nanomedicine, reaching around 400 students across seven middle and high schools in the Tuscany region. The students showed great curiosity and - hopefully - this will inspire the future scientific vocations of many!

MAY

Delving into simulations

From May 22 to 26, the YAMBO school organized by Daniele Varsano delved into materials' excited states, unlocking their mysteries through YAMBO and CHEERS codes. Through theoretical insights and hands-on sessions, participants explored quasiparticles, excitons, and nonlinear optics. Fusing theory and practice, the school emphasized real-world applications. The school was attended by 40 participants from 21 countries, who had the chance of visiting Rome in the social programme. YAMBO is a flagship code of the MaX Centre of Excellence and ICSC PNRR Italian National Centre for HPC, Big Data and Quantum Computing. (https://www.yambo-code.eu/2023/02/18/yambo-school-2023/)

JUNE

20 years of scientific adventure

The 20th anniversary of Cnr Nano's Modena unit, the S3 Centre, was celebrated on June 8-9. More than 130 people including colleagues, alumni, and stakeholders joined in a two-day lively workshop, flipping through over two decades of scientific excellence. Elisa Molinari and Massimo Rontani, past and present directors, went through S3 history, from the conception to the days to come, while warm reunions and greetings marked the occasion; on the second day S3 scientists presented state-of-the-art research activities with a look at their history. A poster session highlighted the young researchers' contribution to research. Thank you, all participants, for celebrating with us!

JUNE

Uplifting Terahertz horizons

Hosted on the stunning Erice hill, from June 23 to 30, the Infrared and Terahertz Quantum Workshop (ITQW) 2023, investigated groundbreaking quantum and electromagnetic phenomena in photonic materials within the infrared and THz frequencies. Organized by Miriam Serena Vitiello and Alessandro Tredicucci, ITQW explored innovative device creation and applications, leveraging the unique properties of this spectral region. It was attended by 150 participants from 18 countries (https://itqw2023.nano.cnr.it).

JULY

Enlightening optogenetics

From July 3 to 5, Modena became the hub for discussing unresolved challenges and advances in understanding photoreceptor mechanisms at the microscopic level. The workshop "Principles of light-induced charge transfer for optogenetics" (CT4OPTO), organised by Laura Zanetti Polzi and Rosa Di Felice, brought together leading experts to explore the untapped potential of photoreceptors in controlling physiological processes, igniting discussions for advancing optogenetics (https://optogenetics.nano.cnr.it/).

SEPTEMBER

Exploring 2D excitonic insulators

The CMD30 – FisMat2023 conference (September 4-8 at Politecnico di Milano) featured a Mini Colloquium on excitonic insulators, exploring their emergence and implications. Spearheaded by visionary physicists, this topic, envisioned over 50 years ago, recently gained momentum in 2D materials.

Organized by Elisa Molinari and Massimo Rontani, the three half-day session sparked discussions among researchers, on the intriguing interacting systems and their potential applications.

SEPTEMBER
Minds & Machines

A public seminar on “Intelligenze al confine tra biologico e artificiale”, was held in Pisa (September 9) to explore the intersection of Biological and Artificial Intelligence. Speakers delved into parallels between human brain function and "Deep Learning" neural networks, as well as analyzed societal impacts of AI dissemination. Chaired by Valentina Tozzini, the seminar also addressed AI's ethical and philosophical dimensions.

SEPTEMBER
Researchers’ night is back!

On September 29 Cnr Nano joined the 2023 European Researchers' Night. In Modena, researchers hosted engaging and interactive activities including the science bash “A far la scienziata comincia tu”, a female scientist centric dialogue on nanoscience's world. Pisa displayed nanotechnology's advancements in health and medicine, unveiling innovative tools for diagnostics, regenerative medicine, and brain studies. These lively events promoted public engagement, showing up Cnr Nano's commitment to bridging the gap between science and society.

NOVEMBER
Acknowledging women in science

"300×100. Protagoniste per la Ricerca", an inspirational video spotlighting 300 female scientists, was premiered during the Cnr's Centennial celebration event on November 18, in Rome. Following the social media campaign #womenatcnr shared by 20 Cnr Institutes, and scripted by Maddalena Scandola and Luisa Neri, the video meant to celebrate the contribution to science of Cnr women researchers, to champion diversity and inclusivity in the scientific community.

People

The list below includes all researchers and staff active at Cnr Nano in 2022-2023. A total of 230 people have been working in our institute (36% female, 64% male), coming from 19 different countries besides Italy (Brazil, Colombia, Cuba, Ethiopia, Germany, Greece, India, Iran, Malaysia, Mexico, Morocco, Pakistan, Portugal, Romania, Russia, Spain, UK, Ukrain, and US). People marked with * are no longer at Cnr Nano.

Cnr Nano Staff

Researchers

Antonella Battisti
Valerio Bellini
Luca Bellucci
Stefania Benedetti
Andrea Bertoni
Giovanni Bertoni
Federica Bianco
Alessandro Braggio
Giorgia Brancolini
Arrigo Calzolari
Michele Campisi
Andrea Camposeo
Alessandra Catellani
Chiara Cavallini
Marco Cecchini
Valdis Corradini
Alessandro Crippa
Pino D'Amico
Giorgio De Simoni
Alessandro di Bona
Rosa Di Felice
Alessandra Di Gaspare
Filippo Fabbri
Riccardo Farchioni
Andrea Ferretti
Maria Cristina Gagliardi
Gian Carlo Gazzadi
Alberto Ghirri
Francesco Giazotto
Angelo Greco
Vincenzo Grillo
Stefan Heun
Gabriele Losi
Paola Luches
Francesca Matino
Andrea Mescola
Riccardo Nifosi
Sibilla Orsini
Fulvio Paleari
Guido Paolicelli
Claudia Maria Pereira Cardoso
Luana Persano
Sergio Pezzini
Valentino Pistore *
Stefano Pittalis
Deborah Prezzi
Gian Michele Ratto *
Elisa Riccardi
Massimo Rontani
Francesco Rossella
Enzo Rotunno
Carlo Andrea Rozzi
Melissa Santi
Chiara Schiattarella
Andrea Secchi
Antonella Sgarbossa
Lucia Sorba
Barbara Storti
Elia Strambini
Fabio Taddei
Ilaria Tonazzini
Valentina Tozzini
Filippo Troiani
Daniele Varsano
Stefano Veronesi
Leonardo Viti
Miriam Serena Vitiello
Laura Zanetti Polzi
Valentina Zannier
Simone Zanotto

Postdoctoral fellows

Omer Arif
Mahdi Asgari *
Shadi Bashiri
Benedetta Bertoni
Miki Bonacci *
Marco Brondi

Luca Bursi *
Sara Chiarugi
Luca Chirolli
Laura Colagiorgio *
Lucian Aurel Constantin *
Jose Gustavo De La Ossa Guerra *
Francesco Delfino *
Chiara De Cesari
Miriam De Sarlo
Andrea Di Ciolo *
Zacharias Fthenakis
Sara Ghayeb Zamharir
Sujoy Kumar Ghosh *
Peter Nicholas Oliver Gillespie
Simone Giubbolini *
Alberto Guandalini *
Manuel Alejandro Justo Guerrero
Savio Laricchia
Dario Alejandro Leon Valido *
Clodoaldo Irineu Levartoski De Araujo *
Tamiru Teshome Mamo *
Daniel Margineda De Godos *
Maria Celeste Maschio *
Alessandro Mossa
Lindsay Elizabeth Bassman Oftelie
Alessandro Paghi
Riccardo Parra *
Vinoshene Pillai *
Claudio Puglia *
Sreyan Raha
Paolo Rosi
Pavel Rukin
Amine Slassi *
Nicola Spallanzani
Maria Spies *
Francesco Tavanti *
Varun Thakur *
Manuela Tore
Giorgia Tori *
Leonardo Vicarelli *

Administrative, technical and support staff

Maria Grazia Angelini
Francesco Baesso
Maria Bartolacelli
Antonio Betzu
Elisa Bolognesi
Davide Calanca
Susanna Cavicchioli
Paola Corezzola
Daniele Desiati
Mara Di Berardo *
Giovanna Diprima
Giuseppe Genovese
Sandro Guerrazzi
Lucia Martorana
Luisa Neri
Francesco Nicolussi Golo
Riccardo Pallini *
Patrizia Pucci
Maddalena Scandola
Federica Sighinolfi
Simone Spinozzi
Anna Grazia Stefani

Support staff located in Genova

Alberto Arnone
Matilde Bolla
Barbara Cagnana
Enrico Camauli
Marco Campani
Paolo Ciocia
Monica Dalla Libera
Roberta De Donatis*
Fabio Distefano
Francesca Fortunati
Danilo Imperatore Antonucci
José Carlos Manganaro

Diletta Miceli
Elisabetta Narducci
Marco Punginelli
Milena Toselli
Claudia Valentini

Affiliated researchers from other institutions

Marco Affronte
Andrea Alessandrini
Maria Allegrini
Fabio Beltram
Giuliano Benenti
Roberto Biagi
Raffaello Bianco
Ranieri Bizzarri
Pietro Bonfà *
Claudio Bonizzoni
Paolo Bordone *
Marilia Junqueira Caldas
Francesco Cardarelli
Franco Carillo
Sara Carpi
Ciro Cecconi
Francesco Ciccarello *
Stefano Corni
Sergio D'Addato
Valentina De Renzi
Elena Degoli
Angelo Di Bernardo
Alberto Di Lieto *
Daniele Ercolani
Rosario Fazio *
Stefano Frabboni
Simone Gasparinetti
Marco Gibertini
Vittorio Giovannetti
Guido Goldoni
Marco Govoni
Alessandro Lascialfari *
Stefano Luin
Rita Magri
Franca Manghi
Ivan Marri
Fabio Mencarelli
Claudia Menozzi
Elisa Molinari
Stefano Ossicini
Gioacchino Massimo Palma
Pasqualantonio Pingue
Dario Pisignano
Alessandro Pitanti
Stefano Roddaro
Alberto Rota
Alice Ruini
Mauro Francesco Sgroi
Alessandra Toncelli *
Mauro Tonelli *
Alessandro Tredicucci
Sergio Valeri *
Giovanni Maria Vanacore
Ylea Vlamidis
Giampaolo Zuccheri

Postdoctoral fellows

Lyudmila Adamska
Ambra Del Grosso
Daniele Montepietra
Giacomo Sesti
Eleonora Spurio
Vittoria Urso*

PhD students

Annachiara Albanese
Luca Basta
Beatrice Bighi
Margherita Bini
Giada Bucci
Lorenzo Castelli

Caterina Chiari
Gloria Conte
Samuele Cornia *
Sofia Cristiani
Matteo D'Alessio
Gaia Forghieri
Gaia Germanese
Davide Giambastiani
Michael Alejandro Hernandez Bertan *
Lorenzo Lavista
Riccardo Magrin Maffei
Nicola Melchioni
Roberta Mezzena
Gabriele Nardi
Alessia Papalini
Samuele Pelatti
Domenic Prete *
Frank Ernesto Quintela Rodriguez *
Franklin Talbert
Simone Vacondio*
Isha Verma *
Andrea Vezzosi
Matteo Zanfrognini *

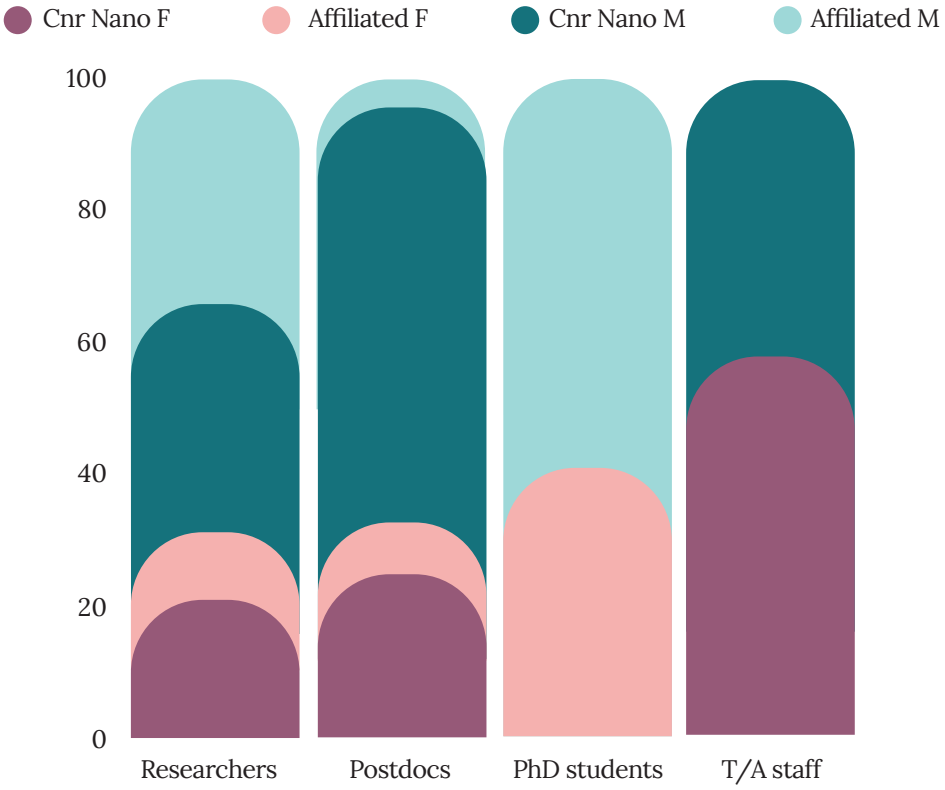

All categories have been normalized to 100 to show the gender distribution within the Institute

Image credits

Cover image
Scanning electron microscope top view image of InSb nanowires. Courtesy of Valentina Zannier (Cnr Nano).

Pag. 9
False-color SEM image of insulin micrometric branched aggregates. Courtesy of Antonella Battisti and Antonella Sgarbossa (Cnr Nano).

Pag. 25
False-color SEM image of a metamaterial composed by an array of L-shape holes etched in a gallium arsenide layer through advanced nanofabrication techniques. Courtesy of Simone Zanotto (Cnr Nano).

Pag. 45
The Superconducting Quantum Interference Proximity Effect Transistor (SQUIPT) is a device able to tune the energy gap of a thin superconducting wire to control the supercurrent flowing through it. Courtesy of Angelo Greco (Cnr Nano).

Pag. 69
Top-view scanning electron microscopy image of a three-dimensional graphene sample functionalized with Pd nanoparticles. Courtesy of Valentina Zannier (Cnr Nano), Emanuele Pompei (Università di Pisa).

Pag. 89
Nanoporous fibers from egg white albumin pyrolysis for water desalinisation. Water (blue) flows through the graphene-like fibers (grey) with O, N and H impurities (red, blue and white), while the ions (Na+, Cl- and Mg2+ : green, pink and yellow) are trapped onto the fibers impurities and defects. Courtesy of Valentina Tozzini (Cnr Nano) and Susanna Monti (Cnr Iccom).

Finito di stampare nel mese di aprile 2024.
Progetto editoriale: Luisa Neri, Cnr Nano.
Progetto grafico: mediamo.net, Modena.

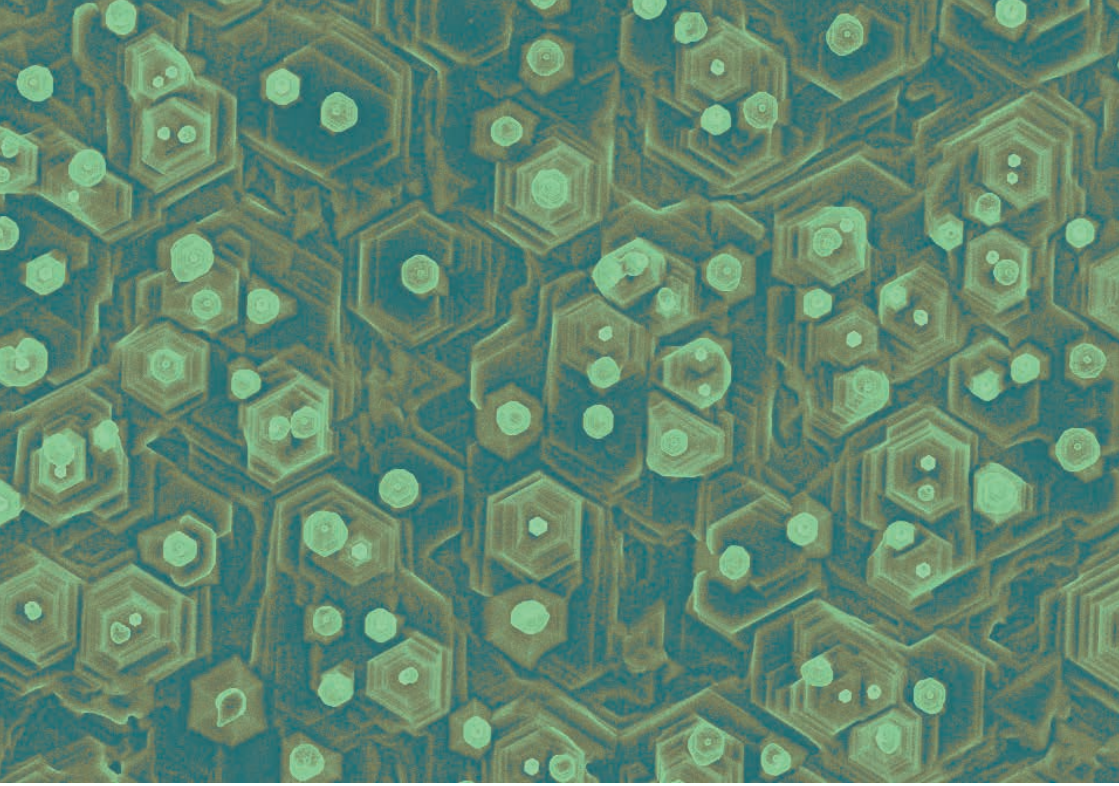

CNRNANO

ISTITUTO NANOSCIENZE CONSIGLIO NAZIONALE DELLE RICERCHE